UNIVERSIDADE DE SÃO PAULO

ESCOLA DE ENGENHARIA DE LORENA

JOSMAN ANDREY VELASCO MENDOZA

Novel *Aspergillus fumigatus* recombinant LPMOs: biochemical characteristics, and their participation in saccharification and photobiocatalysis processes.

Novas LPMOs recombinantes de *Aspergillus fumigatus*: características bioquímicas e sua participação em processos de sacarificação e fotobiocatálise.

Lorena

2022

JOSMAN ANDREY VELASCO MENDOZA

Novel *Aspergillus fumigatus* recombinant LPMOs: biochemical characteristics, and their participation in saccharification and photobiocatalysis processes.

Thesis presented at Escola de Engenharia de Lorena of Universidade de São Paulo to obtain the degree of Doctoral of Science issued by the Programa de Pós-Graduação em Biotecnologia industrial in the field of Biotecnologia Industrial.

Advisor: Prof. Fernando Segato

Original Version

Lorena

2022

JOSMAN ANDREY VELASCO MENDOZA

Novas LPMOs recombinantes de *Aspergillus fumigatus*: características bioquímicas e sua participação em processos de sacarificação e fotobiocatálise.

Tese apresentada à Escola de Engenharia de Lorena da Universidade de São Paulo para obtenção do título de Doutor em Ciências do Programa de Pós-Graduação de Biotecnologia Industrial na área de concentração de Biotecnologia Industrial.

Orientador: Prof. Fernando Segato

Versão Original

Lorena

2022

Ficha catalográfica elaborada pelo Sistema Automatizado
da Escola de Engenharia de Lorena,
com os dados fornecidos pelo(a) autor(a)

Velasco, Josman
Novel Aspergillus fumigatus recombinant LPMOs: biochemical characteristics, and their participation in saccharification and photobiocatalysis processes. / Josman Velasco; orientador Fernando Segato - Versão Original. - Lorena, 2022.
109 p.

Tese (Doutorado em Ciências - Programa de Pós Graduação em Biotecnologia Industrial na Área de Biotecnologia Industrial) - Escola de Engenharia de Lorena da Universidade de São Paulo. 2022

1. Lpmo. 2. Enzymatic saccharification. 3. Aspergillus fumigatus. 4. Aspergillus nidulans. 5. Photobiocatalysis. I. Título. II. Segato, Fernando, orient.

ACKNOWLEDGEMENTS

I thank God for giving me the opportunity to achieve one of the greatest goals of my academic life, for all the care received and surrounding me with fantastic people who enrich my life.

My deep gratitude to my beautiful wife Patricia Quintero for all the support, for the sacrifices made to allow me to carry out this work and grant the greatest joy of our lives... Matias, beloved son and our greatest motivation.

To my family for always believing in me and filling me with confidence, I especially thank my parents for their prayers.

I thank Brazil, a wonderful country that has given us the opportunity to grow up in all aspects of life and that through its development agencies such as CAPES and FAPESP we receive the resources to sustain and carry out this research and also the Departamento de Biotecnologia da Escola de Engenharia de Lorena da Universidade de São Paulo – EEL/USP.

My special thanks to Prof. Fernando Segato for all the years of guidance for sharing with me the invaluable wealth of knowledge, the best counselor I have ever had, thanks for the trust.

To all members of Symb Lab, my work colleagues for friendship, moments of hard work and fun too. Thank you for your contributions in the completion of this work. To the Programa de Pós-Graduação em Biotecnologia Industrial and all the faculty staff who contributed greatly to my doctoral training.

I want to thank the Instituto de Física de São Carlos, especially Prof. Igor Polikarpov and his team who opened the doors of his laboratory, dedicated time to accompany me in conducting experiments and contribute to the scientific rigor of this work.

To Prof. Leandro Cristante de Oliveira of the Department of Physics of the Universidade Estadual Paulista (UNESP) São José do Rio Preto, for his valuable contributions contained in this work.

I would like to thank all my colleagues at industrial biotechnology department and the technicians José Carlos (*Cobrinha*), José Moreira and Barbara Pereira, thank you very much for your friendship and for your contributions to complete this work.

RESUMO

VELASCO, Josman. **Novas LPMOs recombinantes de *Aspergillus fumigatus*: características bioquímicas e sua participação em processos de sacarificação e fotobiocatálise.** 2022. 109 p. Tese (Doutorado em Ciências) – Escola de Engenharia de Lorena, Universidade de São Paulo, Lorena, 2022.

A partir da descoberta do mecanismo oxidativo que as LPMOs usam para promover a degradação de diversos polímeros na natureza, o interesse tanto do setor acadêmico como industrial nessas enzimas tem aumentado vertiginosamente, permitindo, por sua vez, desenvolvimentos tecnológicos como coquetéis enzimáticos que já são usados em processos industriais de conversão de biomassa lignocelulósica. O presente trabalho descreve LPMOs da família AA9 do fungo *Aspergillus fumigatus var. niveus*, enzimas que até o início dessa tese não haviam sido caracterizadas. Após um acurado estudo utilizando ferramentas de bioinformática das diferentes LPMOs, as enzimas foram expressas heterólogamente no fungo *Aspergillus nidulans* usando técnologia de DNA recombinante. Características físicas e bioquímicas, como estrutura 3D, temperatura ótima, efeito do pH na atividade enzimática, temperatura de *melting* e regiosseletividade são consistentemente descritas para três LPMOs (*Af*AA9A, *Af*AA9B e *Af*AA9C), permitindo conhecer as enzimas para serem aplicadas em processos de bioconversão de biomassa vegetal. A aplicação de *Af*AA9A e *Af*AA9B em processos de sacarificação de bagaço de cana sendo acrescentadas no coquetel comercial *Celluclast* 1.5L, permitiu ver um acréscimo na liberação de açúcar de 20% quando a *Af*AA9B esteve presente na reação e ainda mais interessante, a lignina presente na biomassa foi modificada, produto da ação enzimática de acordo com o observado por microscopia confocal de varredura. Por outro lado, foram conduzidos experimentos de fotobiocatálise usando *Af*AA9C, onde sistemas de clorofilina/luz foram usados como doador de elétrons acoplados ou não com agentes redutores químicos. *Af*AA9C demonstrou a capacidade oxidar polissacáridos sendo ativada pelo foto-sistema e foi descrito um efeito sinérgico entre o sistema de doação de elétrons induzido por luz e os agentes redutores químicos, mostrando inclusive uma aparente mudança na seletividade da enzima pelo doador químico quando acoplado ao foto-sistema. Os resultados obtidos aqui mostram o potencial das LPMOs do *A. fumigatus* para impulsionar os processos de sacarificação e participar em fotobiocatálise, mas também abrem novas perspectivas de estudo quanto as caraterísticas estruturais dessas proteínas, o processo de entrega de elétrons e o tipo de mudanças que são ocasionadas na lignina produto da ação enzimática.

Palavras-chave: LPMO. Sacarificação enzimática. *Aspergillus fumigatus*. *Aspergillus nidulans.* Fotobiocatálise.

ABSTRACT

VELASCO, Josman. **Novel *Aspergillus fumigatus* recombinant LPMOs: biochemical characteristics, and their participation in saccharification and photobiocatalysis processes.** 2022. 109 p. Thesis (Doctoral of Science) – Escola de Engenharia de Lorena, Universidade de São Paulo, Lorena, 2022.

From the discovery of the oxidative mechanism that LPMOs use to promote the degradation of several polymers in nature, the interest of both academic and industrial sectors in these enzymes has drastically increased, allowing the technological developments of enzymatic cocktails that are already used in industrial processes to plant biomass conversion. The present work describes the AA9 family LPMOs from *Aspergillus fumigatus var. niveus*, enzymes that until the beginning of this thesis had not been characterized. After an accurate bioinformatic study, the enzymes were heterologous expressed in the fungus *Aspergillus nidulans* using recombinant DNA technology. Physical and biochemical characteristics such as 3D structure, optimal temperature, pH effect on enzyme activity, melting temperature and regioselectivity are consistently described for the three LPMOs (*Af*AA9A, *Af*AA9B and *Af*AA9C) allowing to know the enzymes to be applied in plant biomass bioconversion processes. The application of *Af*AA9A and *Af*AA9B were added to the Celluclast 1.5L commercial cocktail beind applied in the process of sugarcane bagasse saccharification and allowed an increase in sugar release of 20% when *Af*AA9B was present in the reaction and even more interesting, the lignin present in biomass was modified by the enzymatic action as observed by confocal scanning microscopy. On the other hand, photobiocatalysis experiments were carried out using *Af*AA9C using chlorophyllin/light systems as electron donor coupled or not with chemical reductants. *Af*AA9C showed the ability to oxidize polysaccharides being activated by the photosystem and a synergistic effect between the light-induced electron donor system and chemical reductants to increase enzyme activity was detected. The literature describes LPMOs as enzymes that have a type of selectivity for different chemical donors, the experiments performed in this work allowed to describe for the first time an apparent change in enzyme selectivity by chemical donor when coupled to the photosystem. The results obtained here show the potential of *A. fumigatus* LPMOs to boost the saccharification processes and participate in photobiocatalysis, but also open new perspectives for studying the structural characteristics of these proteins, the electron delivery process and the type of changes that are caused in lignin product by the enzyme action.

Keywords: LPMO. Enzymatic saccharification. *Aspergillus fumigatus*. *Aspergillus nidulans*. Photobiocatalysis.

LIST OF ABBREVIATIONS

AA	Auxiliary activity
***Af*AA9A**	LPMO A AA9 family from *Aspergillus fumigatus*
***Af*AA9B**	LPMO B AA9 family from *Aspergillus fumigatus*
***Af*AA9C**	LPMO C AA9 family from *Aspergillus fumigatus*
***Af*AA9D**	LPMO D AA9 family from *Aspergillus fumigatus*
***Af*AA9E**	LPMO E AA9 family from *Aspergillus fumigatus*
***Af*AA9F**	LPMO F AA9 family from *Aspergillus fumigatus*
***Af*AA9G**	LPMO G AA9 family from *Aspergillus fumigatus*
Arg	Arginine
AscA	Ascorbic acid
Asp	Aspartate
BSA	Bovine serum albumin
CBH	Cellobiohidrolase
CBP21	LPMO AA10 family from *Serratia marcescens*
CBS	Center for Biological Sequence analysis
Cel61A	LPMO AA9 family from *Trichoderma reesei*
CAZy	Carbohydrate Active Enzymes
C1	Carbon 1
C4	Carbon 4
C6	Carbon 6
CtPMO1	LPMO from *Chaetomium thermophilum*
CDH	Cellobiose dehydrogenase
CBM	Carbohydrate-binding module
CBX	Enzyme mixture composed of 92% Celluclast, 6% Novozym 188, 2% *T. reesei xylanases*
DMP	Dimethoxyphenol
DNS	Dinitrosalicylic acid
EGL	Endoglucanase

GAX	Glucuronoarabinoxylan
GH	Glycoside hydrolase
GH61	Glycoside hydrolase family 61
GDH	Glucose dehydrogenase
Glu	Glutamine
His	Histidine
HPAEC-PAD	High Performance Anion-Exchange Chromatography with Pulsed Amperometric Detection
HiPMO1	LPMO from *Humicola insolens*
JGI	Joint Genome Institute
Km	Michaelis-Menten constant
L-cys	L-cysteine
LHW	Liquid hot water
LPMO	Lytic Polysaccharide Monooxygenases
Lys	Lysine
NFC	Nanofibrillated Cellulose
NCBI	National Center for Biotechnology Information
PTM	Post-translational modification
pKa	Acid dissociation constant
pfam	Protein families
PyrA	Pyrogallic acid
SEB	Steam exploded bagasse
Tyr	Tyrosine
Tm	Temperature melting
TaGH61A	LPMO from *Termoascus aurantiacus*

LIST OF FIGURES

LIST OF TABLES

SUMMARY

1 INTRODUCTION

It is a common knowledge that the economic system in the world largely depends on hydrocarbons from petroleum, not only as energy sources, but also as raw material for obtaining many products that nowadays are part of human lifestyle. Although this production system be effective for humanking progress it is threatened by non-renewable nature of fossil resources which has been caused several environmental impacts due the high production of waste (mainly carbon derived) that cannot be recycled (Venkata et al., 2016). Several alternatives are being developed by world governments, researchers and companies in order to change the current linear system into a closed circular system, where the production of waste is extremely reduced. Among the alternatives in circular economy models are the bio based ones, which are economic systems closed related to the efficient use of biomass (Venkata et al., 2016). Plant biomass is the most abundant source of biopolymers on Earth (Bar-On et al., 2018), from this renewable raw material, aromatic compounds and polysaccharides can be extracted to be used directly or converted into its monomers to obtain a wide variety of chemical compounds by fermentation processes (Choi et al., 2015; Peralta-Yahya et al., 2012).

However the emerging bioeconomy based in the utilization of plant biomass still present some challenges like: (*i)* its global availability; *(ii)* its recalcitrant nature, that requires pre-treatments steps to facilitate enzymatic saccharification; *(iii)* the efficiency and yield of the saccharification process and *(iv)* the lack of technology for the industrial scaling of biological processes (Chandel et al., 2018). Thus, the discovery of new enzymes that can be able increase the yield of saccharification promote this type of bioeconomy. Cellulose is the main component of plant biomass, its enzymatic deconstruction needs the action of glycosyl hydrolases (GHs), known as cellulases are classified into three groups: endo-β-1,4-glucanases, exo-β-1,4-glucanases or cellobiohydrolases type I and II and β-glycosidases. Endoglucanases (EGLs) randomly hydrolyze the glycosidic bonds, preferentially along the amorphous portion of cellulose, and may or not be processive. Exo-β-1,4-glucanases or cellobiohydrolases (CBHs) cleave bonds in the cellulose chain from its reducing and non-reducing ends (CBH I and CBH II, respectively), releasing cellobiose as a product. Finally, β-glycosidases break down cellobiose or other cellooligosaccharides generated by the two previous types of cellulases (EGLs and CBHs), releasing glucose molecules as product (Horn et al., 2012).

However, since 2011 has been demonstrated that not only the hydrolytic mechanism system can act in biomass deconstruction (Quinlan et al., 2011). Enzymes with oxidative mechanism working collaboratively with each other and with hydrolases in the decomposition of plant materials including cellulose have come and considered as part of the enzymatic catalytic arsenal for the efficient deconstruction of biomass (Beeson et al., 2015; Meier et al., 2018). Among the enzymes capable of oxidizing polysaccharides promoting the spontaneous cleavage of bonds are the LPMOs (lytic polysaccharide monooxygenase).

The present work shows a consistent study of *Aspergillus fumigatus* LPMOs (*Af*LPMOs) belonging to auxiliary activity family 9 (AA9) from CAZy data base (Carbohydrate Active enZymes), in addition to bioinformatic analyzes for all *Af*LPMOs, the recombinant production of *Af*AA9A, *Af*AA9B, *Af*AA9C is reported using *A. nidulans* strain A773 as expression system and their respective functional characterization. The ability to increase the yields in biomass saccharification, lignin modification and participation in photobiocatalysis processes are some of the main results described here.

2 OBJECTIVES

2.1 General Objective

Produce and functionally characterize three recombinant LPMOs of *A. fumigatus var niveus*, evaluating their participation in saccharification and photobiocatalysis processes

2.2 Specific objectives

- *In silico* studies of *A. fumigatus* AA9 LPMOs to identify its physicochemical and structural characteristics;
- Production of three *A. fumigatus* AA9 LPMOs using *A. nidulans* as heterologous expression system.
- Biochemical characterization of recombinant *Af*LPMOs describing its optimal temperature, regioselectivity, thermostability and the effect of pH on enzyme activity;
- Comparative study of two *Af*LPMOs in the saccharification process of pretreated sugar cane bagasse, describing their interaction with commercial cellulases;
- Description of possible physical modifications in the saccharified sugar cane bagasse as a product of enzymatic action;
- Evaluation of chlorophyllin/light photosystems as electron donor for LPMO activation;
- Study the collaborative effect between chemical reducing agents and light induced electron transfer system for LPMO activation.

3 Outline of this thesis

For a better understanding and reading of the research that is recorded in this thesis, three chapters were elaborated.

Chapter I includes a literature review concerning the main aspects of lytic polysaccharide monooxygenases (LPMOs) such as: families, structure, mechanism, regiospecificity, electron donors and main applications. This chapter offers a background of useful information for a better understanding of the later chapters.

Chapter II shows an *in-silico* study of primary structure and phylogeny for all AA9-LPMOs from *Aspergillus fumigatus*, it also reports the process of cloning and heterologous expression of *Af*AA9A and B LPMOs that were studied comparatively in terms of biochemical and functional characteristics being applied in saccharification processes of pre-treated sugar cane bagasse.

Chapter III describes the heterologous expression, biochemical characterization and structural modeling of *Af*AA9C LPMO. In addition, this chapter shows a consistent and innovative study of light-induced electron transfer for *Af*AA9C, where a collaborative effect between chemical reductants and pigment-light system is described to promote the polysaccharides oxidation mediated by *Af*AA9C.

CHAPTER I

LITERATURE REVIEW

According to CAZy data bank (www.cazy.org), Lytic Polysaccharide Monooxygenases (LPMOs) are distributed in eight families of enzymes with auxiliary activity (AA), from AA9 to AA11 and AA13 to AA17 showing differences in source organisms and in the ability to oxidized different types of substrate. Enzymes with auxiliary activity may or may not have a direct activity on a certain polysaccharide, however they can act in conjunction with classic polysaccharide depolymerases, facilitating the hydrolytic processes. The families AA9 and AA16 group together the LPMOs (mainly from fungal source) active in cellulose and xyloglucan (Filiatrault-Chastel et al., 2019; Isaksen et al., 2014; Zhang, 2020); AA10 is one of most complex family being presented in bacteria, archaea, fungi and viruses being active mainly on chitin and some of them in cellulose (Zhou et al., 2019). The AA11 and AA13 are fungal produced enzymes that can oxidize chitin and/or starch respectively (Hemsworth et al., 2014; Vu and Marletta, 2016). The LPMOs belonging to AA14 family are less studied with only two enzymes characterized. These enzymes are mainly present in genomes of filamentous fungi and its activity has been described in the recalcitrant xylan closely associated with cellulose (Couturier et al., 2018). The AA15 family groups enzymes originated from animals like invertebrates and can be active against cellulose and/or chitin (Sabbadin et al., 2018). The new family AA17 was recently described, being active in pectin and participating as virulence factor in the oomycete *Phytophthora infestans* (Sabbadin et al., 2021).

Eriksson and Pettersson (1974) were the first to report the involvement of oxidative enzymes in cellulose degradation by comparing the action of purified endoglucanases from cellulolytic organisms with the secretome of the same organisms in the degradation of cellulose associated to plant biomass. The authors observed that the secretome under aerobic conditions were able to degrade cellulose twice as much compared to anaerobic conditions, and degradation levels in anaerobiosis were similar to those obtained using only endoglucanases.

In 2010, a Novozymes scientists, in order to improve the commercial cocktail Celluclast 1.5L replaced part of the cocktail with some filamentous fungi extracts, showing a synergistic action of cellulases present in Celluclast 1.5L cocktail (Novozymes®) with GH61 enzymes (currently AA9 CAZy family) present in the secretome of *Thermothielavioides terrestris* (formerly *Thielavia terrestris*). Surprisingly, the GH61 potentiated the degradation of cellulose present in pretreated corn stover, however, this effect was not observed with pure cellulose (Harris et al., 2010). In the same year, the oxidative effect of GH61 and its dependence on a metal ion was reported (Phillips et al., 2011; Vaaje-Kolstad et al., 2010), characteristics that promoted the reclassification of GH61 to the AA9 family and the creation of AA class since 2013 (Levasseur et al., 2013). The LPMOs from AA9 family are the most studied, with 34 enzymes characterized according to CAZy (www.cazy.org), multiple works report its application in plant biomass saccharification showing improvement in process efficiency ranging from 5 to 90% depending on the enzyme, typo of biomass and pre-treatment employed (Zhang, 2020). The action of LPMO on cellulose fiber produces new reducing and non-reducing ends by an oxidative mechanism dependent on an electron donor. In addition, in some cases they can decrease the cellulose crystallinity index, oxidizing crystalline regions and facilitating access for cellulases (Martínez, 2016).

1.1 LPMO structural features

1.1.1 Modular architecture and C-terminal extensions

As other CAZy enzymes, LPMOs can show modular architecture, containing, in addition to the catalytic domain, other domains/modules joined together by structures known as linkers (Courtade et al., 2018; Higasi et al., 2021). Among the common LPMO domains are the carbohydrate-binding modules (CBMs) that favor the attachment/interaction of enzyme with the substrate and also provide protection against the auto-oxidation process (Courtade et al., 2018; Forsberg et al., 2017). Recently, the presence of additional modules (different from CBMs) and C-terminal extensions, of unknown biological activity, has been reported in different LPMO families (Hemsworth et al., 2014; Lenfant et al., 2017; Semenova et al., 2020). Hemsworth *et al.* described the presence of a conserved domain which is additional to the catalytic domain of a LPMO from AA11 family. This module, classified as X278 by the authors contains four conserved cysteine residues and an aromatic amino acid. The presence of this module was detected in several enzymes from AA9 and GH18 families

(Hemsworth et al., 2014). A computational analyzes containing 3,400 protein sequences from AA9 was performed by Lenfant *et al.* allowing the identification of five modules (X278, X280-X283) common in the structure of these enzymes (Lenfant et al., 2017). These modules vary in size, for example X283 can present 6 or 7 residues while X280 modules can have up to 60 amino acids (Figure 1.1).

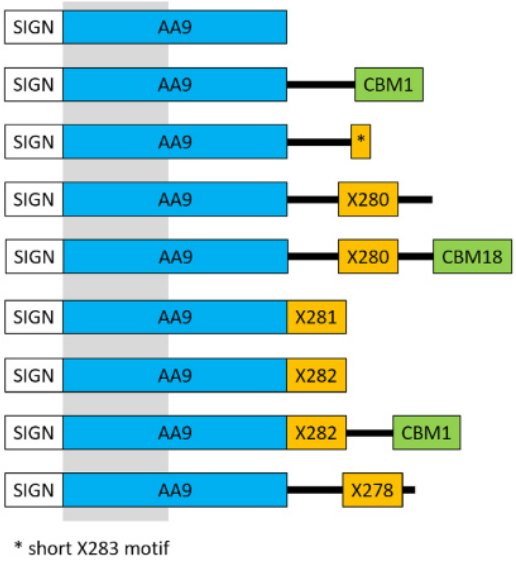

Figure 1.1. Modular architecture that can be present in LPMOs from AA9 family. SIGN: secretion peptide; blue block: catalytic domain; orange block: additional modules; green block: substrate binding modules (CBM) (Lenfant et al., 2017).

In addition to size differences these modules can be differentially located in protein structure, either as a single extra domain (additional to the catalytic domain) or followed by a CBM (Figure 1.1). Another recently described aspect in the architecture of several LPMOs from different families (except AA13 and AA17) is the presence of C-terminal regions. An analysis of 27,060 LPMOs sequences showed that 60% of studied proteins which presented these extra portions vary in length, however its function and folding still are unknown (Tamburrini et al., 2021). In studies carried out by Tamburrini *et al.* showed these predicted terminals were intrinsically disordered regions (IDRs) with differences in its amino acid composition and being described only in LPMOs, so far. The LPMO from the fungus *Penicillium verruculosum* (*Pv*LPMO9A), an enzyme with C-terminal extension was studied in comparison with the same protein without this extra peptide. The analysis showed that the two enzymes had a very similar catalytic behavior such as its optimal pH and temperature values, including the collaborative effect with cellulases, except for the thermostability that

was superior in full-size enzyme (Semenova et al., 2020). This structural feature opens new perspectives in the LPMOs field.

1.1.2 Catalytic domain

Although the different members from LPMOs families show a low similarity between their sequences, all the catalytic domain structures identified so far retain a high degree of similarity (Beeson et al., 2015). The catalytic domain of LPMOs adopts an immunoglobulin-like shape, exhibiting a compact core of beta sheets organized in an antiparallel manner, forming the so-called *β*-sandwich, this core is surrounded and connected by loops that offer flexibility to the structure (Lo Leggio et al., 2018; Span et al., 2017). The loops unite at the end opposite the active site, favoring the conical shape common to these enzymes since the surface near to active site is flat (Figure 1.2). Among the most conserved loops in reported structures are the long C-terminal loop (LC), loop short (LS), L2, L3 and L8, in addition to giving the structure plasticity, some of them are related to substrate recognition as has been reported for the L2, L3 and LC loops (Simmons et al., 2017; Span et al., 2017; Vaaje-kolstad et al., 2017). Some studies point to the LC and LS loops as the coupling structures for cellobiose dehydrogenase (CDH) and they are also the loops with greater mobility (Beeson et al., 2015; Li et al., 2012; Wu et al., 2013).

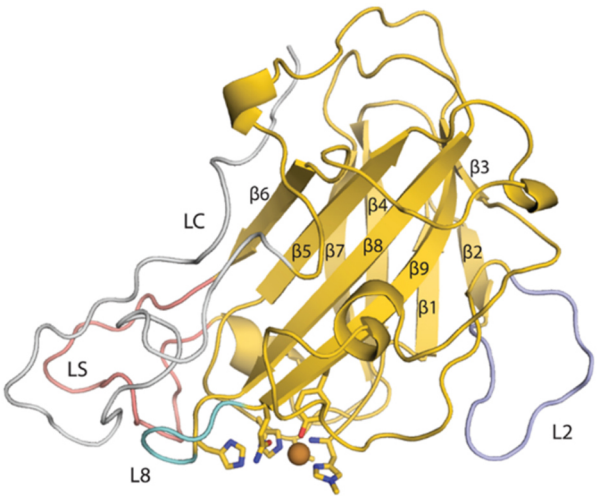

Figure 1.2. Structure of an LPMO from AA9 family obtained by crystallography, beta sheets 1-9 form the *β*-sandwich, the residues that make up the catalytic site in the form of sticks and the copper atom represented by brown sphere. Loop LS pink, LC silver, L8 teal and L2 lavender (Span et al., 2017).

1.1.3 Catalytic site: histidine brace and copper atom

Another highly conserved aspect in all LPMOs families is the so-called histidine brace (His-brace), a structure responsible for coordinating the single copper atom present in catalytic site of these enzymes (Ciano et al., 2018; Quinlan et al., 2011). This structure discovered in 2011 is composed of two histidine residues that fulfill the coordinating function, a first residue located at the N-terminal end of the protein acts as a chelator of the copper atom through amino group and nitrogen atom in π position from imidazole structure, the coordinating function is completed by another nitrogen atom at the τ position of the second histidine residue (whose position in the primary protein structure varies), so the three nitrogen atoms achieve a "T-shaped" geometry to coordinate the copper atom (Figure 1.3) (Ciano et al., 2018; Li et al., 2012; Petrovic et al., 2018).

Although this coordinating system is scientifically proven, some works suggest that the coordination can also be aided by a tyrosine residue in addition to histidines, Leggio *et al* through structural studies reported the tyrosine residue participation in endogenous coordination of copper atom to a LPMO from AA13 family, which has also been reported for LPMOs from AA9, AA10 and AA11 families, thus forming the so-called coordination sphere (Hemsworth et al., 2014, 2013; Lo Leggio et al., 2015; Quinlan et al., 2011). A particular feature of fungal LPMOs is the methylation of N-terminal histidine residue, a post-translational modification (PTM) capable of being performed by filamentous fungi but absent in bacteria. The ability to perform PTMs is a favorable characteristic for chassis organisms used in heterologous expression of LPMOs such as filamentous fungi. LPMOs from filamentous fungi, when heterologously produced in yeasts, do not show methylation due to the absence of methyltransferase (Lo Leggio et al., 2015; Petrovic et al., 2018; Quinlan et al., 2011).

The biological function of this methylation is still unclear but some evidence suggests that methylated histidines have a higher *pKa* value than unmethylated histidines, high *pKa* values increase the affinity for metal ions which favors the presence of copper at active site (Aachmann et al., 2012). However, in a comparative study between two variants of the same LPMO (TaLPMO9A), one with, and one without methylation, it was reported that the presence of this modification had a minimal effect on His-1 *pKa* and its copper affinity, but gave a greater resistance against autoxidation (Petrovic et al., 2018).

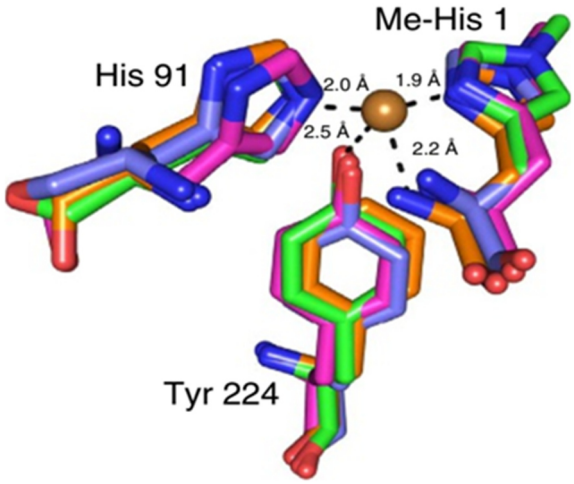

Figure 1.3. LPMOs active site comparison, AA9 (magenta-PDB: 3ZUD), AA10 (Orange-PDB: 2YOY), AA11 (purple-PDB: 4MAI) and AA13 (green-PDB: 4OPB). His: histidine, Tyr: tyrosine, Me-His 1: methylated histidine, dotted line: distance (in angstroms), brown sphere: copper atom (Lo Leggio et al., 2015).

Although the histidine brace is a highly conserved structure, intriguingly, some LPMOs from AA9 family show exceptionally a substitution of histidine (in N-terminal region) for arginine, being called Arg-AA9 (Frandsen et al., 2019). Phylogenetic analyzes have shown presence of these AA9s almost strictly in wood-decomposing fungi from Agaricomycetes class, genes encoding Arg-AA9 in fungi such as *Heterobasidion irregulare*, *Pycnoporus coccineus* and *Polyporus brumalis* have been regulated in lignocellulosic biomass presence (Frandsen et al., 2019; Miyauchi et al., 2018). Structural studies of an Arg-AA9 from *Lentinus similis* fungi showed copper atom absence, inability to chelate metal ions at active site and protein phosphorylation close to the N-terminal arginine. Although the role of these enzymes in biomass degradation is not clear yet, it is possible to assume that they possess a different mechanism than canonical AA9 LPMOs (Frandsen et al., 2019).

The copper atom presence at active site is crucial for LPMO activity, since the initial step in catalytic cycle involves the copper reduction by an external reducing agent, then reduced copper reacts with oxygen to form species with high oxidative power that will remove hydrogen atom from substrate (Aachmann et al., 2012; Beeson et al., 2012; Chaplin et al., 2016). Cooper also provides structural stability to protein, some studies show that Cu^{2+} presence increases protein melting temperature, reaching increases of up to 20 °C (Hemsworth et al., 2013). Again, organisms capable of performing PTMs are desirable to produce LPMOs in their active form, populations of LPMOs can vary in terms of copper content, when bacterial organisms are employed as a chassis for heterologous LPMO

production the apo-enzyme form prevails (Chaplin et al., 2016). Even so, the high affinity that these enzymes have for copper allows that act as copper scavenger agents if it is available in the solution, saturation methods where an apo-enzymes population is arranged in solutions with high copper content have been shown to be effective in increasing the population of metalloenzymes (Loose et al., 2014). When copper saturation processes are used, it is essential to remove all the copper that was not sequestered by LPMOs, since copper under aerobic conditions and in chemical reductant presence (as ascorbic acid) can produce H_2O_2, a molecule with a strong impact on catalytic performance of LPMOs (Hegnar et al., 2019).

1.2 Polysaccharide oxidation: possible catalytic pathways

After more than a decade of studies and a prolific production of LPMOs literature, it has not been possible to accurately describe the mechanism that these enzymes use for polysaccharides oxidation; aspects such as the ideal co-substrate (O_2 or H_2O_2), how the co-substrate activation is coupled to substrate binding and whether Cu(II) reduction or polysaccharide binding happens first are not clear (Wang et al., 2020). Below is a brief overview about mechanistic studies and recent advances that seek to resolve these questions.

1.2.1 Oxidation mechanism using molecular oxygen

The first reports on the LPMO mechanism showed that enzymatic oxidation of polysaccharides did not occur under anaerobic conditions, and through isotope labeling it was revealed that molecular oxygen was the source of oxygen atoms that were incorporated into the solubilized product after enzymatic action. In fact, when the reactions were carried out in cyanide presence, the catalysis was inhibited, however this effect was not observed in catalase or superoxide dismutase presence, reinforcing the hypothesis that the interaction between O_2 and enzyme active site was a critical step in the catalytic process (Vaaje-kolstad et al., 2010). Later structural studies in different LPMOs from *Neurospora crassa* showed the binding of dioxygen species at copper atom (Li et al., 2012; O`Dell et al., 2017), these observations led to conclude that O_2 is directly used by LPMOs to oxidize polysaccharides as shown in equation 1.

$$O_2 + 2e + 2H^+ + R\text{-}H \rightarrow R\text{-}OH + H_2O \quad (1)$$

The cupric ion (Cu^{+2}) is reduced to cuprous ion (Cu^{+}) in electron donor presence, which leads to the subsequent activation of dioxygen intermediate, forming highly reactive copper-oxygen species (Walton and Davies, 2016). Thus, the alternation between the redox states Cu^{+2} and Cu^{+}, in addition to the formation of afore mentioned intermediates during reaction process, involves the abstraction of a hydrogen atom attached to a carbon adjacent to glycosidic bond in polysaccharide chains. Although this proposed mechanism is supported by strong scientific evidence, there are still some uncertainties such as the "timing" from proton and electron transfer and whether the Cu-superoxide or Cu-oxyl complex is responsible for hydrogen abstraction (Beeson et al., 2012; Phillips et al., 2011).

1.2.2 Oxidation mechanism using hydrogen peroxide

Bissaro *et al*. (2017) declare that hydrogen peroxide is the oxidant directly used by LPMOs. These statements are also supported by strong scientific evidence such as: (*i*) increase of LPMOs activity in the presence of moderate levels of H_2O_2 that can be generated *in situ* or added externally, (*ii*) product formation with periodic addition of H_2O_2 under anaerobic conditions coincided with the formation of product in dioxygen presence, (*iii*) using isotope labeling it was shown that the oxygen atoms incorporated into the product by enzymatic action were supplied by H_2O_2 even in O_2 presence, (*iv*) under catalysis conditions using only O_2 as oxidant, horseradish peroxidase addition inhibited the enzymatic activity, although this inhibition is an opposite result to that reported by (Vaaje-Kolstad et al., 2010) using catalase, it was argued that the low *Km* values of peroxidase (compared to catalase) allows for more effective competition with LPMOs for available H_2O_2. Thus, the mechanism that contemplates the use of H_2O_2 as an oxidant is summarized in the equation 2.

$$H_2O_2 + e^- + R\text{-}H \rightarrow R\text{-}OH + H_2O \quad (2)$$

After the "priming" reduction ($Cu^{+2} \rightarrow Cu^{+}$) –LPMO, enzyme in substrate presence reacts with H_2O_2 causing the homolytic breakdown of peroxide with the protonation of distal oxygen to release water and form Cu-oxyl, this complex would remove the hydrogen atom from substrate to form Cu–OH and a substrate radical, the union of Cu-OH complex with substrate radical would produce the final hydroxylation of polymer and regenerating the Cu^{+} for a new catalytic cycle (Bissaro et al., 2017; Meier et al., 2018).

The fact of LPMOs show the ability to produce H_2O_2 (previously activated by a reductant) in the presence of oxygen (Kittl et al., 2012), promotes the debate about which is the oxidizing agent used by these enzymes for substrate hydroxylation. At the same time that the H_2O_2 produced can boost the LPMO activity, its accumulation results in damage to the enzyme by autooxidation. This double effect is known as "futile" cycle and resistance to autoxidation is therefore a desirable characteristic in the prospected LPMOs (Bissaro et al., 2017; Blossom et al., 2020).

1.2.3 Oxygen and hydrogen peroxide pathways connection

Recently, experimental and theoretical studies have expanded the knowledge frontiers about the chemistry of LPMO describing that the mechanism pathways for both O_2 and H_2O_2 may be connected by a common intermediate Cu(I)-H_2O_2 (Wang et al., 2019). In H_2O_2-dependent pathway the Cu(I)-H_2O_2 formation occurs by the interaction between reduced copper and hydrogen peroxide present in the reaction (Figure 1.4)

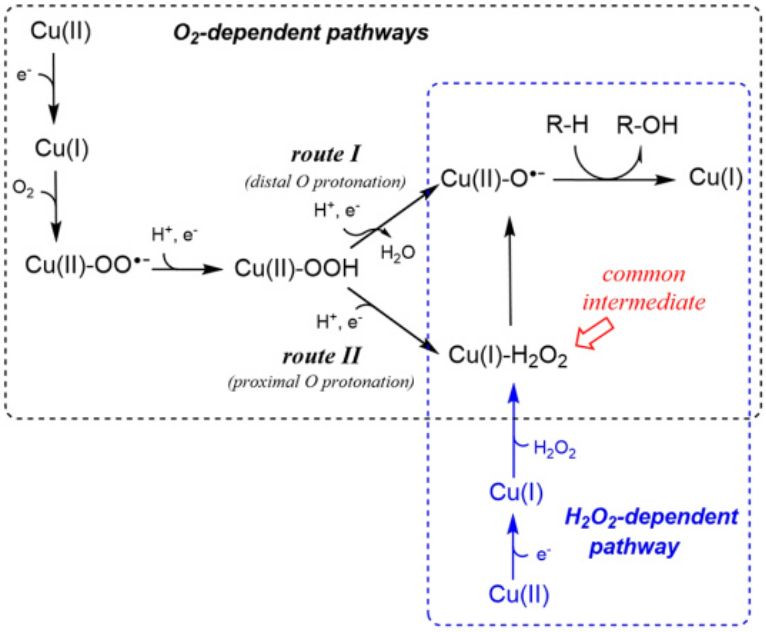

Figure 1.4. Possible LPMOs catalytic mechanism for polysaccharide oxidation by O_2- and H_2O_2-dependent pathways (Wang et al., 2020).

In O_2-dependent pathway after the "priming" reduction and subsequent activation of O_2 the Cu(II)-$OO^{\bullet-}$ is formed. Then, this compound is converted into Cu(II)-OOH by an electron and proton transfer (process apparently regulated by the reducing agent). At this

point, the formation of Cu(I)-H_2O_2 may occur as product of protonation of the proximal oxygen from Cu(II)-OOH (Wang et al., 2020, 2019), as shown in figure 1.4. In the absence of polysaccharide as substrate, Cu(I)-H_2O_2 dissociates leaving the enzyme free and H_2O_2 in solution. This explain the formation of H_2O_2 in LPMO + O_2 + reducing agent reactions (Kittl et al., 2012).

1.3 LPMO regioselectivity and product profile

The oxidation of polysaccharides mediated by LPMOs generates a diversity of oxidized and non-oxidized products as consequence of the chemical selectivity that LPMOs present to execute the hydroxylation in the C1-H or C4-H bonds (or both), adjacent to the glycosidic bond. Enzymes that perform the hydrogen atom abstraction at carbon 1 with subsequent glycosidic bond cleavage produces oligosaccharides with lactone at the reducing end, which is subsequently hydrated and converted to aldonic acid (Beeson et al., 2012; Vu et al., 2014). LPMOs that act preferentially at carbon 4 generate chains with ketoaldoses at non-reducing end (Figure1.5) (Isaksen et al., 2014). A mixture of the products mentioned above and non-oxidized oligosaccharides can be found in reactions catalyzed by LPMOs that act in both C1 and C4. The random action of LPMO in the oxidative process along the polysaccharide chain favors the release of native oligosaccharides (not oxidized) with different degree of polymerization (DP), which are part product profile of the enzyme. It has been shown that LPMOs are able to oxidize soluble cellulose oligomers, promoting bond breaking and concomitant decrease in the DP (Isaksen et al., 2014). Isaksen *et al.* (2014) reported how a C4 oxidizing LPMO, in addition to its activity against cellulose showed the ability to oxidize cellooligosaccharides, being the activity apparently influenced by amino acids that participate in substrate recognition which are close to active site at the flat surface of the protein.

Since the oxidation of C1 and C4 promote the breaking of glycosidic bond boosting the polyssaccharide deconstruction, regioselectivity has become a classification parameter used in studies of biochemical characterization in LPMOs, however, these enzymes can also promote the oxidation at carbon 6 from glucose molecules that do not participate in the glycosidic bonding (Bey et al., 2012; Chen et al., 2018; Quinlan et al., 2011). In initial studies regarding the characterization of LPMOs products, the enzyme potential to oxidize in C6 was already suspected, but similarity molecular weight between C4 and C6 oxidized products did not allowed to confirm the proposed model (Bey et al., 2012; Quinlan et al.,

2011; Vu et al., 2014). Despite of that, Chen *et al.* (2018) reported the C6 oxidation from glucose molecule in cellulose chain by a C1/C4 oxidizing LPMO from the fungus *Chaetomium thermophilum* (*Ct*PMO1) . Mechanism that also had been suggested to LPMOs from *Thermoascus aurantiacus* (GH61A), *Podospora anserina* (GH61B) and confirmed for *Humicola insolens* (*Hi*PMO1) (Bey et al., 2012; Chen et al., 2019; Quinlan et al., 2011).

The biological role from C6 oxidation (generating C6-hexodyaldoses) in cellulose degradation is still unclear since this oxidation does not intervenes in glycosidic bond cleavage, but considering the organized structure of the crystalline portion from cellulose polymer, it is possible to suppose that C6-oxidation can modify the fiber morphology. How?...the free hydroxyls on cellulose surface chain form intra- and intermolecular hydrogen bonds, arranged at specific angles that favor the fiber organization and crystallinity (Chen et al., 2018). One third of free hydroxyls available in cellulose chain are provided by carbon six from glucose molecule, the insertion of an oxygen atom in C6 mediated by LPMOs will alter the strict organization from hydrogen bonds network (Figure 1.5). If these alterations decrease the cellulose crystallinity, it would facilitate the access of LPMOs and hydrolytic enzymes, promoting the deconstruction process.

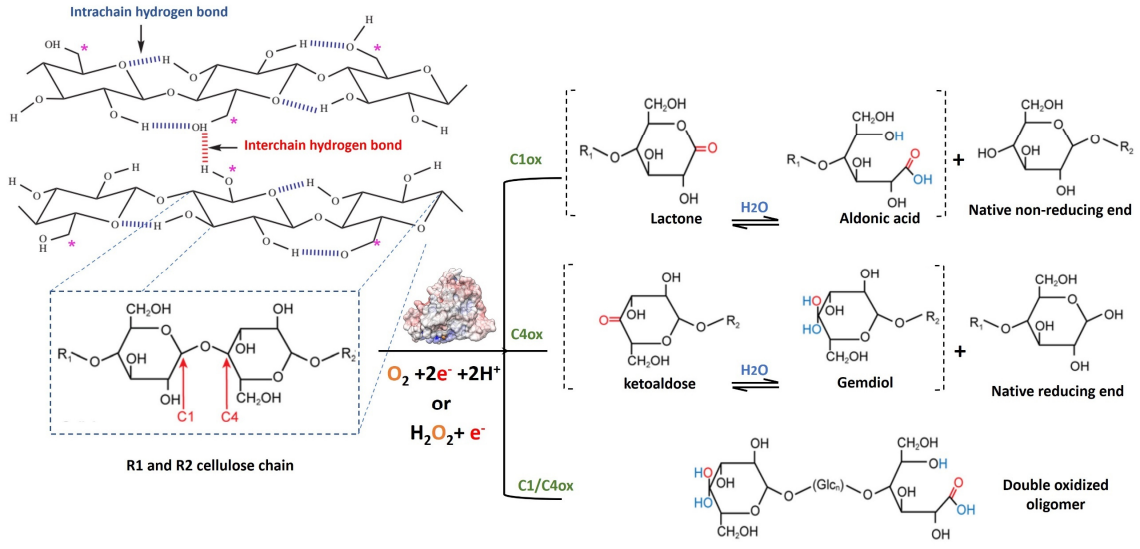

Figure 1.5. Profile of products generated by the regiospecific attack of LPMOs on cellulose structure. Purple star: carbon 6 susceptible to attack LPMO. C1ox, C4ox and C1/C4 ox: oxidative attack at carbon 1, carbon 4 and C1/C4 carbons respectively.

It has also been proposed that cellooligosaccharides containing glucuronic acid (C6-oxidized products) can be further hydrolyzed by *β*-glucuronidases and *β*-glucosidases to produce glucose, glucuronic and saccharic acids, molecules of biological, physiological and

ecological importance to microorganisms (Chen et al., 2019). The reason for the existence of LPMOs showing different regioselectivity is not clear yet, however, it is possible to hypothesize that this selectivity is product of the mode as the enzymes bind to the substrate, indicating that LPMOs can present different binding mechanisms to exposed the surface of the cellulose chain (Vaaje-kolstad et al., 2017; Vu et al., 2014). In addition, considering the resistance that cellulose structure opposes to enzymatic attack due to its conformation, shape and compactness, the hydroxylation of different carbons may be product of an evolutionary strategy of LPMOs to overcome such resistance (Frommhagen et al., 2018a).

As already mentioned, each LPMO family attacks a certain types of polysaccharide (cellulose, chitin, starch, hemicellulose and pectin) with some members that exhibit the ability to oxidize different substrates, like for example, some AA10 and AA15 members that oxidize cellulose and chitin (Forsberg et al., 2017; Sabbadin et al., 2018) and AA9 that oxidize cellulose and xyloglucan (Monclaro et al., 2020; Sun et al., 2020). The large variability in amino acids composition present at the flat surface close to active site and the flexibility provided by structural loops allow the same enzyme to interact and attack substrates with different topologies (Vaaje-kolstad et al., 2017). However, the ability to hydroxylate C1, C4 or C1/C4 has been demonstrated only for members from AA9 family, hitherto none AA10 that hydroxylates only C4 has been reported, in contrast to the only AA17 described so far that predominantly act in C4 from homogalacturonan chain, the other families (AA11, AA13, AA14, AA15 and AA16) had been described as C1-oxidizing (Couturier et al., 2018; Frommhagen et al., 2018a; Sabbadin et al., 2021, 2018; Vu and Marletta, 2016).

In the specific case of AA9 LPMOs, the product profile can also be influenced by the type of cellulosic substrate (Sun et al., 2021). Sun *et al.* (2021) studied the effect of oxidation of different celluloses (bacterial cellulose, regenerated amorphous cellulose and Avicel) mediated by AA9 LPMOs. The authors found that using bacterial cellulose, LPMOs produced mainly cellobionic acid, while with the other substrates oxidized cellooligosaccharides showing different DP were produced, elucidating the idea that the product profile from this enzyme family may be cellulose specificity. It has even been described that the presence of a CBM can interfere in the product profile. As example, the *Sc*LPMO10C a AA10 LPMO carrying a CBM was able to generate shorter oxidized products compared to truncated enzyme (CBM and link removed), however, the same behavior was not detected in the native oligosaccharides produced (Courtade et al., 2018).

1.4 Electron donors

To the oxidation process LPMOs demand electrons from an external supplier for copper atom reduction, a process commonly known as “priming” activation. Until now, a plethora of compounds (enzymatic and non-enzymatic) and systems acting as electron donors for LPMOs have been described (Cannella et al., 2016; Frommhagen et al., 2018a, 2016; Kracher et al., 2016; Westereng et al., 2015), even showing that LPMO can have a type of selectivity towards a certain donor (Frommhagen et al., 2016, 2018a). However, the process to deliver electrons to LPMOs is complex, being affected by factors such as: redox potential (both, enzyme and the donor), temperature, pH, donor and receptor stability and formation of H_2O_2 and other reactive oxygen species that are part of oxidation-reduction process.

The literature shows some works describing the interaction of different electron donors with LPMOs and summarize the types of reductants already described (Frommhagen et al., 2018a; Kracher et al., 2016). For example, Frommhagen *et al.* grouped the reductants into 4 systems depending on: directly or indirectly occurrence of electron transfer, if the donor (enzyme in this case) altered the levels of H_2O_2 or super oxide or whether the system is induced by light. In this review the reducing agents were categorized into 3 groups depending on whether electrons delivery is mediated by enzymes, light or non-enzymatic compounds.

1.4.1 Non-enzymatic electron donors

LPMO reactions can be fueled by low molecular weight compounds such as ascorbic acid, gallic acid, DTT (1,4-dithiothreitol), L-cysteine, reduced glutathione, and in general, phenolic compounds comprising structural features like the 1,2-dihydroxy, 1,2-dihydroxy-6-methoxy, and 1,2,3- trihydroxy moiety (Bissaro et al., 2017; Frommhagen et al., 2016; Kracher et al., 2016; Vaaje-kolstad et al., 2010). These phenolic compounds can be from fungal or plant origin, such as lignin derivatives with different molecular masses (Westereng et al., 2015). Experimentally, the efficiency of a specific compound to reduce LPMO could be determined in reduction potential values, although some studies show that molecules with low reduction potential levels ($\leq$ 250 mV) can cause a better catalytic performance of the enzyme and the electrons transfer also will be dependent of the reduction potential of the enzyme itself as well as the incubation conditions (Frommhagen et al., 2018a; Kracher et al., 2016). Perhaps, the pH value in the incubation conditions is the variable that presents high incidence in the enzyme reduction process. Some authors state that a harsh decrease in pH

values can promote the protonation of the imidazole ring from histidine, affecting the copper atom coordination (Frandsen et al., 2017). On the other hand, it has been shown that alkaline environments favor the H_2O_2 production by some reductants as ascorbic acid and 2,3-dihydroxybenzoic acid (2,3-DHBA) (Hegnar et al., 2019; Stepnov et al., 2021), exerting a ″concomitant effect″ on the catalytic performance of LPMOs both by electron delivery and H_2O_2 generation.

Lignin of different molecular weights and lignin building blocks have been described as efficient reductants for LPMOs, being characterized as the donors (non-enzymatic) with large availability in natural environments where the secretion of LPMOs occurs. Westereng *et al.* suggested that lignin molecules of different sizes can interact with each other generating oxidation-reduction cycles for continuous LPMO activation (Westereng et al., 2015). The electron donor regeneration promotes the reaction sustainability and compounds such as benzoquinones, after delivering electrons to the LPMO can be regenerated by other oxidoreductases, generating a continuous electron donation system.

1.4.2 Enzyme-mediated electron donation

In nature, an arsenal of enzymes acts together for an efficient biomass degradation. Initially, only hydrolytic interactions were thought of, but with the LPMO emergence, it was understood that the process of plant cell wall deconstruction requires the synergic action of enzymes with both hydrolytic and oxidative mechanisms. Nowadays, it's possible to verify that the degradation of lignocellulosic material occurs under conditions of oxidative regulation, in which oxidoreductases act by donating electrons to LPMO regenerating reducing molecules and modifying natural phenolic compounds converting them into efficient electron donors. Enzymes that directly reduce LPMOs or that release/modify reducing compounds are presented below.

1.4.2.1 Direct electron transfer to LPMO

Members from GMC (Glucose-Methanol-Choline) superfamily are found in this group, being cellobiose dehydrogenase (CDH) the most used redox partner in the enzymatic reduction of LPMO studies (Kracher et al., 2016; Phillips et al., 2011; Sygmund et al., 2012). CDH, is a flavoprotein containing a *heme* domain and FAD-cofactor, expressed and secreted only by some fungi (Phillips et al., 2011). CDHs catalyze the oxidation of cellobiose, long

cellodextrins, and other oligosaccharides, resulting in FAD reduction to $FADH_2$ with subsequent electron transfer to *heme* domain, which reduces the copper present in the active site of LPMO (Sygmund et al., 2012). In fungi that are capable of secrete LPMOs and cellobiohydrolases, the presence of CDH is highly conserved. More than 98% of fungi with at least three genes encoding LPMOs also contain CDH-genes in their genomes. In fungal genomes without LPMO the absence of CDH always prevails. *Trichoderma reesei* is apparently an exception due to the inability to produce CDH even though it produces LPMOs (Beeson et al., 2015; Kracher et al., 2016), but CDH absence can be replaced by other enzymes that can also donate electrons to LPMO. A recent study describing new members and characteristics of AA7 family showed the ability of *Fg*CelDH7C (cellooligosaccharide dehydrogenase from *Fusarium graminearum*) to transfer electrons directly from its FAD-cofactor to LPMOs showing a similar performance compared to CDHs (Momeni et al., 2021). Enzymes like aryl-alcohol oxidase (AAO), aryl-alcohol quinone oxidoreductases (AAQO), glucose oxidase (GOx), glucose dehydrogenase (GDH), pyranose dehydrogenase (PDH), from GMC superfamily can also reduce LPMOs or regenerate phenolic compounds (Garajova et al., 2016; Kracher et al., 2016).

1.4.2.2 Production, modification and regeneration of reducing agents mediated by enzymes

After a phenolic compound or quinone deliver electrons to LPMO the compound must be reduced (regenerated) to keep the LPMO activation process. GMC oxidoreductases have been shown as efficient enzymes in regenerating phenolic compounds derived from fungi and plants, thus forming continuous LPMO reduction systems in nature (Kracher et al., 2016). The occurrence of genes encoding GMC oxidoreductases is high in the genomes of biomass-degrading fungi, and when these microorganisms are cultivated in conditions using sole lignocellulosic materials as carbon source, the co-secretion of LPMOs and GMC oxidoreductases is induced indicating the combined participation of these enzymes in biomass degradation (Garajova et al., 2016; Miao et al., 2015).

On the other hand, enzymes with mono- and diphenolase activity are able to modify phenolic compounds making them available to participate in LPMO reduction processes. Frommhagem *et al.* (2017) reported how a polyphenol oxidase from *M. thermophila* (*Mt*PPO7) converted methoxylated phenolic compounds into 1,2-hydroxylated compounds fueling the LPMO activity. The analysis also showed a positive correlation between the

occurrence of PPOs- and LPMO-encoding genes in ascomycetes and basidiomycetes. It is presumed that many other enzymes that modify or release phenolic compounds from plant cell wall such as manganese peroxidases (MnPs), lignin peroxidases (LiPs), versatile peroxidases (VPs), as well as, laccases and ferulic acid esterases can influence the electrons delivery to LPMOs by regulating the availability of non-enzymatic reducing agents (Frommhagen et al., 2018a).

1.4.3 Light-induced electron donors

Simultaneous works carried out by Bissaro *et al* (2016) and Cannella *et al* (2016) described efficient organic and inorganic electron transfer systems induced by light. Bissaro *et al.* (2016) reported the reduction of LPMO through light-driven water oxidation, using vanadium-doped titanium dioxide (V-TiO2) as chemical photocatalyst. In studies developed by Cannella *et al.* (2016) a LPMO from *T. terrestris* was activated in presence of the chlorophyllin/light/ascorbic acid system presenting an increase of up to 100-fold in the catalytic activity of the enzyme. A later study performed by Bissaro *et al.* (2020) showed that LPMOs can be activated using only chlorophyllin/light without the addition of a chemical reductant and the increase in enzyme activity could be proportional to the light intensity employed. Although the light activation mechanism not be completely understood, Bissaro *et al.* (2020) attribute this activation to the formation of superoxide ($O_2^{\bullet-}$) which is later transformed to H_2O_2. Thus, the $O_2^{\bullet-}$ formation may have a "concomitant effect" in the catalytic performance of LPMO acting as electron donor and forming H_2O_2 . Systems added by pigments that capture light (from a natural source or not) causing the electronic excitation that favors the electrons delivery to LPMOs open new possibilities for photobiocatalysis processes applied in plant biomass conversion. Although challenges such as the design of photobioreactors, the optical density of material, cost, among others, must be carefully analyzed (Blossom et al., 2020)

1.5 Applications and new perspectives

Despite the LPMOs mechanism of action is not yet fully understood in addition to some aspects involving LPMOs that still are enigmatic, these enzymes have achieved a leading role in the biotechnology industry for plant biomass saccharification. Due to its ability to

potentiate the processes in synergism with cellulases strong investments have been made by governments (such as the US Department of Energy) and private sector (Novozymes) to include these enzymes in bioconversion processes (Harris et al., 2014; Johansen, 2016). Currently, these enzymes are part of the latest generation enzymatic cocktails used in saccharification of lignocellulosic materials (Harris et al., 2014; Johansen, 2016; Rodríguez-Zúñiga et al., 2015). The addition of LPMO in these cocktails derives from advantageous aspects as: (*i*) increases the saccharification yields: there are many studies demonstrating an increase in saccharification of lignocellulosic material from different sources and using different LPMOs showing at least an improvement of 30% (Zhang, 2020); (*ii*) versatility, different substrates and pre-treatments: the boosting effect of LPMO has been noticed in many industrially relevant substrates showing different composition and subjected to different pretreatments such as corn stover (Harris et al., 2010), wheat (Cannella and Jørgensen, 2014), poplar (Hu et al., 2015), spruce (Dimarogona et al., 2012), soybean residues (Pierce et al., 2017), sorghum straw (Jagadeeswaran et al., 2016) and sugarcane bagasse (Rodríguez-Zúñiga et al., 2015). Previously, it was thought that a complete removal of lignin was desirable in enzymatic saccharification processes, but after insertion of LPMOs changed this scenario, since residual lignin in the material can activate the LPMOs, avoiding the use of external reductants (Hu et al., 2014; Monclaro and Filho, 2017).

Another field that has been exploring LPMOs is nanofibrillated cellulose (NFC) production, Moreau *et al.* (2019) found that treatment of birchwood by LPMO weakened the cellulose fibers cohesion keeping the cellulose crystallinity, showing this step prior to mechanical treatment favored the NFC production. In addition LPMOs can be used for cellulose functionalization (Magri et al., 2021) and, as mentioned above, in plant biomass photobioconversion processes (Blossom et al., 2020). Although, most of LPMOs studies are focused on natural polymers deconstruction, an emerging field of study/application for these enzymes is related to their role in plant pathogenesis and in mutualistic/commensalism symbiosis (Vandhana et al., 2022; Zarattini et al., 2021). Zaratini *et al.* (2021)described that *Arabidopsis* exposure to cellooligosaccharides (COS) or cellulose derivatives generated by an AA9 LPMO from *T. terrestris* stimulated a type of immune response by the plant, even in plants previously treated with AA9_COS the propagation of the plant pathogen *Botrytis cinerea* was inhibited. On the other hand, genomic and transcriptomic studies of *Laccaria bicolor* (a mycorrhizal-forming fungus) showed that AA9 LPMOs expression was stimulated during the establishment of fungal-plant symbiotic relationship, suggesting that

these enzymes may participate in soft plant cell wall remodeling (through cellulose microfibrils loosening) to fungal colonize epidermal root cell (Veneault-Fourrey et al., 2014).

Undoubtedly, LPMOs are important mediators kingdoms interactions in nature and understanding their role in such interactions will allow the construction of knowledge that promotes the technological development of humanity.

CHAPTER II

Comparative analysis of two recombinant LPMOs from *Aspergillus fumigatus* and their effects on sugarcane bagasse saccharification

Based on: Velasco, J., de Oliveira Arnoldi Pellegrini, V., Sepulchro, A.G.V., Kadowaki, M.A.S., Santo, M.C.E., Polikarpov, I., Segato, F., 2021. Comparative analysis of two recombinant LPMOs from *Aspergillus fumigatus* and their effects on sugarcane bagasse saccharification. Enzyme Microb. Technol. 144, 109746. https://doi.org/10.1016/j.enzmictec.2021.109746

2.1 Abstract

Lytic polysaccharide monooxygenases (LPMOs) have been introduced into industrial cocktails used for biomass saccharification due to their capacity to boost enzymatic conversion of recalcitrant cellulose. The genome of the thermotolerant ascomycete *Aspergillus fumigatus* encodes 7 genes for LPMOs that belong to auxiliary activity family 9 (AA9). Here, we cloned, successfully expressed and performed biochemical evaluation of two CBM-less *A. fumigatus* LPMOs (*Af*AA9A and *Af*AA9B). A high-performance anion-exchange chromatography with pulsed amperometric detection (HPAEC-PAD) analysis demonstrated that *Af*AA9A and *Af*AA9B are able to oxide cellulose at C1 and C1/C4 positions, respectively. Synergic effect of LPMOs (separately and in combination) with cellulases were investigated. Supplementation of Celluclast 1.5L with a low concentration of *Af*AA9B improved in 20% the saccharification of sugarcane bagasse pretreated by steam explosion (SEB), while *Af*AA9A did not improved the saccharification. Analysis of the hydrolyzed biomass by confocal laser scanning microscopy (CLSM) showed the LPMOs are promoting lignin oxidation in the lignocellulosic material. This study complements the available results concerning the utilization of LPMOs in the enzymatic saccharification of lignocellulosic biomass.

Keywords: lytic polysaccharide monooxygenases, LPMOs, *Aspergillus*, Cazymes, thermophiles, sugarcane bagasse, enzymatic saccharification

2.2 Introduction

An efficient and sustainable alternative to replace technologies for the production of chemical compounds and fuels based on non-renewable resources relies on the obtaining the precursors from the bioconversion of lignocellulosic biomass. However, even after physicochemical pretreatments recalcitrance of the plant cell walls poses a significant challenge for the enzymatic deconstruction of the plant polysaccharides which remains an obstacle in the development of renewable technologies based on plant biomass (Himmel et al., 2007; Ragauskas et al., 2006). Therefore, to make the process of enzymatic saccharification of plant biomass economically viable it is necessary to use a range of enzymes that acts synergistically in the depolymerization of this complex material (Himmel et al., 2007).

Among the enzyme classes that are capable of acting on lignocellulosic biomass are lytic polysaccharide monooxygenases (LPMOs), copper-based enzymes that act by oxidizing the surfaces of insoluble polymeric substrates, leading to an improved accessibility of hydrolases to the most recalcitrant parts of the substrates (Chylenski et al., 2019; Harris et al., 2014; Hemsworth et al., 2015). The role of oxidative process in cellulose degradation was described as early as 1970's, but remained unexplored until 2010 when LPMO's activity was identified (Bissaro et al., 2017; Eriksson and Pettersson, 1974; Quinlan et al., 2011; Vaaje-Kolstad et al., 2010). Since then, a series of studies has been performed to elucidate the mechanisms of action of this enzyme class in the context of biomass bioprocessing optimization (Cannella and Jørgensen, 2014; Horn et al., 2012; Rodríguez-zúñiga et al., 2015). *Aspergillus* species present many copies of genes encoding LPMOs from different auxiliary activity families (AA). Regarding to AA9 LPMOs, *A. niger* and *A. oryzae* which are two industrially relevant strains have 7 and 8 LPMO genes in their genomes, while other economical important strains such as *A. nidulans*, *A. flavus*, *A. terreus* and *A. fumigatus* have 9, 7, 12 and 7 genes encoding LPMOs in its genomes, respectively (Sugui et al., 2015; Vries et al., 2017). In this study we compared biochemical properties of two auxiliary activity family 9 (AA9) LPMOs from *A. fumigatus* var. *niveus* (*Af*AA9A and *Af*AA9B), a saprophytic and thermotolerant fungus (optimal growth 37 °C, good growth between 30 and 45 °C, maximal growth at 52 °C), that plays an essential role in the recycling of environmental carbon and nitrogen due to the capacity to grow up in various niches including soils, dead matter and animals (Couger et al., 2018; Latgé, 1999; Vries et al., 2017). Both

genes were successfully cloned by Gibson Assembly® method, which allows the *in vitro* recombination of DNA fragments containing small overlapping sequences (between 15 to 30 bp) in an isothermal reaction and expressed in *A. nidulans* (Gibson et al., 2009). In this work, aspects such as amino acid sequence, homology, biochemical characteristics and the performance of two *A. fumigatus* LPMOs in the biomass depolymerization process were investigated.

2.3 Materials and methods

2.3.1 Sequence analysis and tridimensional homology model

The protein sequences of the enzymes were analyzed using NCBI database (National Center for Biotechnology Information), Pfam (Protein families) and other bioinformatic tools such as MycoCosm from JGI (Joint Genome Institute), CBS (Center for Biological Sequence Analysis) and ProtParam from the ExPASy-SIB (Bioinformatics Resource Portal) server, for the identification of the signal peptide, conserved domains, molar mass, isoelectric point and molar extinction coefficient.

Phylogenetic analysis was performed using multiple sequence alignment generated with MUSCLE (Edgar, 2004) and a consensus tree using MEGA software version 10.1.7 (Kumar et al., 2018). The sequences of *Af*AA9A (KEY82006.1), *Af*AA9B (KEY76044.1) and the following AA9s with protein structures and regioselectivity determined experimentally were compared: *Af*AA9B (PDBid 6H1Z), *Cv*AA9 (PDBid 5NLT), *Hj*AA9A (PDBid 5O2W), *Hi*AA9B (PDBid 2VTC), *Ls*AA9A (PDBid 5ACF), *Mt*AA9D (PDBid 5UFV), *Nc*AA9A (PDBid 5FOH), *Nc*AA9C (PDBid 4D7U), *Nc*AA9F (PDBid 4QI8), *Nc*AA9M (PDBid 4EIS), *Pc*AA9D (PDBid 4B5Q), *Ta*AA9A (PDBid 2YET) and *Tt*AA9E (PDBid 3EII). The neighbor-joining method and a bootstrap of 1000 replicates were used to infer the consensus tree. The structure-based sequence alignment was generated with T-Coffee (Di Tommaso et al., 2011).

A tridimensional model of *Af*AA9A was generated using the Swiss-Model Automated Comparative Protein Server (https://swissmodel.expasy.org/) (Waterhouse et al., 2018) using the crystal structure of *Pc*AA9D from *Phanaerochaete chrysosporium* as a template. The experimental and theoretical models of *Af*AA9B (PDBid 6H1Z) (Lo Leggio et al., 2018) and *Af*AA9A, respectively, were compared and generated using the PyMOL Molecular Graphics System (Version 1.5.0.4 Schrödinger, LLC, New York, NY, USA).

2.3.2 Chemicals, microbial strains, cultivation, and plasmid

All chemicals were molecular biology grade. The substrates 2,6-dimethoxyphenol (2,6-DMP), Avicel PH-101, carboxymethylcellulose (CMC), 4-nitrophenyl β-D-glucopyranoside (pNPG), 4-nitrophenyl β-D-xylopyranoside (pNPX) and 4-nitrophenyl β-D-cellobioside (pNPC) were obtained from Sigma-Aldrich (St. Louis, USA). Phosphoric acid swollen cellulose (PASC) was prepared from Avicel PH-101 (Walseth, 1952). The pretreated biomass, steam-exploded bagasse (SEB), was kindly provided by Prof. Dr. George Jackson de Moraes Rocha (Brazilian Biorenewables National Laboratory, Brazil) (Wanderley et al., 2013). The oligonucleotides were purchased from Exxtend Biotechnology Ltd. (Campinas, Brazil) and maltose used as inducer was purchased from WE Consultoria (Porto Alegre, Brazil).

A. nidulans strain A773 (*pyrG89; wA3; pyroA4*) was purchased from the Fungal Genetic Stock Center (FGSC, Manhattan, USA). *A. nidulans* A773 was cultivated in a minimal medium as previously described (Velasco et al., 2019). *A. fumigatus* var. *niveus* was kindly provided by Prof. Rolf Prade from Oklahoma State University (Stillwater, USA) and cultivated in potato dextrose agar medium (PDA – Sigma-Aldrich) for 2 days at 45 °C. The pEXPYR vector was used for cloning and expression of *Af*AA9A and *Af*AA9B genes into *A. nidulans* A773 (Segato et al., 2012a). The plasmids carrying the polymerase chain reaction (PCR) amplified fragments corresponding to the *Af*AA9B and *Af*AA9A genes were propagated using high efficiency NEB1 Turbo competent *Escherichia coli* (New England BioLabs, Ipswich, USA).

2.3.3 Cloning, heterologous expression, purification and identification

The genomic DNA (gDNA) from fresh mycelia of *A. fumigatus* var. *niveus* was extracted with Wizard® Genomic DNA Purification kit (Promega, Madison, USA). The full-length coding sequence (CDS) of *Af*AA9A and *Af*AA9B were used for primers construction (accession XM_750694.1 and XM_746947.1, respectively). For gene cloning, appropriate regions were added in the oligonucleotides pEXPYR fwd (5' **CCGGCACGGGAC**TTCTAGTGATTTAATAGCTCCATGTCAACA 3') and pEXPYR rev (5' **CATTGCTGAGGTGTA**ATGATGCTGGGGGTG 3') used to linearize pEXPYR expression vector to allow correct gene insertion by Gibson Assembly® Method (Gibson et

al., 2009; Velasco et al., 2019). *Af*AA9A and *Af*AA9B genes were amplified from gDNA by PCR using Phusion® High-Fidelity DNA Polymerase (New England BioLabs) with the oligonucleotides *Af*AA9A fwd (5' **CATTACACCTCAGCA**ATGAAGCTGTCCCTTCTTGCT 3'), *Af*AA9A rev (5' **GTCCCGTGCCGGTTA**TTAGGGCTTGAACTGACGAGCGTGCCGGCG 3'), *Af*AA9B fwd (5' **CATTACACCTCAGCA**ATGACTTTGTCCAAGATCACT 3') and *Af*AA9B rev (5' **GTCCCGTGCCGGTTA**TTAAGCGTTGAACAGTGCAGGACCAGGAAT 3'), including specific regions to assemble the genes into PCR-linearized pEXPYR vector (Velasco et al., 2019). For cloning 50 ng of vector and 200 ng of each gene were mixed with 2× Gibson Assembly® Master Mix (New England BioLabs) and incubated for 1 h at 50 °C. Next, the products were used to transform *E. coli* cells by heat shock method. Cells were cultured in LB-ampicillin medium added by agar 2% and colonies were selected to confirm the presence of genes of interest by colony PCR. To propagate plasmids positive colonies were cultured in LB-ampicillin broth and plasmids were extracted by Wizard Plus SV Minipreps DNA Purification System kit (Promega) and used to transform *A. nidulans* A773 protoplasts mediated by polyethylene glycol (PEG) as previously described (Tilburn et al., 1983).

Colonies of *A. nidulans* A773 showing the capacity to grow up in minimal medium without the addition of uracil and uridine were selected and verified for secretion of recombinant LPMOs. To confirm the secretion of *Af*AA9A and *Af*AA9B a screening of 16 randomly selected colonies was carried out by inoculating 10^7 – 10^8 spores/ml of each transformant in 20 ml of minimal medium with 3% maltose and pyridoxine (1 mg/L - inducing medium) in Petri dishes for 48 h at 37 °C, under static conditions. Secretion of the proteins was visualized by SDS-PAGE (Shapiro et al., 1967) and, for each LPMO transformants revealing highest secretion levels of active protein were selected for enzyme production and purification. The enzymatic activity from supernatants produced by the selected transformants was evaluated by measuring the LPMO peroxidase activity using 1 mM 2,6-DMP as chromogenic substrate, 100 µM of H_2O_2 as co-substrate at 35 °C for 5 min using 100 mM phosphate/succinate buffer, pH 8. The LPMO activity in low concentration can be detected using absorption coefficient of the coerulignone (ε_{469} = 53,200 M^{-1} cm^{-1}) by this sensitive assay (Breslmayr et al., 2018).

For enzyme production selected transformants for *Af*AA9A and *Af*AA9B were cultured in 1 L of inducing medium as previously described (Berto et al., 2019). The culture extracts

were filtrated in a qualitative membrane (Miracloth, MilliporeSigma, Burlington, USA), concentrated and buffer-exchanged (100 mM Tris, pH 8.0) using an Amicon® Stirred Cell (10 kDa cut-off polyethersulfone membrane, MilliporeSigma). Purification of proteins were performed in two steps: ion exchange and size exclusion chromatography. In the first step, the concentrated extracts were injected into 5 ml DEAE-Sepharose CL6B resin (GE Healthcare Life Sciences, Marlbourough, USA) packed in Econo-Pac® Chromatography Column (Bio-Rad, Hercules, CA, USA) equilibrated with 100 mM Tris pH 8. Protein elution was performed in the same buffer using a gradient of NaCl (0.05 – 1 M). All resulting samples were applied on 15% SDS-PAGE to verify the fractions where the enzymes of interest eluted. In the second purification step, the LPMO-containing fractions were concentrated in Vivaspin 6 ultrafiltration device (GE Healthcare Life Science) with a 10 kDa cut-off membrane at 5000 x g, to a final volume of 10 ml. The injections were performed on the HiLoad® 16/600 Superdex® 75 pg column integrated into the Äkta Pure 25 M system (GE Healthcare Life Science). The protein fractions were collected and analyzed in SDS-PAGE. Fractions containing the purified proteins of interest were put together and stored at 4 °C. Prior the experiments *Af*AA9A and *Af*AA9B were saturated with copper sulfate (3 times of molar concentration of protein for 30 min at 16 °C), and further purified by size exclusion chromatography as previous described to remove the excess of copper.

The corresponding bands at SDS-PAGE for *Af*AA9A and *Af*AA9B were excised, reduced, alkylated and submitted to *in situ* trypsin gel digestion. A RP-nanoUPLC (nanoAcquity, Waters, Milford, USA) equipment coupled with a Q-TOF Ultimamass Spectrometer (Waters) with nano-electrospray source was used to analyze the protein fragments. The spectra were obtained though the software MassLynx v.4.1 (Waters) and the raw data files were converted to a peak list by the software Mascot Distiller v.2.3.2.0, 2009 (Matrix Science Ltd., London, UK). The MS/MS profiles were searched against predicted protein sequences of *A. fumigatus* var. *niveus* using Mascot engine v.2.3 (Matrix Science Ltd.) (Shevchenko et al., 1996). Tests against the synthetic substrates pNPG, pNPC and pNPX and polysaccharides (cellulose and xylan) without the addition of the reductant were performed to verify the presence of hydrolytic enzymes in LPMOs fractions. In these tests 2.5 µg of protein was added to the reactions which were performed in 50 mM sodium acetate buffer pH 5 containing substrate (1 µM pNP derived and 1% for polysaccharides substrates) and incubated at 45 °C for 1 h. After, the enzymatic reaction was interrupted by addition of 1 M sodium carbonate and the absorbance was measured at 405 nm (Textor et al., 2013).

2.3.4 Functional characterization of recombinant LPMOs

The pH effect on peroxidase activity of LPMOs *Af*AA9A and *Af*AA9B was evaluated by Breslmayr assay method using sodium acetate buffers (pH 4 - 6), 100 mM sodium phosphate buffer pH 7, and 100 mM sodium borate buffer (pH 8 – 10) (Breslmayr et al., 2018). The absorbance scan at 469 nm were performed at 30 °C for 30 min with readings every 15 sec in triplicates. To assess the stability of *Af*AA9A and *Af*AA9B in different pH, 1 µM of each enzyme was incubated for different periods of time (0.5, 1, 3, 6, 16 and 24 h) at room temperature in 0.1 M phosphate/succinate buffer adjusted to different pH values (6, 7 and 8). After incubation, the *Af*AA9A and *Af*AA9B were evaluated by peroxidase activity using Breslmayr assay method at 30 °C and compared with the enzyme activity without previous incubation period.

*Af*AA9A and *Af*AA9B stability at different pH and temperatures were determined by thermal shift assay (Thermofluor) at different pH (2-10) by mixing 7.5 µg of enzyme with SYPRO Orange stain (Invitrogen, Carlsbad, USA), in a molar ratio of 4-fold related to enzyme. The thermal unfolding of each LPMO was observed in 48 different conditions in temperatures ranging from 25 to 95 °C (increments in temperature of 1 °C/min). In some conditions 0.3 M of NaCl was added in the reaction. The reactions were monitored by change in fluorescence using a CFX96 Touch Real-Time PCR Detection System (Bio-Rad, Hercules, USA). The melting temperature average (Tm) was calculated from values obtained in tested conditions in thermal-shift assay. To determine the optimal temperature of the enzymes, Breslmayr assay based in 2,6-DMP method was used by incubating the reactions in phosphate/succinate buffer 0.1 M pH 7 for 10 min at different temperatures (30 - 60 °C), as previously described (Breslmayr et al., 2018)

2.3.5 LPMOs regiospecificity and SEB saccharification

The oxidative effect of *Af*AA9A and *Af*AA9B on cellulose was evaluated using reactions of 1 ml with the following final concentrations: 2 µM enzyme, 5% Avicel, 1 mM ascorbic acid (AscA) in 100 mM phosphate/succinate buffer. Reactions at pH 5 and 7 were incubated in 45 °C for 16 h at 800 rpm. After incubation, the reactions were heated for 10 min at 95 °C, centrifuged at 10,000 x g for 5 min, supernatants were recovered, filtrated and analyzed using high-efficiency anion exchange chromatography (HPAEC) equipped with pulsed amperometric detection (PAD) (Westereng et al., 2016). The Dionex™ CarboPac™ PA1

Analytical column (4 × 250 mm) and a pre-column Dionex™ CarboPac™ PA1 guard column (4 × 50 mm) coupled to the Dionex ICS 5000 system (Dionex, Sunnyvale, USA) was used to analyze the oxidized and non-oxidized soluble oligosaccharides. To evaluate the collaborative effect of *Af*AA9A and *Af*AA9B with cellulases in biomass saccharification, reactions using steam exploded sugarcane bagasse (SEB) as substrate were performed. Reactions with 12.5 ml final volume consisted in 0.5 g of SEB and enzyme load of 5 mg of total protein/g of substrate in 50 mM sodium acetate buffer pH 5 incubated in a rotatory shaker at 50 °C, 180 rpm for 72 h. The bagasse was grounded and granulometry adjusted to 65 mesh. A cocktail was prepared by adding different concentrations of commercial cellulases and hemicellulases (CBX). Each 100 mg of CBX cocktail was composed in Celluclast 1.5L (92 mg), β-glucosidase (6 mg), xylanase GH11 from *T. reesei* (2 mg) and used as control under the conditions mentioned above. For all experiments were used the same load of total proteins (2.5 mg) except for CBX mix that was replaced in 20% by LPMOs or BSA as follow: (a**)** 100% CBX; (b) 80% CBX + 20% BSA; (c) 80% CBX + 20% *Af*AA9A; (d) 80% CBX + 20% *Af*AA9B and (e) 80% CBX + 10% *Af*AA9B + 10% *Af*AA9A. AscA in a concentration of 1 mM was used as a reducing agent whereas in control reactions the LPMOs were replaced by BSA. Samples were withdrawn in the defined periods of time (3, 8, 24, 48, 72 h), heated and centrifuged as previously described, supernatant was recovered and filtered in a 0.22 μm filter to sugar quantification by HPLC and also DNS method (Miller, 1959). Glucose concentrations were determined by HPLC Shimadzu LC-10AD (Shimadzu, Kyoto, Japan), equipped with refractive index detector and a UV spectrophotometer. An ion exchange column HPX87H (Bio-Rad) was used at 65 °C working temperature and the elution was done with 5 mmol/L sulfuric acid with a rate of 0.6 ml/min.

2.3.6 Structural changes in substrates introduced by enzymatic hydrolysis

To evaluate structural changes introduced by enzymatic activity in pretreated lignocellulosic biomass, the residual solids were collected, dried, and analyzed using X-ray diffraction (XRD) and confocal laser scanning microscopy (CLSM). XRD was applied to evaluate cellulose crystallinity indices (CrIs) and to calculate an average crystallite sizes in the samples. Using Cu Kα radiation (λ = 1.5406 Å), Miniflex 600 (Rigaku, Tokyo, Japan) was set to operate at 40 kV, with 15 mA and 2 θ scans were measured from 5 to 50° in 0.05-

degree steps with an X-ray exposure of 15 s per step. Apparent crystallinity indices (CrIs) were calculated based on the individual diffraction peaks extracted from the curve-fitting process from the experimental diffraction scans. The PeakFit program (www.systat.com) was used and the average size of cellulose crystallites was determined by Scherrer equation (Bernardinelli et al., 2015; Monshi et al., 2012). The samples after enzymatic reactions were further analyzed by CLSM to map lignin distribution and to obtain information on its molecular arrangement within the samples (Coletta et al., 2013; Yu et al., 2014). Confocal microscopy images were collected from the surface of the samples using Zeiss LSM 780 confocal microscope with a Coherent Chameleon laser (Tisapphire) as a source for two-photons (2P) excitation experiments and a Plan-Apochromat objective lens (20x in water immersion) (Coletta et al., 2013). The total number of dots per image was 1024 x 1024 (Coletta et al., 2013; Espirito Santo et al., 2018).

2.4 Results and discussion

2.4.1 Bioinformatic sequence analyses

Analysis of *A. fumigatus* var. *niveus* genome identified the presence of seven genes encoding LPMOs from family AA9 (GenBank accession#: KEY83569.1, KEY81994.1, KEY77159.1, KEY82006.1, KEY80517.1, KEY80276.1, KEY76044.1), and allowed mapping of different conserved catalytic domains and cellulose binding modules (CDs and CBMs, respectively) of the enzymes (Couger et al., 2018; Segato et al., 2014a). The CBMs were present in three enzymes (KEY83569.1, KEY77159.1 and KEY80517.1) (Figure 2.1A). In all cases it was possible to verify the presence of a histidine residue in the N-terminal region after the signal peptide, characteristic of LPMOs (Quinlan et al., 2011). The LPMOs showed significant differences in the regions comprising signal peptides, CDs, CBMs and encoded LPMOs with different molecular masses (Figure 2.1A).

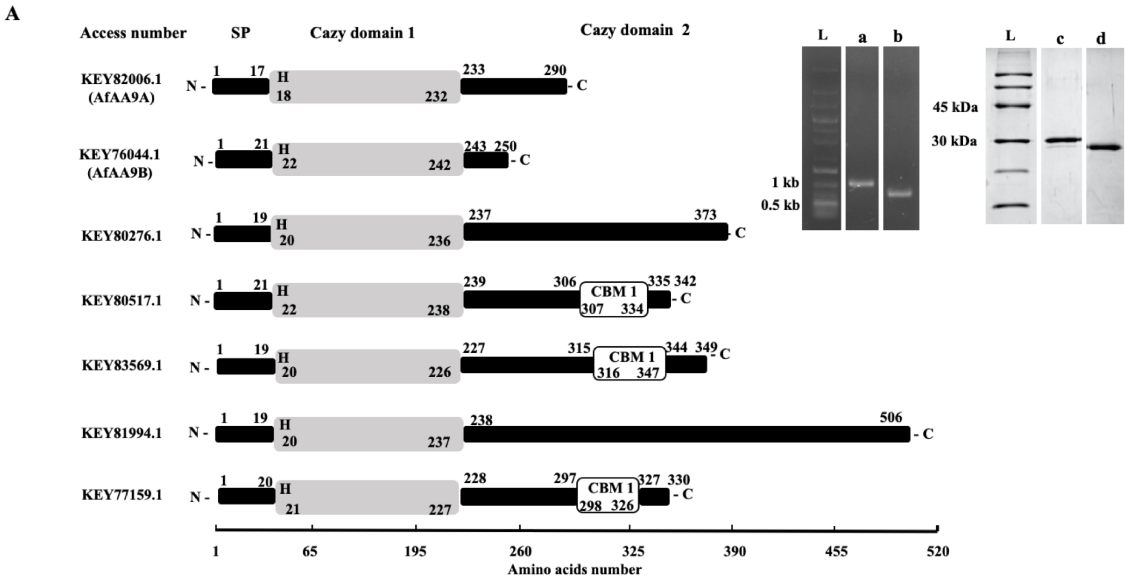

B

HYFFDVLVIDGKETRSNEFVR**SNTRPAKYNPTK**WK**NIRDDMTPDMPDFR**CNK**GAFTFAGQTGTAEVK**AGSKLAMK**LAVGATM**
QHPGPALVYMSKAPSSAK**TYEGDGDWFKIHEEGVCNK**NADFTK**DAWCTWDKDRIEFTIPADLPDGEYLIRPEHIGLHGAHDG**
QAEFYYTCAQVKVVGGGTGTPGPTIKFPGGYKKDDPSFNFSLWNGYKDYPMPGPTVWTGGSGSGSSSYSKVANVTSSDESSQ
SGASSSQGTVSTCPNKYNRRHARQFKP

C

HGFVSGIVADGKYYGGYLVNQYPYMSNPPDTIAWSTTATDLGFVDGTGYQSPDIICHRDAKNGKLTATVAAGSQIEFQWTTW
PESHHGPLITYLAPCNGDCATVDK**TTLKFVK**IAAQGLIDGSNPPGVWADDEMIANNNTATVTIPASYAPGNYVLR**HEIIALH**
SAGNLNGAQNYPQCFNIQITGGGSAQGSGTAGTSLYKNTDPGIKFDIYSDLSGGYPIPGPALFNA

Figure 2.1. (A) Comparative analysis of LPMOs from *A. fumigatus*, SP: signal peptide; CAZy domain 1 and 2 refers to the catalytic and CBM if present; H: histidine; N-: amino terminal region; -C: carboxy terminal region. In set: (L) Molecular weight, (a and b) agarose gel electrophoresis for *Af*AA9A and *Af*AA9B genes (accession XM_750694 and XM_746947, respectively), (c and d) SDS-PAGE of purified recombinant LPMOs *Af*AA9A and *Af*AA9B. (B and C) Identified peptides of recombinants LPMOs by LC-MS/MS yielding a sequence coverage of 64% for *Af*AA9A and 31% for *Af*AA9B, respectively

The presence of genes encoding LPMOs from family AA9 in the genome of *A. fumigatus* var. *niveus* suggests that proteins might have different functions and complement each other for effective degradation of biomass in nature. For example, a fact that 3 out of 7 *A. fumigatus* var. *niveus* LPMOs have CBMs, not only shows considerable structural differences among them but also indicates possible differences in their substrate affinity, products size and auto-oxidation resistance (Courtade et al., 2018; Forsberg et al., 2017). Although the histidine-brace residues are highly conserved in LPMOs there are some enzymes with one of His-residue is substituted for arginine. Such type of Arg-AA9 has been recently described as a group of proteins present in wood-degrading fungi belonging to the phylogenetic class of *Agaricomycetos* (Frandsen et al., 2019). The analysis of LPMO from

family AA9 codified by *A. fumigatus* var. *niveus* genes using the SignalP 5.0 server (total of 7 proteins) showed that these enzymes have a histidine at the N-terminus, including *Af*AA9A and *Af*AA9B.

The LPMOs *Af*AA9A and *Af*AA9B contains 273 and 229 residues in mature enzymes, respectively, being smaller CBM-less LPMOs (Figure 2.1A). In order to propose the putative regioselectivity of each target LPMO, alignments and phylogenetic analysis were performed by comparing the 7 LPMOs codified in the *A. fumigatus* var. *niveus* genome (Figure 2.2) and also the proteins *Af*AA9A, *Af*AA9B evaluated in this work together AA9s with structures and regioselectivity previously reported (Figure 2.3 and Figure 2.4).

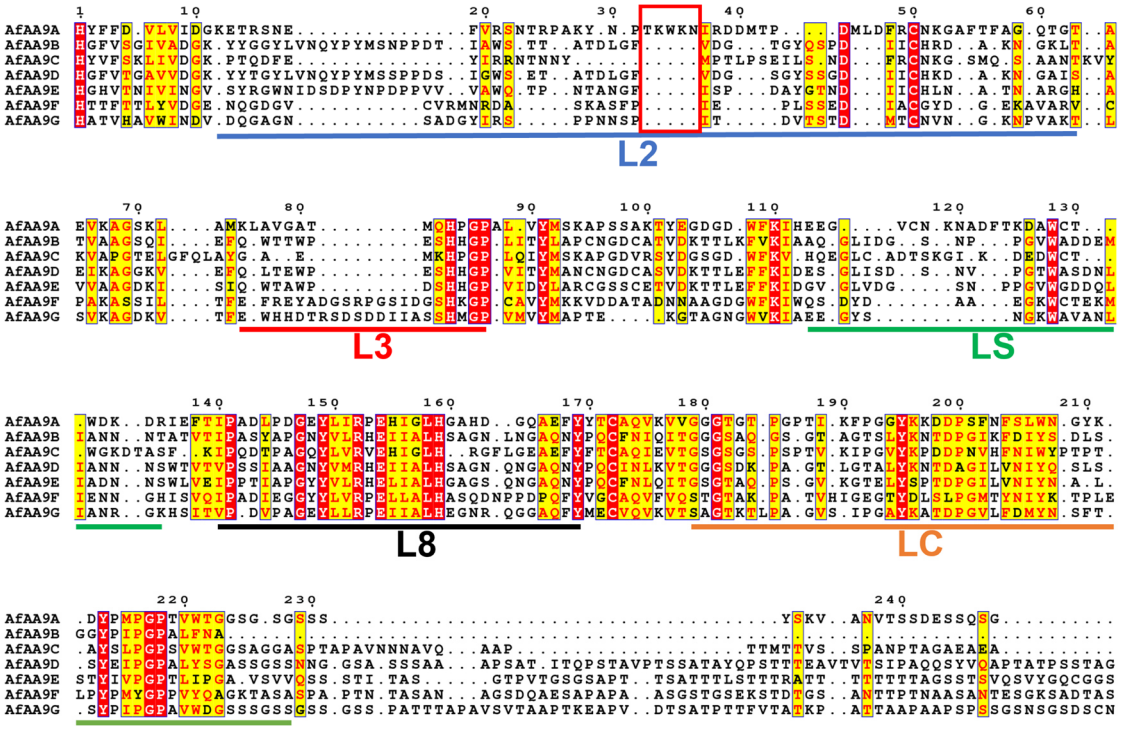

Figure 2.2. Structure based multiple sequence alignment (MSA) of AA9 LPMOs from *A. fumigatus*. The amino acid sequences of seven AA9 LPMOs were aligned using TCoffee. *Af*AA9A (GenBank accession#: KEY76044.1), *Af*AA9B (KEY77159.1), *Af*AA9C (KEY80276.1), *Af*AA9D (KEY80517.1), *Af*AA9E (KEY81994.1), *Af*AA9F (KEY82006.1) and *Af*AA9G (KEY83569.1). The extra element region found just on *Af*AA9A sequence is indicated inside the red box. The loop regions found in the carbohydrate binding surface are underlined in different colors (Loop L2 in blue; L3 in red; LS in green; L8 in black; LC in orange).

The sequences of *Af*AA9A and *Af*AA9B share low identity (26%) suggesting divergence in structure and oxidative specificity between *A. fumigatus* var. *niveus* enzymes. The highest sequence identity of *Af*AA9B was shared with the *Ta*AA9A (72%) and *Hj*AA9A (55%), both C1/C4 specific LPMO (Figure 2.3A) (Harris et al., 2010; Tanghe et al., 2015). On the other hand, *Af*AA9A and *Pc*AA9D, a C1 specific LPMO, clustered together with 41%

identity. These analyses suggest *Af*AA9A as a C1 specific AA9. Such predictions were further validated by HPAEC-PAD analysis of the oxidized products, confirming of the predictions described above.

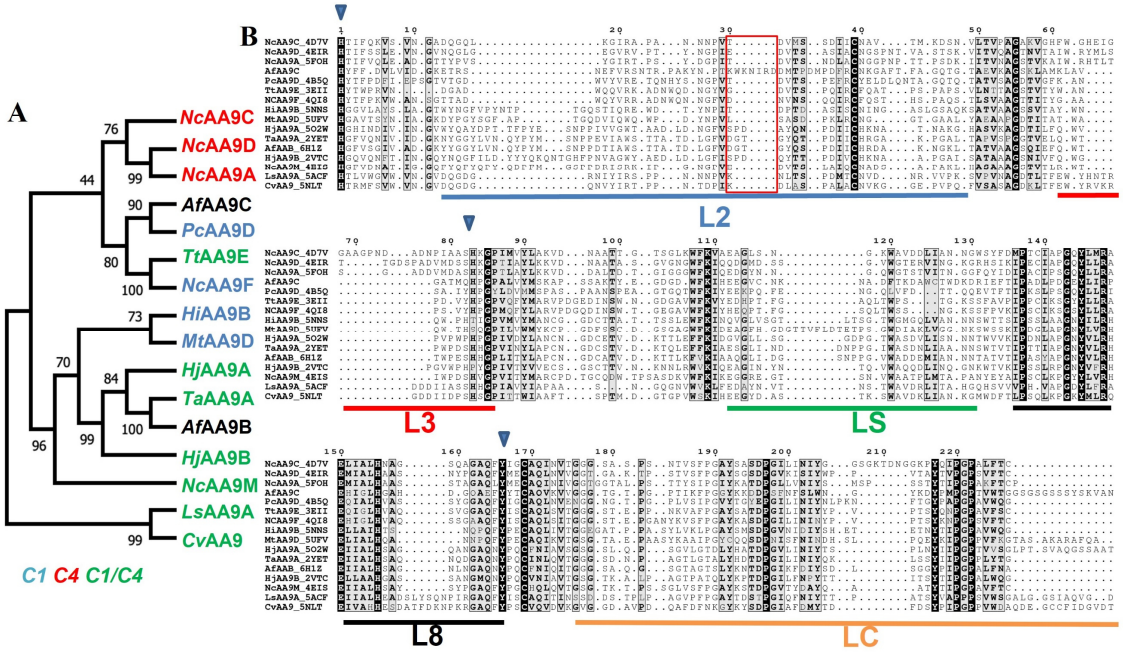

Figure 2.3. Sequence-based and structural comparison of LPMO9s. (A) Consensus phylogenetic tree of biochemically and structurally characterized LPMO9s. Multiple sequence alignment based on catalytic modules. The oxidative regiospecificity (C1, blue; C4, red; C1/C4, green) is indicated for each LPMO. (B) Structure based multiple sequence alignment (MSA) of *Af*AA9A, *Af*AA9B and LPMO with tridimensional structures determined by X-ray crystallography. The conserved residues involved in copper ion coordination are indicated by blue arrows. The extra element region found just on *Af*AA9A sequence is indicated inside the red box. The loop regions found in the carbohydrate binding surface are underlined in different colors (Loop L2 in blue; L3 in red; LS in green; L8 in black; LC in orange).

A closer analysis of LPMO sequences using structural-guided multiple sequence alignment indicate that *Af*AA9A and *Af*AA9B share a conserved catalytic core and the copper coordinating residues His1, His86/84 and Tyr175/169 (Figure 2.3B). The structure of *Af*AA9B has already been determined by X-ray crystallography (Lo Leggio et al., 2018) and showed structural features considered characteristic of C1/C4-oxidizing LPMOs such as a Pro83 residue close to the copper center (Borisova et al., 2015) and four aromatic residues (Tyr24, Phe43, Trp82, Tyr212) on the surface of the flat active site (Danneels et al., 2019). All these descriptions support the C1/C4 specificity of *Af*AA9B.

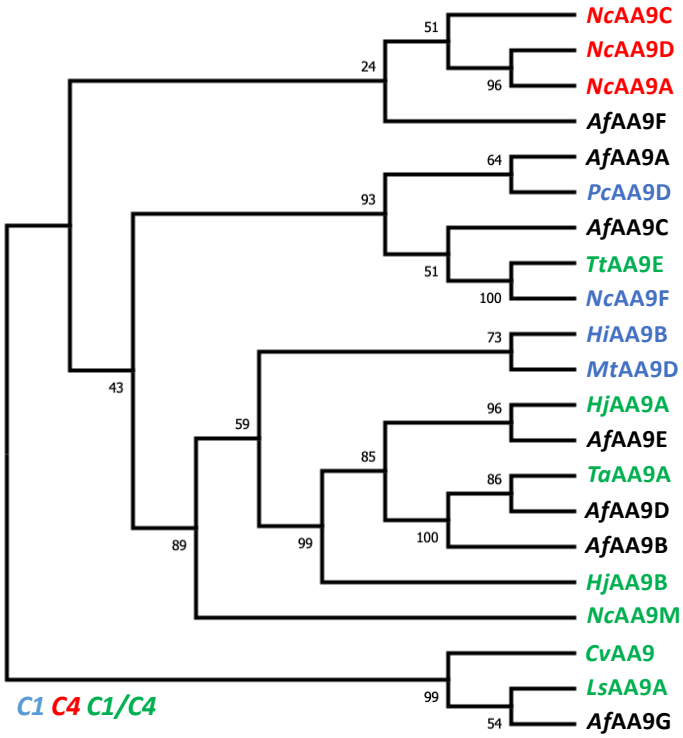

Figure 2.4. Regioselectivity prediction based on sequence-based comparison of LPMO9s. Consensus phylogenetic tree of biochemically and structurally characterized LPMO9s and the annotated enzymes from *A. fumigatus*. Multiple sequence alignment based on catalytic modules. The oxidative regiospecificity (C1, blue; C4, red; C1/C4, green) is indicated for each characterized LPMO. This analysis suggests the following regioselectivity for the seven AA9s from *A. fumigatus*: *Af*AA9A (C1), *Af*AA9B (C1/C4), *Af*AA9C (C1 or C1/C4), *Af*AA9D (C1/C4), *Af*AA9E (C1/C4), *Af*AA9F (C4) and *Af*AA9G (C1/C4).

The MSA show that *Af*AA9A missed the C1/C4 specific elements listed above as well as the L3 loop characteristic of C4 LPMOs corroborating with a C1 prediction. Moreover, this analysis revealed an extra sequence inside the L2 region not reported before (Figure 2.3B). To assess the putative position of this element, the tridimensional homology model of *Af*AA9A was constructed (Figure 2.5). This extra element comprises a loop of 11 residues (30-41) found in the catalytic surface and close to the copper center (Figure 2.5 and Figure 2.2). The presence of the extra loop and the predicted C1-oxidant capacity make *Af*AA9A an enzyme with interesting and contrasting characteristics to be compared with *Af*AA9B (considered by us as the model LPMO of *A. fumigatus*)

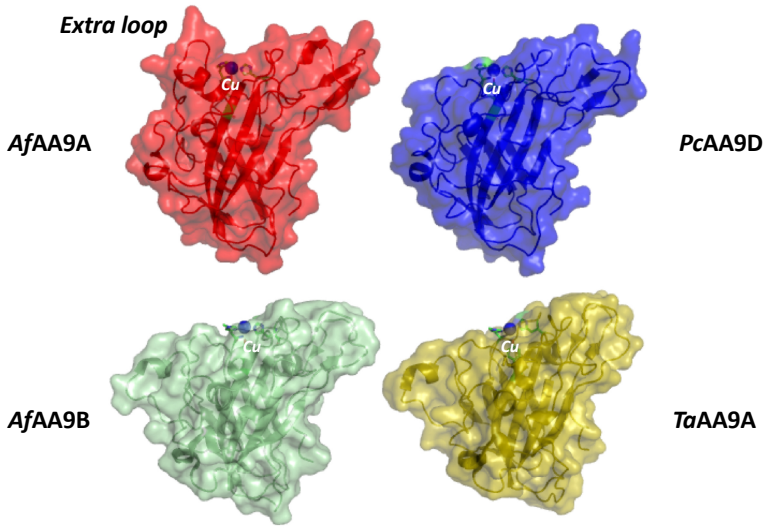

Figure 2.5. Structural comparison of *Af*AA9A and *Af*AA9B with close correlated AA9s. The *Af*AA9A (red structure) was modelled based on the experimental structure of *Pc*AA9D (PDBid 4B5Q, blue structure). The crystallographic structures of *Af*AA9B (PDBid 6H1Z, green structure) and *Ta*AA9A (PDBid 2YET, yellow structure) are also compared. The extra element found in *Af*AA9A is indicated. The proteins are shown in transparent surface and secondary structure cartoon representation. The copper ion is shown as a blue sphere.

2.4.2 Cloning, transformation and protein identification

The genes codifying the *A. fumigatus* var. *niveus* LPMO proteins *Af*AA9A (KEY82006.1) and *Af*AA9B (KEY76044.1), have 995 and 862 bp in length containing 2 introns each corresponding in 122 and 109 bp that after post-transcriptional modification results in 873 and 753 bp, respectively. Both genes were PCR-amplified from *A. fumigatus* var. *niveus* gDNA and successfully cloned into pEXPYR vector by Gibson Assembly® and heterologous expressed in *A. nidulans* A773 (Figure 2.1A). Transformants for both LPMOs efficiently secreted *Af*AA9A and *Af*AA9B in inducing medium. The SDS-PAGE analysis shows bands with 30 and 26 kDa for *Af*AA9A and *Af*AA9B, respectively (Figure 2.1A). The LC-MS/MS analyzes allowed to identify 10 peptides for *Af*AA9A (Figure 2.1B) and 4 peptides for *Af*AA9B (Figure 2.1C) with sequence coverage of 64 and 31%, respectively. Purified enzymes did not show hydrolytic cellulase and/or xylanase activity on tested substrates. *A. nidulans* plus pEXPYR system reveals itself very efficient in processing and secretion of LPMO *Af*AA9B. This system was developed and adapted in our group to express genes encoding LPMOs. The patented *A. oryzae* expression systems (patent number WO2012044836) was previously used to express *Af*AA9B. Another expression system was

E. coli DH5α, that does not have essential post-translational modifications for LPMOs activity and does not secrete the protein to the extracellular medium (Gouvêa et al., 2019; Lo Leggio et al., 2018).

2.4.3 LPMO functional characterization

LPMO *Af*AA9B has been a subject of studies aimed at improving its thermal resistance. This enzyme was used to generate several chimeras with differences in thermostability and cellulose degradation (Lo Leggio et al., 2018). The structural characterization and mutation of 4 amino acids from native protein *Af*AA9B was also performed, resulting in improved thermostability (Lo Leggio et al., 2018). Previous works report the effect of Celluclast 1.5L supplemented with high load of *Af*AA9B in the saccharification of steam exploded sugar cane bagasse (Gouvêa et al., 2019). Despite of that, no detailed biochemical and functional characterization in combination with the supplementation of commercial cocktail with low concentration of this enzyme has yet been described.

Figure 2.6A shows the results of the scan of absorbance performed at different pH for the LPMOs using Breslmayr assay method. In general, *Af*AA9B is more efficient than *Af*AA9A in the conversion of the substrate 2,6-DMP in all tested pH. For both LPMOs the conversion of 2,6-DMP to the product coerulignone at pH 4 - 5 and 4 - 6 (*Af*AA9B and *Af*AA9A) was very low, while in pH 6 - 7 for *Af*AA9B and only pH 7 for *Af*AA9A was higher compared to pH 4 - 5. However, from pH 4 to 7 the conversion of 2,6-DMP into coerulignone by LPMOs remained increasing constantly for 30 min, while in pH 8 - 10 the conversion was very fast in initial minutes and started to decrease after 3 min. The pH curves were plotted using the highest values of absorbance obtained in the analysis for each pH in the scan analysis and showed that *Af*AA9A and *Af*AA9B are more active at pH 8 (Figure 2.7). LPMOs with better performance at pH higher than 7 have already been reported both for peroxidase activity in the Breslmayr assay with 2,6-DMP (Semenova et al., 2020) and for activity on cellulose (Breslmayr et al., 2018; Frommhagen et al., 2018b; Hegnar et al., 2019). *Af*AA9A was more stable at all tested pH, maintaining residual activity above 90% for 24 h, whereas *Af*AA9B showed a slight decrease in activity after 6 h, losing up to 38 and 22% after 24 h in pH 6 and 7, respectively (Figure 2.7A). It is important to note that in incubation conditions tested (in the absence of reductant), the conversion of O_2 to H_2O_2 and reactive O_2 species that can cause oxidative damage to enzymes are avoided (Hegnar et al., 2019).

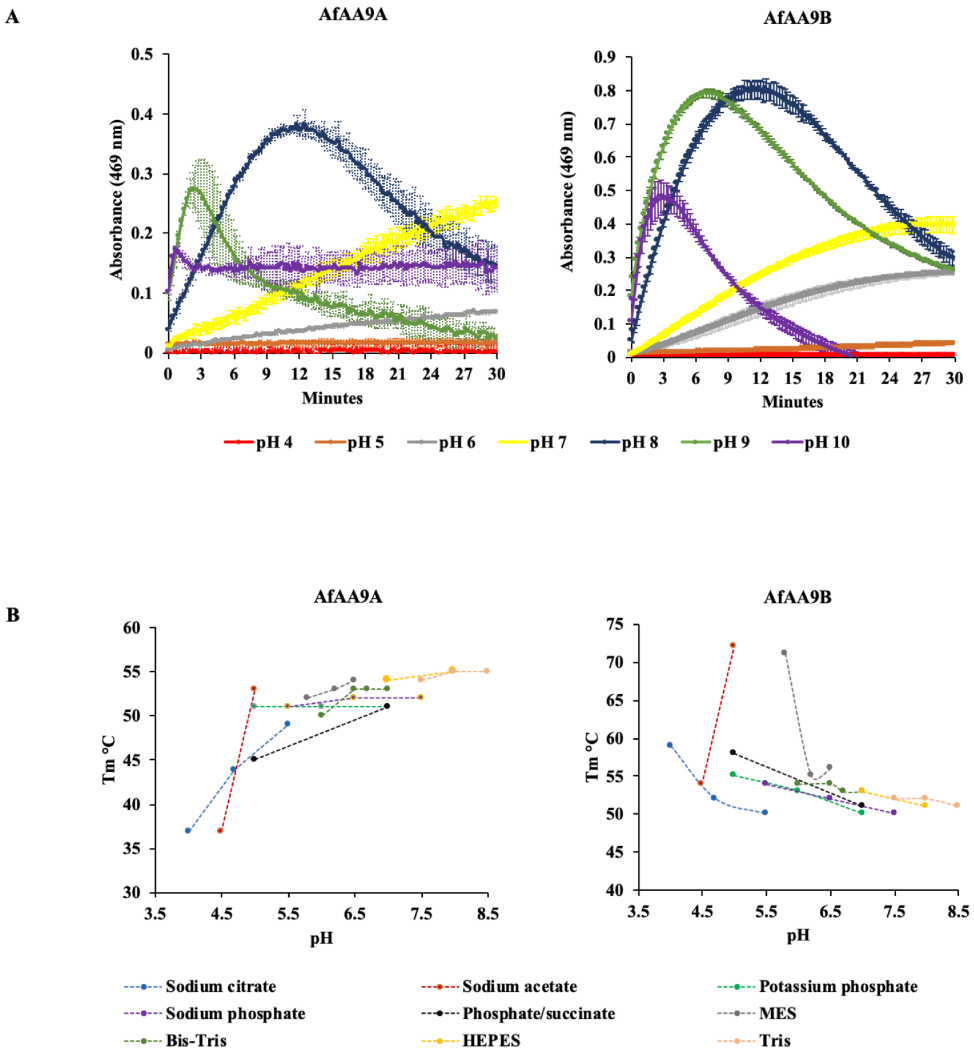

Figure 2.6. (A) pH scan analysis for recombinant LPMOs and (B) analysis of pH effect on *Af*AA9A and *Af*AA9B Tm by thermo-shift assay.

The LPMOs showed differences in their thermal stability behavior, with different values of Tm depending on the tested buffer/pH/NaCl conditions, *Af*AA9B showed the highest value of Tm (72 °C) in sodium acetate buffer pH 5, while *Af*AA9A showed highest value (55 °C) in HEPES pH 8 and Tris pH 8.5 (Table 2.1). Thermal unfolding of the enzymes for the condition where the highest Tm values were obtained is given in figure 2.7C. Tm values of around 70 °C have been reported for *Af*AA9B under the same conditions tested here, however the effect related to this value decreases sharply in different buffers has not been previously described (Lo Leggio et al., 2018).

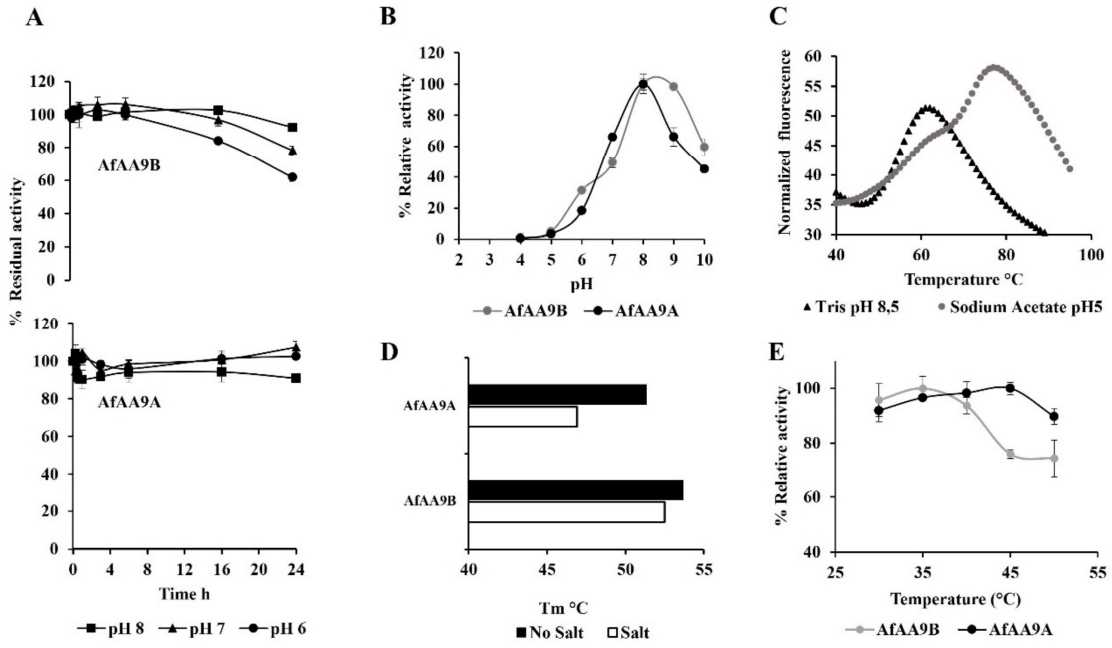

Figure 2.7. (A) Stability of LPMOs A*f*AA9A and A*f*AA9B at different pH using Breslmayr assay. (B) pH curves for the peroxidase activity of A*f*AA9A and A*f*AA9B. (C) Shift in fluorescence signal for the conditions where the highest Tm values were obtained, triangle represents A*f*AA9A and circle A*f*AA9B. (D) Tm average for A*f*AA9A and A*f*AA9B in presence/absence of 0.3 M of NaCl. (E) Optimal temperature for LPMOs evaluated by Breslmayr assay/peroxidase activity.

The enzymes showed contrasting results with respect to pH effects on Tm, showing that conditions with low pH were more favorable for *Af*AA9B (sodium acetate pH 5) whereas alkaline pH showed be more advantageous for *Af*AA9A (Tris pH 8.5) (Figure 2.7C). A more detailed analysis of pH effect on Tm is given in figure 2.6. An increase in pH also increases the Tm values for *Af*AA9A, a contrasting result for *Af*AA9B where the slope lines shows that for all buffers (except sodium acetate) while the pH increase Tm decreases (Figure 2.6B). Furthermore, a comparative analysis of the Tm of *Af*AA9A and *Af*AA9B for the tested conditions with 0.3 M of NaCl using thermal shift assay showed a decrease in Tm values for both LPMOs, being the effect most severe for *Af*AA9A that the average in Tm values reduced by 4 °C (Figure 2.7D). The pH not only affects enzymes, but also influences reductant redox potential and the conversion of O_2 into H_2O_2 when the enzyme is not bound to the substrate, in the process known as a futile cycle (Hegnar et al., 2019).

Table 2.1. Melting temperature values for *Af*AA9B and *Af*AA9C determined by Thermal shift assay. ND: no determined.

pH	Buffer (50 mM)	NaCl (mM)	Tm °C AfAA9B	Tm °C AfAA9A
-	H2O	0	53,00	54,00
5	Phosphate/succinate	0	58,00	45,00
2,0	HCl	0	51,00	47,00
7	Phosphate/succinate	0	46,00	51,00
4,0	Sodium citrate	0	59,00	37,00
4,5	Sodium acetate	0	54,00	37,00
4,7	Sodium citrate	0	52,00	44,00
5,0	Sodium acetate	0	72,00	53,00
5,0	Potassium phosphate	0	55,00	51,00
5,5	Sodium citrate	0	50,00	49,00
5,5	Sodium fosfate	0	54,00	51,00
5,8	MES	0	71,00	52,00
6,0	Potassium phosphate	0	53,00	51,00
6,0	Bis-Tris	0	54,00	50,00
6,2	MES	0	55,00	53,00
6,5	Sodium phosphate	0	52,00	52,00
6,5	Sodium cacodilate	0	ND	54,00
6,5	Bis-Tris	0	54,00	53,00
6,5	MES	0	56,00	54,00
6,7	Bis-Tris	0	53,00	53,00
7,0	Potassium phosphate	0	50,00	51,00
7,0	HEPES	0	53,00	54,00
7,0	Bis-Tris	0	53,00	53,00
7,3	Ammonium acetate	0	53,00	55,00
7,5	Sodium phosphate	0	50,00	52,00
7,5	Tris	0	52,00	54,00
8,0	Imidazole	0	49,00	54,00
8,0	HEPES	0	51,00	55,00
8,0	Tris	0	52,00	55,00
8,0	Bicina	0	51,00	52,00
8,5	Tris	0	51,00	55,00
9,0	Bicina	0	49,00	51,00
9,5	Sodium carbonate	0	47,00	51,00
10,0	Sodium carbonate	0	46,00	48,00
3,0	Citric acid	300	42,00	ND
4,5	Sodium acetate	300	55,00	26,00
5,0	Potassium phosphate	300	51,00	46,00
5,5	Bis-Tris	300	54,00	48,00
5,5	Sodium citrate	300	50,00	48,00
5,8	MES	300	72,00	47,00
6,0	Bis-Tris	300	53,00	47,00
6,5	Sodium cacodilate	300	53,00	50,00
6,5	Sodium phosphate	300	52,00	50,00
7,0	Bis-Tris	300	51,00	49,00
7,0	HEPES	300	53,00	50,00
7,3	Ammonium acetate	300	51,00	50,00
7,5	Tris	300	50,00	49,00
8,0	HEPES	300	50,00	51,00

The 2,6-DMP method does not use reductants which facilitates the analysis of the enzyme in different pH values, however, shows limitations including substrate oxidation in alkaline pH, which might result in higher apparent activity (Breslmayr et al., 2018). At alkaline pH, the radicals formed by the oxidation of 2,6-DMP can react with the coerulignone in polymerization reactions that cause its decolorization (Figure 2.6A). Since the Breslmayr assay based in 2,6-DMP method has some limitations, the enzymes were evaluated by HPAEC-PAD revealing a better activity for both enzymes at pH 7 as compared to pH 5 (Figures 2.8A and 2.8B).

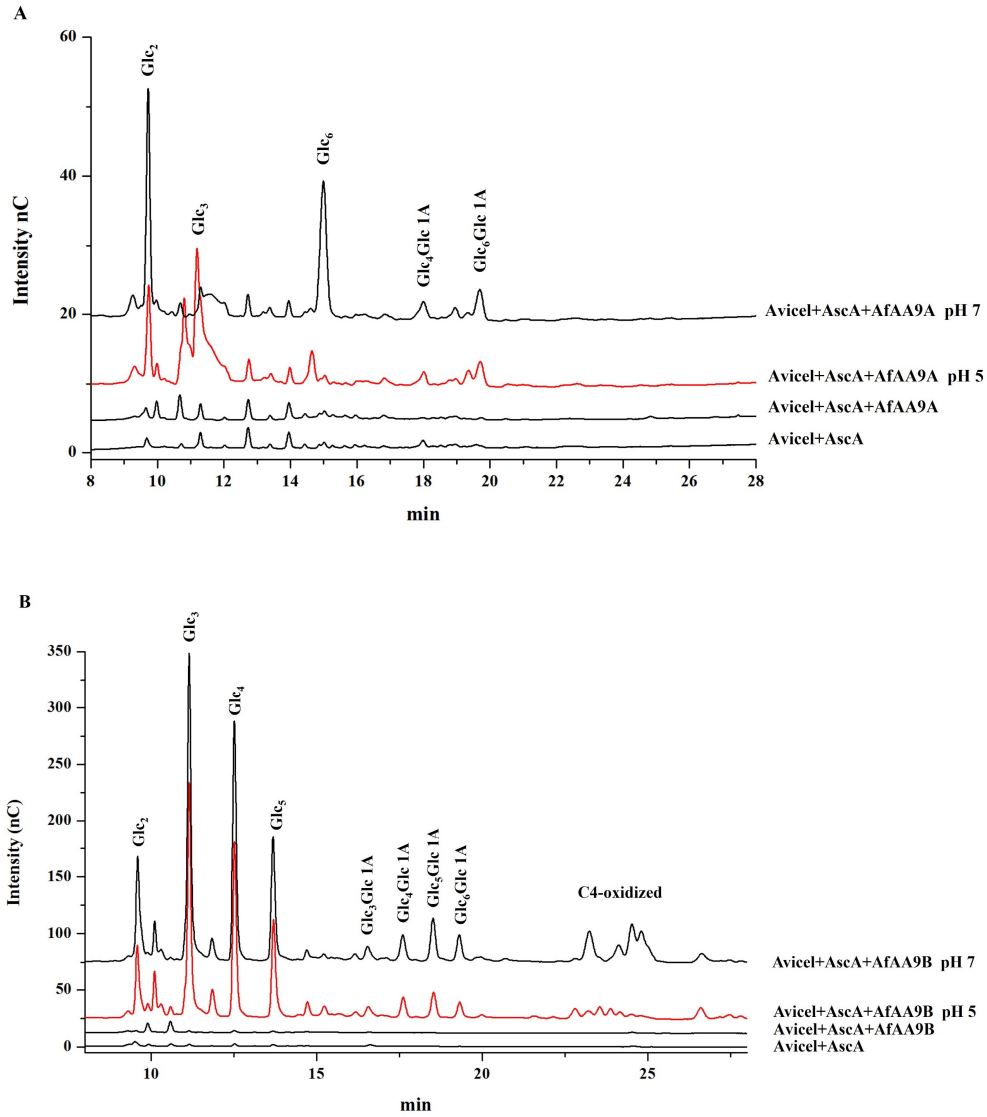

Figure 2.8. (A) Oxidation of cellulose at 45 °C using A*f*AA9A at pH 5 and pH 7 evaluated by HPAEC-PAD. The same experimental conditions were maintained in control reactions without the addition of LPMO or reductant. (B) Oxidation of cellulose at 45 °C using *Af*AA9B at pH 5 and pH 7 evaluated by HPAEC-PAD. The same experimental conditions were maintained in control reactions without LPMO or reductant addition.

This result is in agreement with previous study that reported a greater release of oxidized products at pH 7 for a LPMO from *Gloeophyllum trabeum* as compared with pH 6 (Hegnar et al., 2019). Frommhagen *et al*. (2018b) described the high activity for two *T. thermophilus* LPMOs at pH 7 - 8. Our group obtained similar results with LPMOs from *T. thermophilus* and *T. reesei* (unpublished data).

The optimal temperature for peroxidase activity of each LPMO is shown in figure 2.7E. *Af*AA9A maintained its activity above 80% between temperatures ranging from 30 to 50 °C and has an optimal temperature of 45 °C, while *Af*AA9B is more active between 30 and 40 °C (Figure 2.7E). Considering the enzymes from the same organism, one can expect them to perform best at similar temperatures. The analysis of optimal temperature based in peroxidase activity were also detected with values near to 40 °C and have also been reported for LPMOs of *T. reesei*, *Thermoascus aurantiacus* and *Talaromyces cellulolyticus* showing that these enzymes had their activity largely reduced by temperatures above 45 °C (Zhang et al., 2019). This is clearly not the case for *Af*AA9A and *Af*AA9B that retain 90 and 75% of their activity at 50 °C, respectively.

2.4.4 Regiospecificity and saccharification effect of LPMOs

Analysis of products released by recombinant LPMOs using HPAEC-PAD technique showed that *Af*AA9B enzyme is more efficient in oxidative cellulose cleavage when compared to *Af*AA9A (Fig. 2.8). The products released by the recombinant enzymes allowed the classification of *Af*AA9A as type one and *Af*AA9B as type two, since these LPMOs are able to oxidize at carbon C1- and C1/C4 of pyranose ring, respectively, which is consistent with bioinformatic analysis (Figures 2.3A and 2.4), demonstrating production of cellodextrins (Glc_n) and aldonic acids (Glc_nGlc1A) with different degree of polymerization (DP). For cellodextrins with different DP were detected cellobiose (Glc_2), cellotriose (Glc_3), cellotetraose (Glc_4) and cellopentaose (Glc_5) and aldonic acids were detected cellotrionic acid (Glc_3Glc1A), cellotetraonic acid (Glc_4Glc1A), cellopentaonic acid (Glc_5Glc1A) and cellohexaonic acid (Glc_6Glc1A). In addition to the regiospecificity of LPMOs, the results demonstrate that enzymes are more active at pH 7 (Figure 2.8, black lines), corroborating with previous analysis using Breslmayr method that showed the LPMOs have an increased peroxidase activity in pH values above 5 (Figure 2.7B). The effect of pH in the mechanism of LPMOs on cellulose oxidation must be carefully analyzed

since the pH can affects the reductant redox potential, influencing peroxide production (Hegnar et al., 2019). This affects enzymatic performance since peroxide accumulation can enhance LPMOs activity, and also can cause oxidative damage (depending on the amount of H_2O_2 produced) (Bissaro et al., 2017; Hangasky et al., 2018). The large amount of cellodextrins detected for *Af*AA9B is common for LPMOs C1/C4-oxidizing when the products are analyzed by HPAEC-PAD, since alkaline conditions employed by this technique favor the conversion of ketoaldoses (glucooligosaccharides oxidized at carbon 4) into cellodextrins (Westereng et al., 2016). The discrete activity obtained for *Af*AA9A allows to infer that the enzyme might have higher efficiency in non-soluble products, which would require longer reaction times to solubilize and detect the products (Frommhagen et al., 2018b). Considering that HPAEC-PAD data allows to evaluate only the generated soluble products and disregard the enzyme effects on insoluble portion, the LPMOs activity is often underestimated (Eijsink et al., 2019).

Supplementation of CBX cocktail with LPMO enhanced the saccharification of SEB (Figures 2.9 and 2.10) after 72 h of incubation. The addition of *Af*AA9B showed a positive effect in the saccharification of SEB increasing in 20% the release of glucose compared to the sample containing only CBX. The addition of *Af*AA9A to the CBX did not show positive effect in SEB saccharification with almost the same behavior promoted by the addition of BSA. This difference between the LPMOs agrees with biochemical data (HPAEC-PAD analysis) where *Af*AA9B showed a better performance in cellulose degradation (Figure 2.8). On the other hand, a mixture of the two LPMOs improved saccharification for the first 48 h showing a similar performance to the treatment with the mixture containing 80% CBX + 20% *Af*AA9B, however after this period of time the glucose yield did not improve, resulting in almost the same amount of glucose produced by 100% CBX after 72 h of reaction (Figure 2.9). Previous studies demonstrated that BSA can be adsorbed on lignin present in the lignocellulosic substrates and disable potential unproductive binding of cellulases, which will in turn enhance soluble sugars release as a result of cellulase action (Pielhop et al., 2015). Therefore, the increment in enzymatic hydrolysis observed in the presence of *Af*AA9B (14.44 mg/ml of glucose released) could be attributed to the catalytic capacity of the LPMO and not to the unproductive absorption effects, since the experiments containing BSA in equal load did not have the same effect because the amount of released glucose was lower (10.15 mg/ml) due to the enzymatic load reduction (80% CBX supplemented with 20% BSA, Figure 2.9).

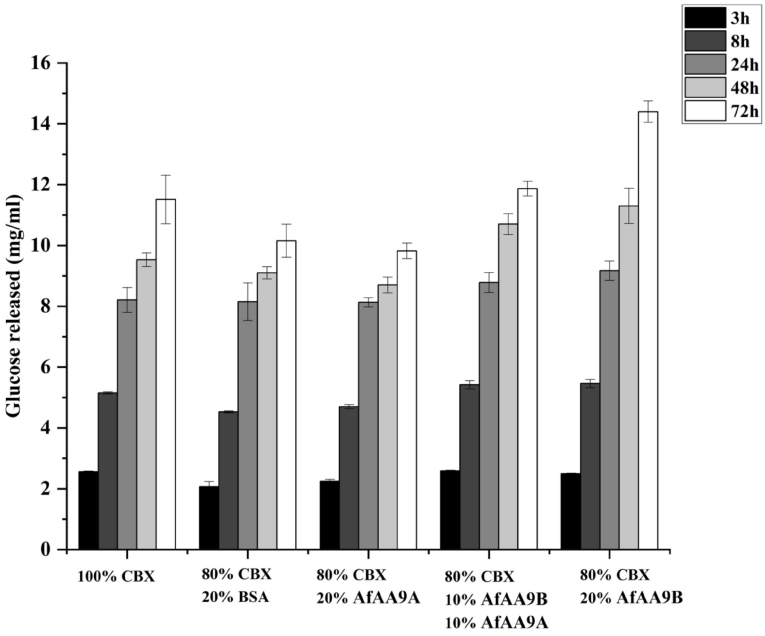

Figure 2.9. Effect of LPMOs in saccharification of steam explosion pretreated sugarcane bagasse. CBX (92% Celluclast 1.5L, 6% β-glucosidase (Novozym 188), 2% *T. reesei* xylanase).

It is interesting to note that enzymatic hydrolysis with CBX supplemented with both LPMOs (80% CBX + 10% *Af*AA9A + 10% *Af*AA9B, Figure 2.9), compared with enzymatic hydrolysis of CBX + 20% *Af*AA9B, showed almost the same sugar release efficiency until 48 h of incubation. Although sugar yields be very close the enzymatic load of *Af*AA9B (in treatment using combined LPMOs) was 50% compared with the reaction that only *Af*AA9B was added. Presumably, this effect is mediated by *Af*AA9A contribution to the enzymatic hydrolysis. To confirm whether this behavior could be attributed to the collaborative effect between LPMOs or only 10% of *Af*AA9B could be contributing to the observed saccharification effect, an additional assay was performed using 90% of CBX and 10% of *Af*AA9B (Figure 2.10). The figure 2.10 shows the same pattern of reducing sugar release for the treatments using 10% *Af*AA9B and the combined LPMOs (80% CBX + 10% *Af*AA9A + 10% *Af*AA9B) demonstrating that when the two LPMOs are mixed only *Af*AA9B promotes the release of sugar with no apparent effect for *Af*AA9A. These results show that not all LPMOs are able to improve cellulose saccharification processes, even obtained from the same source. Harris and colleagues studied six LPMOs from *T. terrestris* and showed that only few LPMOs boosted cellulose hydrolysis present in corn stover substrate (Harris et al., 2010).

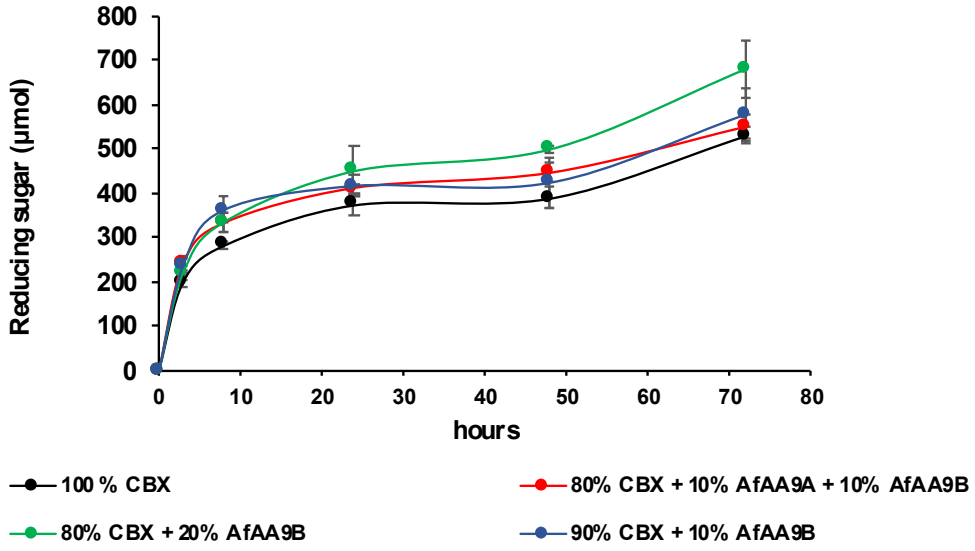

Figure 2.10. Analysis of the effect of LPMOs in saccharification of steam explosion pretreated sugarcane bagasse by DNS method. CBX (92% Celluclast 1.5L, 6% β-glucosidase (Novozym 188), 2% *T. reesei* xylanase).

The *Af*AA9B boosting effect had already been reported by de Gôuvea and co-workers increasing the hydrolytic capacity of Celluclast 1.5L on SEB by 22%, an increase similar to reported here (20%) however using two times higher enzymatic load than that used in present study (10 mg/g of substrate) (Gouvêa et al., 2019). This promising result not only further confirms a potential of this enzyme to be used as an additive to commercial cocktails, but also demonstrates that synergistic effects can be increased by adjusting the conditions of enzymatic hydrolysis.

2.4.5 Structural changes of hydrolyzed substrate

The crystallinity indices (CrIs) of control and hydrolyzed samples were determined from their X-ray diffraction patterns (Table 2.2) (Bernardinelli et al., 2015; Park et al., 2010). Although CrIs of the enzymatically hydrolyzed residual samples were somewhat smaller as compared to pretreated biomass samples used as controls, the differences in average crystallinities are not significant (Table 2.2). Therefore, we can conclude that enzymatic saccharification of SEB did not change crystallinity of the remaining solid fraction significantly (Table 2.2). This implies that the enzymatic hydrolysis reactions wear out crystalline and amorphous fractions of the biomass samples in approximately equal degree. Taking into consideration that enzymatic hydrolysis of lignocellulosic biomass is a

heterogeneous catalytic reaction which occurs at the interface between liquid media containing the catalysts (enzymes) and the insoluble solid substrate (lignocellulosic biomass), it seems reasonable to suppose that both crystalline and amorphous regions at the surface layers of the biomass have to be digested and solubilized before the enzymes access to internal layers of polysaccharides. This should result in approximately homogeneous degradation of lignocellulosic biomass biopolymers from outside inwards, with the remaining solids having approximately the same crystallinities as the original pretreated samples.

Table 2.2. Crystallinity index (CrI) of steam exploded bagasse (SEB) and hydrolysed samples.

Sample	ICr (Park)	Crystallite (nm)
SEB	52.1 ± 2.7	4.4 ± 0.4
100% CBX	50.1 ± 1.0	4.4 ± 0.3
80% CBX + 20% *Af*AA9A	50.6 ± 1.0	4.5 ± 0.4
80% CBX + 20% *Af*AA9B	48.6 ± 1.2	4.3 ± 0.1
80% CBX + 10% *Af*AA9A + 10% *Af*AA9B	51.1 ± 1.3	4.1 ± 0.2

This notion is further supported by the results of evaluation of the average crystallite sizes (Table 2.2). The size of an average crystallite in the pretreated samples and samples remaining after enzymatic hydrolysis were not impacted by the enzymatic hydrolysis with the average of about 4.3 nm before and after enzymatic hydrolysis (Table 2.2). This is consistent with a notion of a (quasi) homogeneous surface erosion catalyzed by the applied enzymatic mixtures, both in the absence and in the presence of the evaluated LPMOs. Next, changes introduced in the lignin fraction of the pretreated lignocellulosic biomass samples by the enzymatic hydrolysis, were evaluated by confocal laser scanning microscopy (CLSM), allowing measuring the emission spectra of lignin to verify its distribution and changes in fluorescence emission spectra, which could report on possible modifications in lignin electronic states (Figure 2.11) (Coletta et al., 2013; Espírito Santo et al., 2019; Westereng et al., 2015). Steam explosion pretreatment causes considerable redistribution of lignin in the bagasse samples resulting in spectral changes in CLSM reporting on modifications of the plant cell walls (Espírito Santo et al., 2019; Yu et al., 2014). Prior to enzymatic saccharification a significant part of residual lignin from pretreated sugarcane bagasse kept emitting fluorescence green-bluish wavelength spectra (Figure 2.11A), which is a characteristic of none or just minor modifications in the residual lignin (Coletta et al.,

2013; Espírito Santo et al., 2019; Espirito Santo et al., 2018). CLSM analysis demonstrated that enzymatic saccharification introduced important changes in lignin autofluorescence, shifting it to the longer wavelength region (toward yellow and red, Figure 2.11B-E).

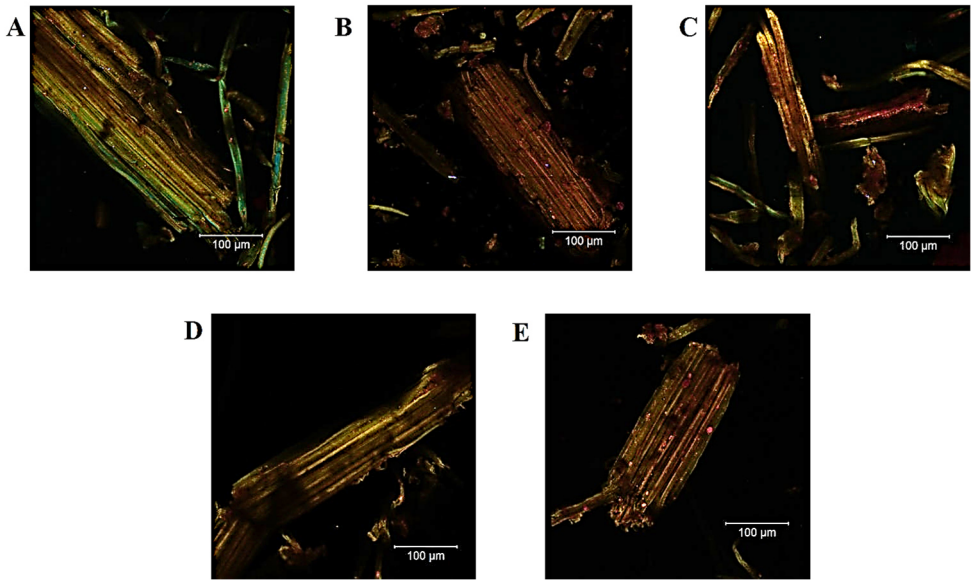

Figure 2.11. CLSM spectral image of steam exploded bagasse samples after enzymatic hydrolysis. (A) Control, (B) 100% CBX, (C) 80% CBX + 20% *Af*AA9A, (D) 80% CBX + 20% *Af*AA9B and (E) 80% CBX + 10% *Af*AA9A + 10% *Af*AA9B.

Remarkably, the observed shift of the fluorescence to red is pronounced in samples that was efficiently hydrolyzed, particularly when reactions occurred in the presence of LPMO *Af*AA9B (Figure 2.9, Figure 2.11D and Figure 2.11E). The less efficiently hydrolyzed samples such as that containing the LPMO *Af*AA9A still reveal a presence of lignin partially emitting in green (Figure 2.9 and Figure 2.11C).

It is known that lignin can positively interact with LPMOs by electron transfer from lignin particles boosting the enzymatic hydrolysis of cellulose (Rodríguez-Zúñiga et al., 2015; Westereng et al., 2015). Electron donation by lignin might have effects on its chemical structure which results in changes in its autofluorescence. This effect can be associated to the efficiency of lignin-mediated electron transfer since it is likely to be LPMO-specific. Comparison of figure 2.11C with the figures 2.11D and figure 2.11E indicates that the samples after enzymatic hydrolysis by the cocktail containing LPMO *Af*AA9B are more homogeneously shifted to red, which might suggest that electron transfer from lignin to boost *Af*AA9B activity of cellulose is contributed to this phenomenon, with the positive effects on the biomass hydrolysis yields (Figure 2.9 and Table 2.2).

2.5 Conclusions

Since the discovery of LPMOs showing that the collaborative effect of these enzymes can considerably improve the biomass saccharification by cellulases, much attention has been given to this class of enzymes, however, there is still a lack of studies focused on the analysis of its biochemical characteristics. AA9 LPMOs are abundant and widely distributed in filamentous fungi genomes showing a large variety of sequences. Therefore, thorough analysis of LPMOs still is a demand and can provide essential information to improve the biomass saccharification. The genes encoding *Af*AA9A and *Af*AA9B were successfully cloned and expressed in *A. nidulans* using pEXPYR vector. Biochemical characteristics of both LPMOs were determined and the combination of LPMOs and LPMOs-cellulases in the saccharification of pre-treated sugarcane bagasse were tested, revealing positive effects of *Af*AA9B addition resulting in a reduced enzyme load. Our CLSM analysis demonstrated that the tested LPMOs modify autofluorescence of lignin after the saccharification, indicating LPMO-mediated modifications of this macromolecule. Thus, the *A. fumigatus* var. *niveus* LPMO *Af*AA9B reveals itself as a promise candidate to be added in cocktail preparations used in the saccharification of pre-treated plant biomass.

CHAPTER III

Light boosts activity of novel LPMO from *A. fumigatus* leading to oxidative cleavage of cellulose and hemicellulose.

Based on: Velasco, J., Sepulchro, A.G.V., de Oliveira Arnoldi Pellegrini, V., Cannella, D., Cristante. L., Polikarpov, I., Segato, F., 2022. Light boosts activity of novel LPMO from *A. fumigatus* leading to oxidative cleavage of cellulose and hemicellulose. ***Under review in ACS Sustainable Chemistry and Engineering.***

3.1 Abstract

Lytic polysaccharide monooxygenases (LPMOs) are copper dependent enzymes that potentiate the deconstruction of polysaccharides through oxidative mechanism. The oxidative catalysis performed by LPMOs is dependent of a reductant to promote the divalent copper ion in the metalloenzyme to its monovalent state. In the present work, we report the biochemical characterization of a novel LPMO from *Aspergillus fumigatus* (*Af*AA9C), as well as the computational modeling of its three-dimensional structure. *Af*AA9C showed the ability to oxidize cellulose and xyloglucan being activated by light. The evaluation of different electron donors coupled to the chlorophyllin+light photosystems allowed to elucidate the existence of a collaborative effect between chemical reducing agent and light-induced electron transfer systems promoting changes in LPMO activity which is reducing agent type-dependent. These findings are of general importance for the utilization of LPMOs in reactions applying photobiocatalysis and in sustainable industrial processes such as the depolymerization of plant biomass.

Keywords: Photobiocatalysis, Lytic polysaccharide monooxygenases, Cellulose, Xyloglucan

3.2 Introduction

Microorganisms such as filamentous fungi have a relevant role in the complex decomposition and recycling of lignocellulosic materials, since these organisms are able to mediate a large number of biochemical processes which make available the carbon and other compounds entrapped in these materials (C.P. Kubicek and E.M. Kubicek, 2016; Kües, 2015). Currently, the biorefinery concept supports the implementation of renewable carbon sources such as lignocellulosic materials being considered as environmentally friendly alternative for common, oil-based refineries (Carmona-Cabello et al., 2018) . In nature, the depolymerization of these materials is catalyzed by multiple enzymes produced by myriad of microorganisms. Due to these characteristics the composting process has been a target environment for recover biomass-degrading microorganisms including those defined as thermotolerant (López et al., 2021).

The microbial metabolism under composting conditions produce heat which determines the dynamic and structure of microbial population in the environment and, depending to the microorganism adaptation during the temperatures changes at the process, most of them are defined as thermotolerant (Moreno et al., 2021). Among the fungi, *Aspergillus fumigatus* has been detected in composting process because of specific characteristics such as thermotolerance and capacity to secrete hemi- and cellulolytic enzymes allowing the fungus to proliferate efficiently (Vivek-Ananth et al., 2018). The protein machinery of *A. fumigatus* has been studied for depolymerization of plant polysaccharides due the large number of genes encoding Carbohydrate-Active EnZymes (CAZymes) in its genome, making this fungus a model specie in carbon cycle (Couger et al., 2018; Miao et al., 2015).

Environmental concerns regarding the greenhouse effect make the bioconversion of lignocellulosic materials a significant source to produce biochemicals and biofuels to achieve a circular economy in the future (Carmona-Cabello et al., 2018; Sheldon, 2014). However, the efficient conversion of this recalcitrant material requires a combined action of hydrolytic and oxidative enzymes. Then, the discovery of new and better oxidative enzymes presenting high levels of synergism with hydrolytic enzymes is fundamental to turn this process economically feasible (Obeng et al., 2017; Scheller and Ulvskov, 2010). In this scenario, lytic polysaccharide monooxygenases (LPMOs) emerged as promising biocatalysts assisting hydrolytic enzymes in the depolymerization of polysaccharides. Currently, these proteins are classified as auxiliary activity enzymes (AA) in the CAZy database within families AA9-AA11; AA13-AA17 (Sabbadin et al., 2021). Previously, it

has been demonstrated that LPMOs from family AA9 improve the catalytic efficiency of cellulases and increase the saccharification yields of biomass polysaccharides (Harris et al., 2014). Therefore, LPMOs are able to boost the capacity of cellulolytic cocktails, thus allowing improvements in the general process that generate value-added products from plant biomass. Although the entire molecular mechanisms of LPMO still not fully elucidated, discovery of these enzymes resulted in a biotechnological shift in the production of biofuels turning themselves into essential components of new generations of industrial cocktails applied for biomass saccharification (Johansen, 2016).

The three-dimensional structures of LPMOs share an immunoglobulin-like β-sandwich fold having an active site exposed at the surface that coordinate the copper atom by a conserved His-brace structure, which still is a paradigm for LPMOs (Beeson et al., 2015; Hemsworth et al., 2015; Tandrup et al., 2018). As exemplified by other CAZymes, LPMOs can also harbor a carbohydrate binding module (CBM family 1 and/or 18) attached by a linker at C-terminal region of the catalytic domain (Lenfant et al., 2017). Previous sequence analysis demonstrated that LPMOs also can carry modules of unknown function (X278, X280, X281 and X283), tandem-associated or not to the CBMs (Lenfant et al., 2017). More recently, C-terminal disordered extensions not found in other CAZymes were reported for LPMOs (Tamburrini et al., 2021).

The oxidative cleavage of the cellulose mediated by LPMOs depends on the presence of chemical or biological agents to reduce the copper atom (Cu II $\rightarrow$ Cu I) at the catalytic site. So far, most of studies report the use ascorbic acid as reducing agent, however these enzymes demonstrate a certain promiscuity in accepting electrons from different sources (lignin-derived phenols, enzymes and prosthetic groups) (Brenelli et al., 2018; Kracher et al., 2016; Westereng et al., 2015). Interestingly, comparisons among the reducing agents showed a differential amount of oxidized and non-oxidized oligosaccharides released as products from cellulosic substrate, apparently indicating the existence of a complex and poorly understood phenomenon governing the electron donation to LPMOs (Agger et al., 2014; Beeson et al., 2012; Kadowaki et al., 2018; Velasco et al., 2021).

Recently, an alternative mechanism for electron transfer to LPMOs driving the catalytic process involves the use of light-induced system, comprising a photosensitizer only or in combination with reducing agents leading to a significant improvement in the efficiency of the process (Bissaro et al., 2016; Cannella et al., 2016). Light is widely available and sustainable energy source to improve the catalytic process promoted by LPMOs in biomass saccharification, which makes it very attractive (Blossom et al., 2020; Labourel et al., 2020;

Maciá-Agulló et al., 2015). However, Photo-LPMO-Catalysis (PLC) reaction systems are highly complex due to the number of variables involved in the process such as the type of reducing agent (if present), photosensitizer, light intensity, LPMO autoxidation, generation/accumulation of reactive oxygen species (ROS), and the cross-effects among these variables.

It was initially postulated that ROS did not play a role in light driven LPMO reactions (Möllers et al., 2017). However, it is known that photo-excited chlorophyllin can reduce O_2 to $O_2^{\bullet-}$ in PLC systems resulting in spontaneous conversion to H_2O_2 by disproportionation or by chemical reduction promoted by reducing agent (*e.g.* ascorbic acid) (Bissaro et al., 2020; Nishikimi, 1975). H_2O_2 plays a dual role in catalysis (activation/deactivation). On one hand, LPMOs can efficiently use it as co-substrate to increase its catalytic effect to oxidize polysaccharides (Bissaro et al., 2017; Müller et al., 2018). On the other hand, high levels of H_2O_2 are harmful to LPMO since they promote an autoxidation of the catalytic site and deterioration of the photosensitizer (Bissaro et al., 2017). The presence of ascorbic acid in PLC system contribute to H_2O_2 production, but is affected by light intensity which impact in the effect exerted on the system by (*i*) priming reduction of LPMO; (*ii*) reduction of $O_2^{\bullet-}$ to H_2O_2 and (*iii*) H_2O_2 production in reaction with metals as free copper (commonly present in LPMO reactions), turning PLC system dependent of an appropriate balance in all these parameters (Bissaro et al., 2020; Stepnov et al., 2021).

Until recently, only few studies reported the use of different reducing agents in combination with light system (Cannella et al., 2016). The current work reports the three-dimensional model, the functional characterization of an AA9 LPMO from *A. fumigatus* var. *niveus* (*Af*AA9C) and the evaluation of three different reducing agents combined with light-induced electron transfer system composed by chlorophyllin to investigate the mutual influence on the oxidative activity of *Af*AA9C on cellulose and hemicellulose.

3.3 Materials and methods

3.3.1 Sequence, computational analysis and homology molecular modeling

The sequences of LPMOs from family AA9 from *A. fumigatus* var. *niveus* (*Af*AA9C) and *Thermoascus aurantiacus* (*Ta*AA9A) (accession numbers KEY80276 and ACS055720, respectively), were obtained from National Center for Biotechnology Information (NCBI, Bethesda, MD, USA). The domains were validated with InterProScan software (Jones et al., 2014) and the potential sites for N- and O-glycosylation were verified based in amino acid

sequence of mature protein at NetNGlyc 1.0 and NetOGlyc 4.0 Servers using default parameters (Steentoft et al., 2013). The analysis of secretion signal peptide was performed at SignalP-5.0 Server. Molar mass, extinction coefficient and isoelectric point (pI) were determined by ProtParam tool (Gasteiger et al., 2005).

A three-dimensional model of *Af*AA9C was built using Robetta (Kim et al., 2004) and I-TASSER web servers employing the primary sequence without the signal peptide (Yang et al., 2015). The copper position was selected based on structural alignment with the templates from *T. aurantiacus*, *A. fumigatus*, *Talaromyces verruculosus*, *Trichoderma reesei*, *Malbranchea cinnamomea*, *Neurospora crassa* and *Heterobasidium irregulare* (PDB ids: 2YET:A, 6HA5:A, 6H1Z:A, 5O2W:A, 4EIS:B and 5NNS:A.

The reasonableness of selected model was evaluated using the score function provided by QMEAN (Benkert et al., 2011) and QMEANDisCo (Studer et al., 2020) varying from 0 to 1, where higher values indicate more reliable models. The constructed model was also compared with the cellulose-specific LPMO from *T. aurantiacus* (*Ta*AA9A - PDB id: 2YET:A), which presents high coverage and percentage of identity in the crystallographic structure. Protein representations were prepared using UCSF Chimera v 1.16 and the electrostatic surface potential calculated through DELPHI web server using standard parameters and setting up the salt concentration to 1 mM to allow the net neutralization under the evaluated pH. The partial charges were assigned via PDB2PQR through APBS web server accordingly to AMBER force field (Dolinsky et al., 2007; Pettersen et al., 2004; Sarkar et al., 2013). Primary sequence evaluations and representations were produced using ALINE editor with secondary structure calculations using DSSP (Bond and Schüttelkopf, 2009; Touw et al., 2015).

3.3.2 Microbial strains and culture conditions

The *A. fumigatus* var. *niveus* strain was kindly provided by Prof. Rolf Prade from Oklahoma State University (Stillwater, OK, USA). *A. nidulans* strain A773 (*pyrG89*; *wA3*; *pyroA4*) was purchased from Fungal Genetic Stock Center (FGSC, Manhattan, KS, USA). Both *A. fumigatus* and *A. nidulans* A773 were cultivated in minimal medium composed of salt solution, trace elements, 1% (w/v) glucose, pH 6.5. For *A. nidulans* A773 the medium was supplemented with pyridoxine, uracil, and uridine, as previously described (Segato et al., 2012). *Escherichia coli* Turbo strain (New England BioLabs, Ipswich, MA, USA), used for plasmid replication was cultivated in 50 ml centrifuge tube containing 10 ml of Lysogeny

Broth (LB) medium added by ampicillin (100 µg/ml) at 37 °C and 180 rpm for 16 h. For heterologous protein expression, the recombinant strain was cultivated in liquid minimal medium supplemented with 3% (w/v) maltose and pyridoxine (1 mg/L) for 2 days at 37 °C without shaking (Velasco et al., 2020).

3.3.3 Construction of pEXPYR-*Af*AA9C plasmid and transformation

The gene sequence encoding the full-length *Af*AA9C including introns and signal peptide (accession number XM_747533/AFUA_1G12560A) was amplified by polymerase chain reaction (PCR) using genomic DNA (gDNA) from *A. fumigatus* var. *niveus* extracted with Wizard Genomic DNA Purification kit (Promega, Madison, WI, USA) as template. The PCR amplified fragment was obtained using Phusion® High-Fidelity DNA Polymerase (New England Biolabs) with the oligonucleotides (Exxtend Biotechnology Ltd., Campinas, SP, Brazil) AFAA9C forward (5'-**CATTACACCTCAGCA**ATGTCTGTCCCTAAGATTGCA-3') and AFAA9C reverse (5'-**GTCCCGTGCCGGTTA**CTAAGCAGAGAGATCACGAGCGTGCACCTT-3'), containing specific regions (in bold) to allow the gene insertion into pEXPYR expression vector by Gibson Assembly® method as previously described (Gibson et al., 2009; Velasco et al., 2019, 2020). The resulting reaction was used to transform Mg^{+} competent *E. coli* Turbo® cells (New England BioLabs) by heat-shock and the resulting ampicillin-resistant colonies were randomly screened by colony PCR technique. A positive clone was cultured as previously described to propagate the recombinant plasmid, followed by extraction with Wizard Plus SV Minipreps DNA Purification System kit (Promega). Approximately 20 µg of the recombinant plasmid containing the gene for *Af*AA9C was transformed into *A. nidulans* A773 (FGSC, *pyrG89; wA3; pyroA4*) by integration mediated by polyethylene glycol (PEG) (Segato et al., 2012; Tilburn et al., 1983). The resulting *A. nidulans* recombinant strains were selected by the replacement in *pyrG89* gene which revert uracil and uridine auxotrophic marker and a strain showing the capacity to secrete *Af*AA9C in the expression medium was used to produce the recombinant protein as previously described (Berto et al., 2019).

3.3.4 Heterologous expression, purification and identification of recombinant *Af*AA9C

For spore production the recombinant strains for *Af*AA9C was inoculated in a Petri dish containing solid minimal medium added with pyridoxine and incubated as previously described. The spores were harvested with a spatula and transferred to a 50 ml centrifuge tube containing saline solution (0.9% NaCl). Approximately 10 ml of saline solution containing 10^7 to 10^8 spores/ml was used to inoculate 1 L of minimal medium supplemented with pyridoxine (1 mg/L) and maltose 3% (w/v), which was distributed in 250 ml trays, followed by incubation at 37 °C for 2 days without agitation (Berto et al., 2019; Velasco et al., 2021). Next, the medium was recovered by filtration through the qualitative membrane to remove mycelia and cell debris (Miracloth, MilliporeSigma, Burlington, MA, USA). The filtered medium containing *Af*AA9C was concentrated 10-fold by ultrafiltration using an Amicon® Stirred Cell device coupled with a 10 kDa cut-off polyethersulfone (PES) membrane (MilliporeSigma).

The recombinant *Af*AA9C was purified in two chromatographic steps, which included an ion exchange and a size exclusion as previously described (Berto et al., 2019). Purified protein was saturated with copper by incubating the enzyme in $CuSO_4$ solution for 30 min at 16 °C, in a molar ratio of 3:1 (copper:*Af*AA9C). Subsequently, the protein was loaded into an ÄKTA Pure M25 system coupled with a HiLoad 16/600 Superdex 75 pg size exclusion column (Cytiva Life Sciences) to remove unbound copper ions. The resulting sample was evaluated in SDS-PAGE followed by Breslmayr assay method using 2,6-dimethoxyphenol (2,6-DMP) as substrate which is able to detect the LPMO peroxidase activity (Breslmayr et al., 2018). In mode to confirm the recombinant protein, the band corresponding to *Af*AA9C on SDS-PAGE was excised, reduced, alkylated and analyzed by LC-MS/MS at Mass Spectrometry Facility of Brazilian Biosciences National Laboratory (LNBio) from Brazilian Center for Research in Energy and Materials (CNPEM, Campinas, SP, Brazil) (Shevchenko et al., 1996)

3.3.5 Thermal shift assay (Thermofluor)

Thermofluor was employed to evaluate *Af*AA9C stability in different conditions (buffers and temperatures). The analyses were performed by mixing 10 µM of enzyme with 40 µM of SYPRO™ Orange dye (ThermoFisher). The thermal stability of *Af*AA9C was evaluated in 48 different conditions incubated in temperatures ranging from 25 to 95 °C with increments of 1 °C per min. The concentration of buffer solutions in the reactions was 50

mM and 300 mM for NaCl when added. The reactions were monitored by following changes in fluorescence using a CFX96 Touch Real-Time PCR Detection System (Bio-Rad, Hercules, CA, USA). The melting temperature (Tm) averages were calculated by measuring the fluorescence in the tested conditions using an excitation and emission wavelengths of 490 nm and 530 nm, respectively.

3.3.6 Biochemical characterization of *Af*AA9C

The purified *Af*AA9C was tested for the presence of cellulases and xylosidase contaminants using specific substrates. Reactions were performed with 1 µM of enzyme and 0.25% of carboxymethylcellulose (CMC) and/or 1 mM of synthetic substrates 4-nitrophenyl β-D-glucopyranoside (*p*NPG), 4-nitrophenyl β-D-cellobioside (*p*NPC) and 4-nitrophenyl β-D-xylopyranoside (*p*NPX) (Sigma-Aldrich) in 50 mM sodium phosphate buffer pH 5.0. Reactions were incubated at 50 °C for 30 min at 1000 rpm in a Thermomixer (Eppendorf), afterwards 1 M sodium carbonate was added and the absorbance of *p*NP released was read at 405 nm (Textor et al., 2013).

To monitor the reducing sugars released in reactions with CMC, 100 µl of 3,5-dinitrosalicylic acid (DNS) was added to 100 µl reaction, the mixture was boiled for 5 min and the absorbance read at 545 nm (Miller, 1959). Besides to evaluate the oxidative activity of *Af*AA9C and the absence of cross activity of cellulases and hemicellulases, assays using cellulosic and hemicellulosic substrates were performed including controls without the addition of reducing agent. The products released by *Af*AA9C in the reactions were analyzed by HPAEC-PAD (High-Performance Anion-Exchange Chromatography with Pulsed Amperometric Detection, ICS5000+, ThermoFisher, Waltham, MA, USA).

To determine the optimal temperature of *Af*AA9C, the reactions were incubated for 10 min in different temperatures (30 to 60 °C) in 100 mM phosphate/succinate buffer, pH 7.0 using 2,6-DMP as substrate. The effect of pH on *Af*AA9C peroxidase activity was monitored using 100 mM sodium acetate (pH 4.0 – 6.0), 100 mM sodium phosphate (pH 7.0) and 100 mM sodium borate (pH 8.0 – 10.0) buffers, followed by absorbance measurements at a wavelength of 469 nm at 30 °C for 30 min with intervals of 15 sec. To assess the effect of pH on catalytic stability of *Af*AA9C, 1 µM of enzyme was incubated in 100 mM phosphate/succinate buffer pH 6.0, 7.0 and 8.0 for 0.5, 1, 3, 6, 16 and 24 h at room temperature. After incubation, the peroxidase activity of *Af*AA9C was measured and

compared to the activity of the enzyme without incubation at previously mentioned conditions.

In order to evaluate the oxidative behavior of *Af*AA9C on cellulose at different pH, reactions using 5% Avicel PH-101 (w/v) as substrate (Sigma-Aldrich), 2 μM of copper saturated enzyme, and 1 mM ascorbic acid (AscA) as a reducing agent were performed. The reactions were incubated at 40 °C in 100 mM phosphate/succinate buffer (pH 5.0 and 7.0) for 16 h, samples were withdrawn, boiled at 95 °C for 5 min, centrifuged at 9,600 × *g* for 10 min at 4 °C and separated from insoluble fraction by filtration in a 0.22 μm syringe filter (Whatman Cytiva, Maidstone, UK). Products were analyzed by HPAEC-PAD system equipped with a Dionex CarboPac™ PA1 guard column (4 × 50 mm) and a Dionex CarboPac™ PA1 analytical column (4 × 250 mm) in a Dionex ICS5000+ (ThermoFisher). Non-oxidized cello-oligosaccharides were purchased from Megazyme® and C1-oxidized cello-oligosaccharides were prepared using iodine oxidation and used as standards (Keller et al., 2020). The chromatograms were recorded and analyzed using Chromeleon 7.0 software (ThermoFisher).

The activity of *Af*AA9C on different carbohydrates was evaluated using Avicel PH-101, phosphoric acid swollen cellulose (PASC) prepared from Avicel PH-101 as described by Wood (1988), bacterial cellulose, filter paper, and xyloglucan from tamarind seed (Megazyme®) as substrates. The reactions were composed by 1 μM *Af*AA9C, 0.3% (w/v) of each substrate mixed in 20 mM sodium phosphate buffer pH 6.0 using 1 mM AscA as reducing agent. Reactions were incubated for 2 h at 50 °C, 1000 rpm in a Thermomixer and resulting products analyzed by HPAEC-PAD as described above. The influence of different reducing agents in *Af*AA9C activity was evaluated using AscA, L-cysteine (L-cys) and pyrogallic acid (PyrA) in a final concentration of 1 mM. The reactions were incubated for 0.5, 1 and 2 h using PASC and xyloglucan as substrate in previously mentioned conditions and released products were analyzed by HPAEC-PAD.

3.3.7 Light activation of *Af*AA9C

The effect of chlorophyllin/light (Chl/light) in the activity of *Af*AA9C was first evaluated as a function of time for 10, 30 and 60 min using 0.3% of PASC (w/v), 1 μM of *Af*AA9C in 20 mM sodium phosphate buffer pH 6.0 at 50 °C and 1000 rpm. Reactions were set in the presence or absence of 1 mM AscA as a reducing agent with 500 μM of Chl and released

products were analyzed by HPAEC-PAD. A stock solution of Chl 50 mM was freshly prepared prior each experiment and maintained at 4 °C in the dark. Before beginning of the reactions, the solution was thawed in the dark at room temperature for 1 h to dissipate possible photoinduced pigments. For all reactions using light, the average photon irradiance in the system was 220.8 μmol/sec (22.08 $W.m^{-2}$). Reactions were placed at 50 °C for 10 min before activation by light and/or addition of reducing agent (Blossom et al., 2020; Cannella et al., 2016). The reactions were performed in triplicate and a control was used for each one.

Subsequently, the effect of AscA, L-cys and PyrA as electron donors coupled to the Chl/light system on *Af*AA9C activity was evaluated using PASC and xyloglucan as substrates. Reactions were performed at 50 °C for 30 min and 1000 rpm in a Thermomixer using 0.3% of PASC or xyloglucan (w/v) and 1 mM of each reducing agent. Light intensity, pH, protein load and Chl addition were the same used in the previous experiment. Controls were employed for each reaction; the darkness control experiments were performed in dark conditions from Chl preparation to the sample centrifugation for soluble/insoluble fraction separation before products detection by HPAEC-PAD.

3.4 Results and discussion

3.4.1 *In silico* evaluation of *Af*AA9C model

The LPMO *Af*AA9C has 373 residues of which the first 19 comprise the signal secretion peptide (Figure 3.1A). After post-translational modification the mature *Af*AA9C consists of 354 residues (from His1 to Ala354) with a predicted molecular weight of 36.6 kDa and a pI of 4.8. The AA9 domain comprise 226 residues (His1 to Tyr226), according to the alignment with the model LPMO TaAA9 from *T. aurantiacus* (Figure3.2A). In addition, *Af*AA9C presents at the C-terminus an extra region of 128 residues (Ser227 to Ala354) that cannot be ascribed to any annotated function and has been described as a disordered region present in LPMOs and lacking in other CAZymes (Tamburrini et al., 2021). The recombinant protein showed 2 and 48 sites for N- and O-glycosylation, respectively with 45 out of the 50 predicted glycosylation sites located on the disordered regions at the C-terminus (128 residues, Figure 3.1).

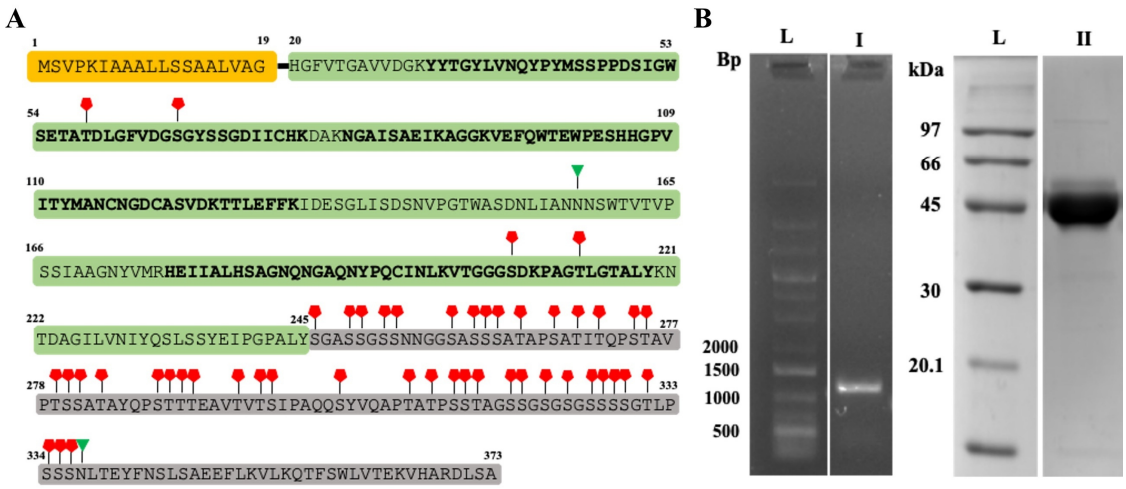

Figure 3.1. (**A**) *Af*AA9C sequence, signal peptide (yellow box), catalytic domain (green box), extra region (gray box) predicted *O*-glycosylation (red pentagon) and *N*-glycosylation (green triangle) sites. The amino acids highlighted in bold were identified by LC-MS/MS. (**B)** gene cloning and protein expression, L: ladder, I: *Af*AA9C gene, II: *Af*AA9C LPMO.

There are evidences that some CAZymes can have intrinsically disordered regions (IDRs) in their structures. Indeed, recent computational analyses showed that LPMOs from families AA9 to AA16 display extensions at C-terminus which are not present in other CAZymes (Tamburrini et al., 2021). From 7 AA9 LPMOs encoded by *A. fumigatus* var. *niveus*, 3 harbor a CBM1 (KEY80517, KEY83569 and KEY77159), 2 show a short sequences commonly found in this family (KEY82006 and KEY76044), and the other 2 have extensions at the C-terminal region which do not show similarity with other domains (KEY81994 and KEY80276-*Af*AA9C) (Figure 2.1) (Velasco et al., 2021). The extension of *Af*AA9C presented a remarkable Ser, Thr, Ala and Pro rich region comprising 25.2, 14.2, 12.6 and 6.3% of the sequence which is characteristic of IDRs, corroborating with glycosylation prediction (Tamburrini et al., 2021). An analysis against the GenBank showed the IDR region from *Af*AA9C has similarity only with proteins from other *Aspergillus* species (Table 3.1)

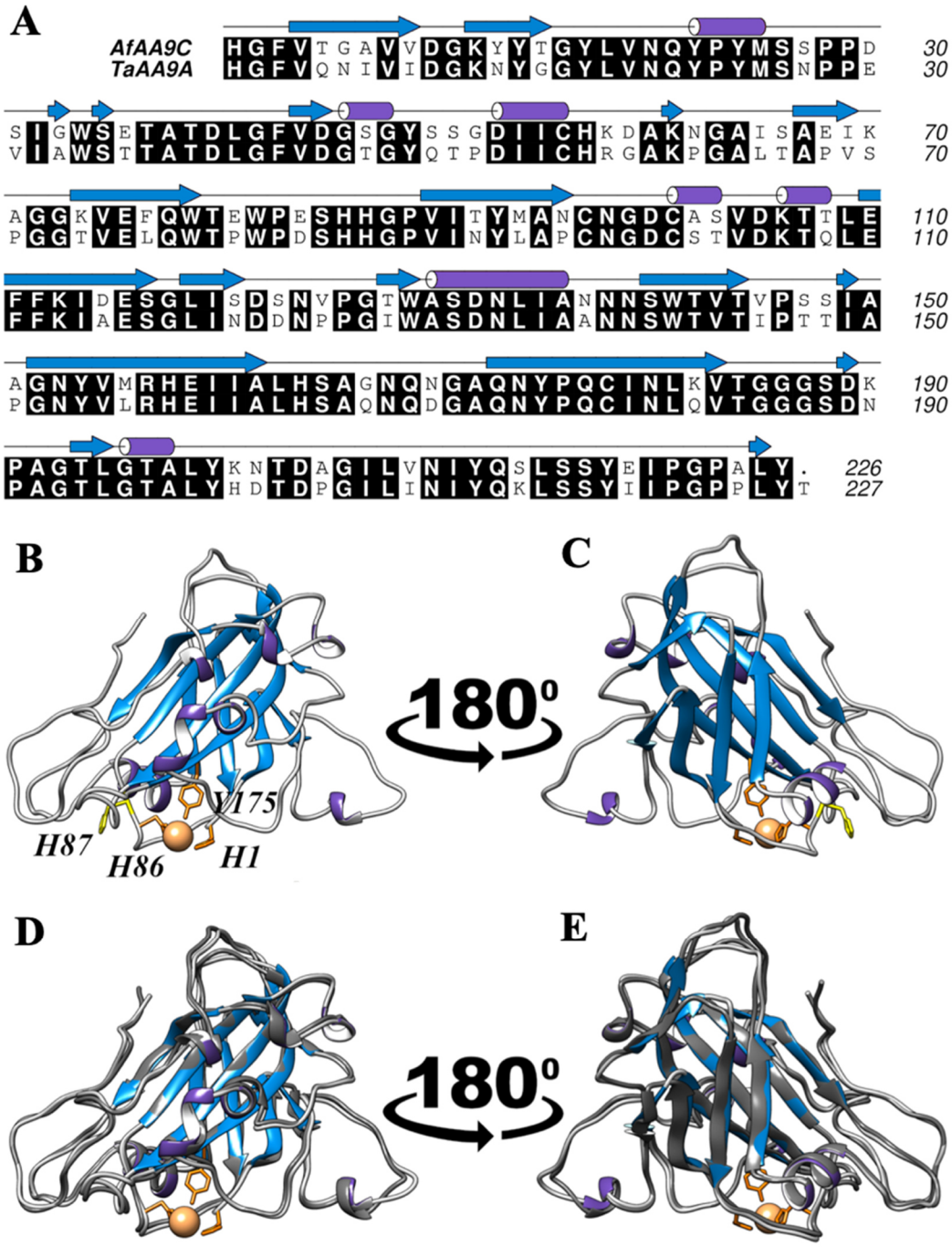

Figure 3.2. Computational modeling of *Af*AA9C LPMO. (**A)** Alignment of *Af*AA9C primary sequence against *Ta*AA9A highlighted by identity. Over the primary sequence there is a representation of the secondary structure (DSSP calculation) that follows the color pattern indicated in **B** and **C**. **(B)** Cartoon representation of *Af*AA9C tridimensional model based on residues 1 to 226 (neglecting the signal peptide sequence). Alpha helices, beta sheets and coils are in purple, blue and white, respectively. The residues *H1*, *H86* and *Y175* are labeled and represented by sticks in orange as well as the residue H87 in yellow. The cooper ion was positioned based on the alignment of homologue proteins and represented by a sand color sphere. (**C)** Tridimensional representation of the model rotated by 180° around its Y-axis. **(D)** Structural alignment of *Af*AA9C model against *Ta*AA9A crystal structure (in gray) and **(E)** its rotation by 180° around its Y-axis.

Table 3.1. Results of BLASTp from the extra region of *Af*AA9C against the GenBank. The results returned similarity only with sequences from other *Aspergillus* species. Excepted the synthetic construction from *Talaromyces cellulolyticus*. QC – query coverage.

Accession	Description	e-value	QC (%)	*Aspergillus* species
XP_752626	putative endoglucanase	8e-75	100	*A. fumigatus* Af293
XP_033411806	endoglucanase-4	3e-39	85	*A. lentulus*
XP_043127715	uncharacterized protein	2e-38	82	*A. viridinutans*
GFF87836	endoglucanase-4	5e-38	82	*A. udagawae*
KAF7161613	hypothetical protein	1e-36	82	*A. felis*
XP_001264507	putative endoglucanase	3e-35	82	*A. fischeri* NRRL 181
QDK56837	AA9 synthetic construct	3e-35	82	*Talaromyces cellulolyicus*
XP_026617457	hypothetical protein	1e-34	84	*A. thermomutatus*
KAF4219826	hypothetical protein	2e-31	81	*A. fumigatiaffinis*
XP_024682709	putative endoglucanase	2e-31	82	*A. novofumigatus* IBT 16806
XP_043154526	uncharacterized protein	8e-31	82	*A. pseudoviridinutans*
KAF7113654	hypothetical protein	2e-22	65	*A. hiratsukae*
XP_025550284	hypothetical protein	8e-20	90	*A. homomorphus* CBS 101889
XP_024698912	uncharacterized protein	1e-19	74	*A. steynii* IBT 23096
XP_001269010	putative endoglucanase	2e-18	100	*A. clavatus* NRRL 1
XP_025491679	hypothetical protein	2e-18	90	*A. uvarum* CBS 121591
XP_025506867	hypothetical protein	2e-18	89	*A. aculeatinus* CBS 121060
PYI08701	hypothetical protein	5e-18	90	*A. sclerotiicarbonarius* CBS 121057
XP_040797861	endoglucanase	5e-17	82	*A. fijiensis* CBS 313.89
XP_025445904	hypothetical protein	5e-17	82	*A. brunneoviolaceus* CBS 621.78
XP_025524161	hypothetical protein	2e-16	82	*A. japonicus* CBS 114.51
EHA18110	hypothetical protein	1e-14	77	*A. niger* ATCC 1015
XP_001818766	unnamed protein product	3e-14	75	*A. oryzae* RIB40
XP_041149593	uncharacterized protein	6e-14	75	*A. flavus* NRRL3357
XP_001210534	endoglucanase IV precursor	2e-10	30	*A. terreus* NIH2624

For *Af*AA9C modeling, the IDR of the primary sequence was excluded allowing to build a more robust three-dimensional model for the sequence corresponding to the region of AA9 domain. In order to do so, the primary sequence (Figure 3.2A) was submitted to Robetta and I-TASSER web servers. Since the best models provided were practically identical, the

result from Robetta was chosen (Figure 3.2B and C). Next, the model quality was evaluated via QMEAN4 and QMEANDisco, resulting in 0.90 and 0.86 ± 0.06 values, respectively, indicating that the modeling procedure returned a reliable three-dimensional model for *Af*AA9C. The presence of extra regions containing modules appended to the catalytic domain has already been described for LPMOs from families AA9, AA11 and AA16 (Filiatrault-Chastel et al., 2019; Lenfant et al., 2017; Semenova et al., 2020). In the case of AA9 LPMOs the non-CBM modules such as X278 and X280-X282 at the C-terminus region have been identified, however, their biological function remains unknown (Lenfant et al., 2017). Another interesting feature found in the proposed model is the high similarity (75%) of the catalytic domain of *Af*AA9C with *Ta*AA9A (Figure 3.2 A, D and E), including the configuration of the active site of both proteins and the presence of the conserved residues His86 and His87 (orange and yellow sticks at Figure 3.2B and C) also present in other *A. fumigatus* LPMOs (Velasco et al., 2021). The His87 residue has been proposed as part of a possible electron transfer pathway in AA9 family forming a putative tunnel with His86 (copper ion coordination motif) to deliver electrons from external regions to the active site of the protein (Cannella et al., 2016; Onuchic et al., 1992). The long amino acid pathway, which is followed by outer electrons to reach the copper atom at the active site of LPMOs (either by direct delivery, via long-range transfer, or both) forms a basis for the hypothesis, which however still has to be proved experimentally (Cannella et al., 2016; Wang et al., 2021).

3.4.2 Gene cloning, heterologous expression and identification of *Af*AA9C

The genomes of biomass-degrading microorganisms contain hundreds of genes encoding proteins highly specialized in plant biomass deconstruction, which are grouped in many CAZyme families. Genes encoding AA families are very abundant in their genomes especially those from AA9 with some species harboring over 20 genes (Fig. 3.3) (Berka et al., 2011). In *Aspergillus* species the AA9 encoding genes can be present in copy numbers ranging from 6 to 12 in *A. clavatus*, *A. flavus*, *A. nidulans* and *A. terreus*, or in cases like the thermotolerant species *A. niger* and *A. fumigatus* which harbor 7 copies of genes encoding AA9 LPMO each (Segato et al., 2014b; Velasco et al., 2021). From the 7 genes encoding AA9 LPMO in *A. fumigatus* (*Af*AA9A to *Af*AA9G), only *Af*AA9A and *Af*AA9B were well studied and described so far, with the remaining 5 genes to be investigated and explored

(Leggio et al., 2018; Velasco et al., 2021). *A. fumigatus* is commonly found in biomass composting communities and occurs in all stage of composting maturation, thus containing strains with mesophilic or thermotolerant characteristics (Couger et al., 2018; López et al., 2021). Due to its characteristics and versatility, the secretome of *A. fumigatus* cultured in different polysaccharides as carbon sources have been investigated, demonstrating this microorganism is able to secrete a large range of CAZy proteins to the extra cellular medium including LPMOs from family AA9, among them the *Af*AA9C (Gouvêa et al., 2018).

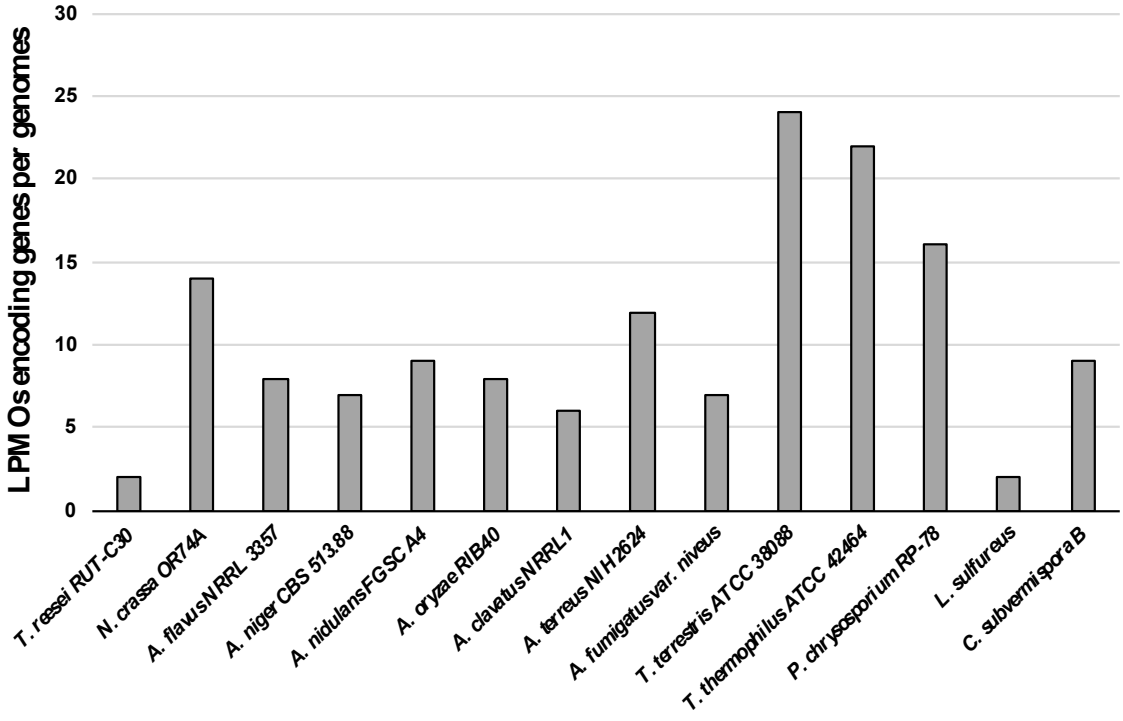

Figure 3.3. Evaluation of number of genes encoding LPMOs from family AA9 in the genome of filamentous fungi of relevance. The data was compiled from NCBI, MycoCosm and CAZy databanks.

The *Af*AA9C gene was successfully amplified by PCR from gDNA of *A. fumigatus* var. *niveus* (Figure 3.1B, lane I), cloned into pEXPYR vector by Gibson Assembly® method, transformed and expressed in *A. nidulans* A773 (Velasco et al., 2019, 2020). The recombinant LPMO shows a molecular weight (MW) of approximately 45 kDa, as indicated in the SDS-PAGE analysis (Figure 3.1B, lane II). The evaluated size of the recombinant protein is larger than that predicted *in silico* (36.7 kDa) this difference can be associated to the post-translational modifications such as glycosylation which frequently occur in *A. nidulans* (Rubio et al., 2016). Considering LPMOs were formerly classified as endoglucanases from CAZy family GH61 (Levasseur et al., 2013), the LC-MS/MS analysis of the recombinant protein identified *Af*AA9C as an endoglucanase from *A. fumigatus* in

GenBank, using MASCOT search engine software, showing 9 identified peptides with a coverage of 38% (highlighted in bold on Figure 3.1A).

3.4.3 Analysis of temperature and pH effect in *Af*AA9C activity

After purification, fractions containing the recombinant enzyme were pooled and used for further experiments. The assay with purified *Af*AA9C did not show any residual cellulase or hemicellulose activities on specific substrates such as CMC, *p*NPG, *p*NPC and *p*NPX under experimentally tested conditions. Furthermore, the enzyme was also tested using PASC and xyloglucan as putative substrates without the addition of reducing agent but the HPAEC-PAD analyses did not show any contamination with cellulases or hemicellulases. *Af*AA9C saturated with copper was submitted to Thermofluor analysis using several buffers (Table 3.2) demonstrating an apparent melting temperature of 45 °C in sodium citrate buffer pH 5.5 supplemented by 300 mM NaCl (Figure 3.4A). The assays also detected conditions not favorable for the enzyme stability, as manifested by lower Tm values (Table 3.2).

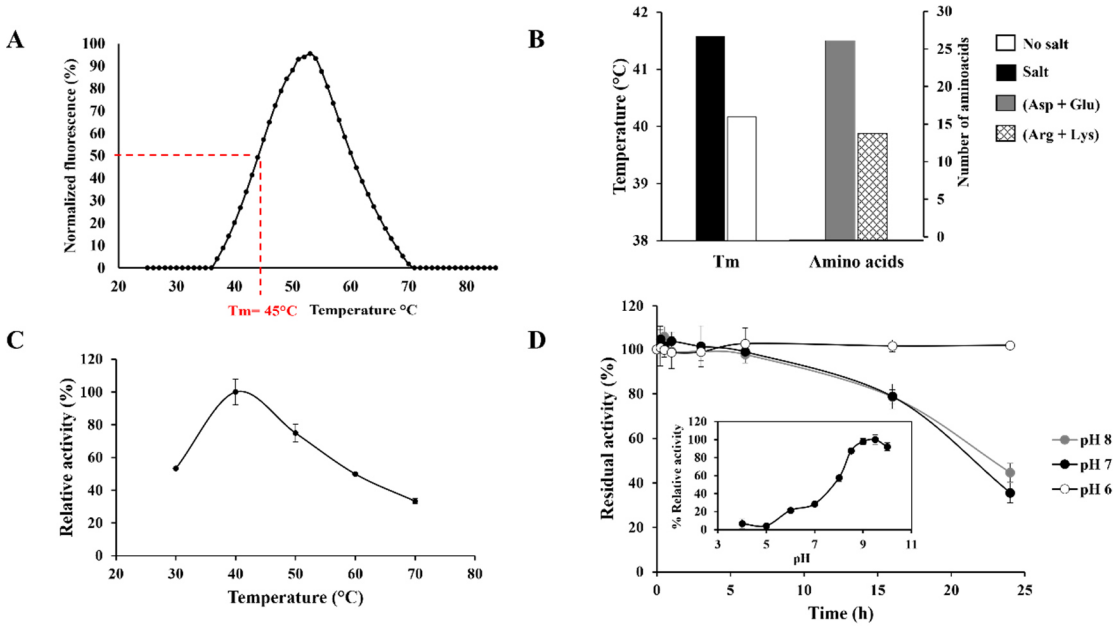

Figure 3.4. A) *Af*AA9C thermal denaturation in sodium citrate buffer pH 5.5 and 300 mM of NaCl; (**B**) correlation in Tm average and (Asp + Glu)/(Arg + Lys) ratio; (**C**) *Af*AA9C optimal temperature and (**D**) effect of pH on catalytic stability, inset pH curve.

Table 3.2. *Af*AA9C melting temperatures measured by thermal shift assay. ND: no detected

pH	Buffer (50 mM)	NaCl (mM)	Tm °C
-	H_2O	0	44.0
5.0	Phosphate/succinate	0	43.0
2.0	HCl	0	43.0
7.0	Phosphate/succinate	0	26.0
4.0	Sodium citrate	0	43.0
4.5	Sodium acetate	0	42.0
4.7	Sodium citrate	0	42.0
5.0	Sodium acetate	0	44.0
5.0	Potassium phosphate	0	43.0
5.5	Sodium citrate	0	41.0
5.5	Sodium Phosphate	0	43.0
5.8	MES	0	41.0
6.0	Potassium phosphate	0	43.0
6.0	Bis-Tris	0	42.0
6.2	MES	0	40.0
6.5	Sodium phosphate	0	43.0
6.5	Sodium cacodylate	0	ND
6.5	Bis-Tris	0	42.0
6.5	MES	0	42.0
6.7	Bis-Tris	0	42.0
7.0	Potassium phosphate	0	43.0
7.0	HEPES	0	43.0
7.0	Bis-Tris	0	42.0
7.3	Ammonium acetate	0	39.0
7.5	Sodium phosphate	0	40.0
7.5	Tris	0	40.0
8.0	Imidazole	0	37.0
8.0	HEPES	0	40.0
8.0	Tris	0	40.0
8.0	Bicine	0	40.0
8.5	Tris	0	38.0
9.0	Bicine	0	39.0
9.5	Sodium carbonate	0	26.0
10.0	Sodium carbonate	0	26.0
3.0	Citric acid	300	26.0
4.5	Sodium acetate	300	40.0
5.0	Potassium phosphate	300	44.0
5.5	Bis-Tris	300	44.0
5.5	Sodium citrate	300	45.0
5.8	MES	300	43.0
6.0	Bis-Tris	300	43.0
6.5	Sodium cacodylate	300	44.0
6.5	Sodium phosphate	300	44.0
7.0	Bis-Tris	300	43.0
7.0	HEPES	300	43.0
7.3	Ammonium acetate	300	44.0
7.5	Tris	300	42.0
8.0	HEPES	300	42.0

The role of copper ion in the protein structure mobility is important since the absence of metal ion in the protein active site can reduce the enzyme stability, resulting in the reduction of Tm and a loss of activity (Sabbadin et al., 2021). In summary, an addition of NaCl promoted a positive effect on protein stability increasing the averaged Tm in 1.5 °C. This behavior may be related to the presence of solvent-exposed acidic amino acids such as aspartic acid (Asp) and glutamic acid (Glu) on the protein surface (Figure 3.4B and Figure 3.5) (Li et al., 2017; Nakamura et al., 2018). The acidic amino acid residues at the surface of the protein can generate a negative electrostatic potential in the protein surface improving its solvation (Kern et al., 2013; Siglioccolo et al., 2011)

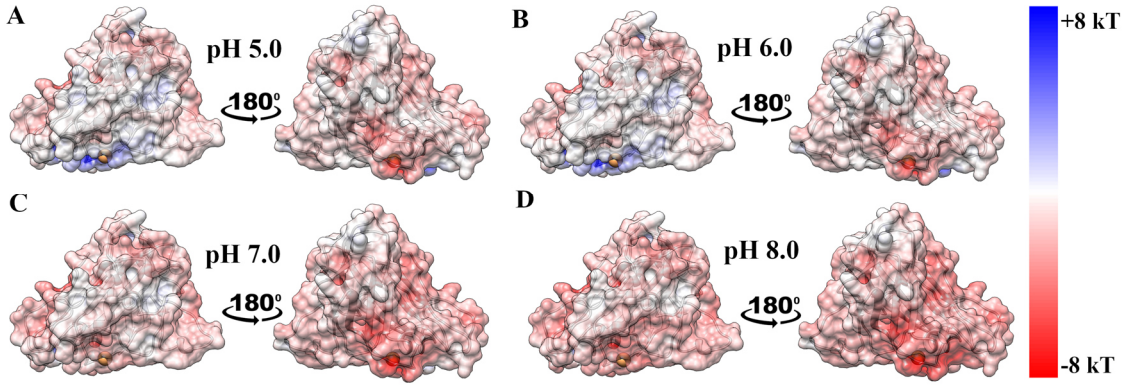

Figure 3.5. Surface representation colored by the electrostatic potential from -8 *kT* (red) to 8 *kT* (blue) as presented in the right color bar for the pH 5.0 (A), 6.0 (B), 7.0 (C) and 8.0 (D) in 1 mM salt concentration. Inside the surface a cartoon representation is presented to facilitate the visualization of the orientation. The copper ion is presented as a sand color sphere.

Analysis in the ratio of acidic to basic amino acid residues (Asp+Glu / Arg+Lys) in the enzyme primary structure showed that *Af*AA9C contains two times more Asp+Glu as compared to Arg+Lys residues (Figure 3.4B). The surface electrostatic potential of *Af*AA9C calculated using DELPHI web server demonstrated that *Af*AA9C has a significant charge distribution at its surface with a higher number of acidic amino acid residues, corroborating with our previous results (Figure 3.5).

The peroxidase activity of *Af*AA9C was highest at 40 °C and maintained 75% of its relative activity at 50 °C (Figure 3.4C). Using Breslmayr 2,6-DMP method, Zhang et al. 2019 reported similar values of 40 °C as optimal temperature for LPMOs from *T. aurantiacus, T. reesei* and *Talaromyces cellulolyticus*, however these enzymes lost 50% of their activity at 50 °C (Zhang et al., 2019). These thermal characteristics allow to explore a possibility of using *Af*AA9C together with commercial *T. reesei* cellulosic cocktails.

The absorbance values from peroxidase activity assays at different pH showed that *Af*AA9C was able to constantly convert the substrate 2,6-DMP into the product coerulignone at pH ranging from 4.0 to 7.0 over the 30 min (Figure 3.6). However, for pH 8.0 and above it, the detection of product release started to decrease after 10, 6 and 4 min for pH 8.0, 9.0 and 10, respectively. This characteristic of LPMOs was already described (Higasi et al., 2021; Velasco et al., 2021) and is related to the polymerization reaction that occurs between the radicals coerulignone and 2,6-DMP, which is stimulated at higher pH values (Figure 3.6) (Breslmayr et al., 2018).

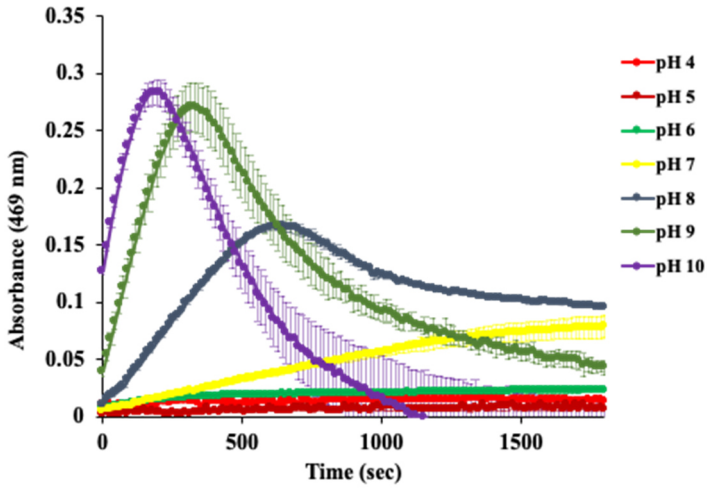

Figure 3.6. *Af*AA9C peroxidase activity at 469 nm in different pH values based in Breslmayr method. Absorbance readings were made every 15 seconds for 1800 s.

The highest absorbance values obtained for each evaluated pH are shown in figure 3.4D (inset) and the apparent improvement in *Af*AA9C activity at alkaline pHs could be explained by the associated action of enzymatic activity and reduction in the oxidation potential of substrate in this pH range (Breslmayr et al., 2019). Despite changes in oxidation potential of 2,6-DMP substrate, two different forms of LPMOs (*Pv*LPMOA9-hm and *Pv*LPMOA9-Im) with better performance in assays measuring the peroxidase activity of the enzyme at pH 7.5 were reported, with a reduction above 20% of its activity in pH 8.0 (Semenova et al., 2020). Regarding the catalytic stability of *Af*AA9C using 2,6 DMP at different pH, the enzyme remained stable and maintained 100% of its activity in pH 6.0 for 24 h. However, the enzyme was able to maintain its activity at pH 7.0 and 8.0 for up to 5 h, with a remaining activity of 80 and 40% after 16 and 24 h, respectively in both pH (Figure 3.4D). This negative effect promoted by alkaline pH in *Af*AA9C activity corroborate with the results of

the Thermofluor assays without addition of NaCl demonstrating that Tm of *Af*AA9C started to decrease in pH above 7.0. The prolonged catalytic stability in acid pH demonstrated by *Af*AA9C is another favorable characteristic for supplementation of commercial cocktails containing cellulases.

3.4.4 Analysis of pH effect in the catalytic activity of *Af*AA9C on crystalline cellulose

The results of oxidative activity of *Af*AA9C (at pH 5.0 and 7.0) against Avicel PH-101, a model crystalline cellulose substrate, demonstrated a better performance at pH 7.0 since the enzyme was able to release large amounts of products in that condition compared to pH 5.0 (Figure 3.7 inset). Previous investigations showed the same behavior for other recombinant LPMOs from *A. fumigatus* and *T. thermophilus* (Higasi et al., 2021; Sepulchro et al., 2021; Velasco et al., 2021). The analysis of the products profile generated by *Af*AA9C allowed the classification of the enzyme as a type 3 LPMO since the enzyme was able to oxidize the substrate at C1 and C4, releasing cellodextrins (Glc_2 – Glc_6), aldonic acids (Glc_2Glc1A – Glc_6Glc1A) and ketoaldoses (C4-oxidized, $GlcgemGlc_n$) in evaluated conditions (Figure 3.7).

This result corroborates with previous performed *in silico* analysis, which applied alignment and phylogenetic tools to predict the regioselectivity of *Af*AA9C (Velasco et al., 2021). Although the type of products detected was almost the same in the evaluated conditions (pH 5.0 and 7.0), a high amount of cellobiose, aldonic acids and ketoaldoses were detected in assays with pH 7.0 (Figure 3.7). The pH effect on cellulose oxidation mediated by LPMOs must be carefully analyzed since the optimal conditions can be affected by changes in redox potential of the reducing agent, which is essential for LPMO activation and also influence the production of H_2O_2 when the enzyme is not bound to the substrate in O_2 and reducing agent presence (Hegnar et al., 2019). LPMOs showing better oxidative performance at alkaline pH have already been reported in reaction systems using AscA as reducing agent (Frommhagen et al., 2018b). Some previous reports showed that the effect of AscA as a reducing agent increases in alkaline pH, simultaneously with the increase in H_2O_2 production and these factors might explain why *Af*AA9C has higher apparent activity in the assays with pH above 5.0 (Frommhagen et al., 2018b; Hegnar et al., 2019).

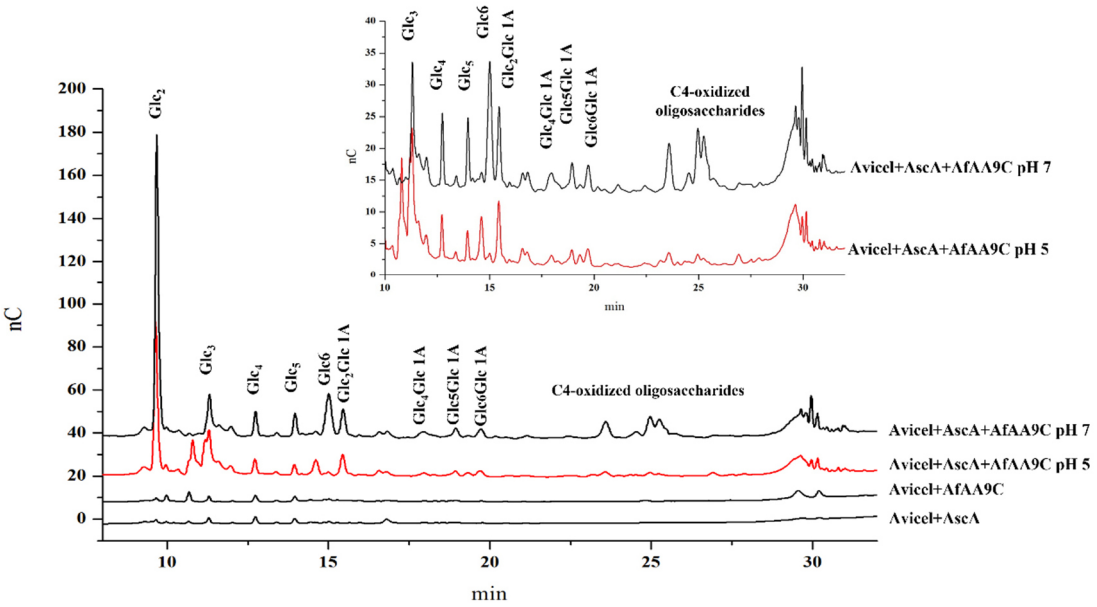

Figure 3.7. *Af*AA9C cellulose oxidative activity at pH 5.0 and pH 7.0 using 5% of Avicel as substrate and 1 mM of ascorbic acid (AscA), the reactions were incubated at 40 °C in 100 mM phosphate/succinate buffer for 16 h Glc: cellodextrins (DP2-6), GlcGlc1A: aldonic acids (DP2-6), in set: comparison of products detected after cellotriose elution at pH 5 and pH 7. Products detected using HPAEC-PAD.

3.4.5 *Af*AA9C activity in the presence of different substrates and reducing agents

Among the tested substrates, *Af*AA9C revealed higher activity on Avicel, PASC and xyloglucan, while acting on bacterial cellulose and filter paper the solubilized oligos were not apparent after LPMO treatment under the tested conditions (data not shown). Due to humongous availability and variations among LPMOs from ascomycetes, enzymes showing activity on both cellulosic and hemicellulosic substrates have already been reported (Agger et al., 2014; Bennati-Granier et al., 2015). Regarding the cleavage of hemicellulosic substrate by LPMOs, the correct identification of the peaks proved to be difficult because of the absence of standards as well as to the heterogeneity in the composition of xyloglucan from tamarind which present backbone composed by glucose containing highly substitutions of xylose residues that also can be further substituted by galactosyl groups. However, there is no doubt that *Af*AA9C is able to oxidize xyloglucan generating a range of products shown in figures 3.8D to F.

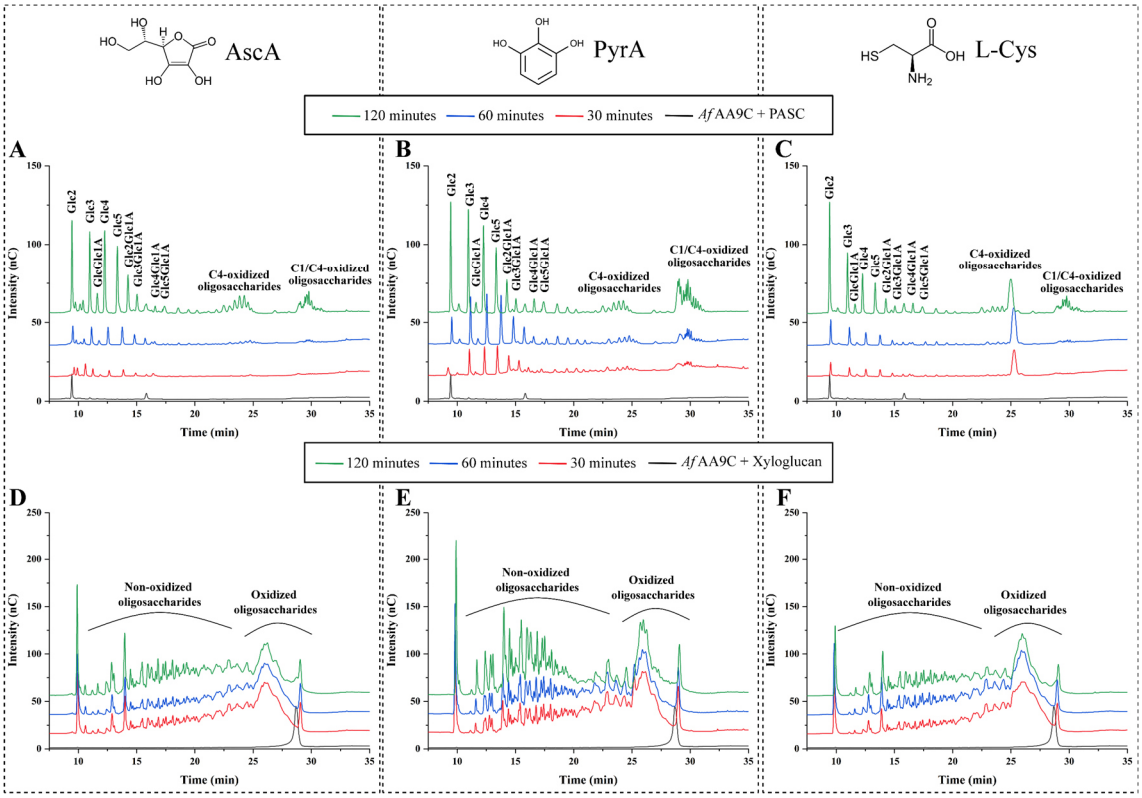

Figure 3.8. *Af*AA9C activity over time (30, 60 and 120 min) using different substrates and reducing agents. PASC oxidation (**A-C**) – (**A**) ascorbic acid, (**B**) pyrogallic acid, (**C**) L-cysteine. Xyloglucan oxidation (**D-E**) – (**D**) ascorbic acid, (**E**) pyrogallic acid, (**F**) L-cysteine. Products detected using HPAEC-PAD.

AA9 LPMOs with the activity against xyloglucan can be sub-classified as enzymes tolerant and intolerant to substitutions contained in the substrate. The tolerant sub-class are able to randomly oxidatively cleave the glucosidic bonds that joins the glucopyranose residues regardless substitutions, thus generating a diversity of products, while the non-tolerant sub-class can only oxidize glucose residues without substitutions (Monclaro et al., 2020). The range of products generated and detected by the action of *Af*AA9C on xyloglucan indicate that this enzyme could be a substitution-tolerant xyloglucan-active LPMO.

Since PASC and xyloglucan were identified as the preferred substrates of *Af*AA9C, the effect of different chemical reducing agents in *Af*AA9C activity against these substrates was evaluated. The investigated reducing agents are classified into three different groups accordingly to its chemical structure: (*i*) AscA – group which does not contain phenolic ring or sulfur atom; (*ii*) PyrA – group showing a 1,2,3-benzenetriol fraction and (*iii*) L-cys – group which contains sulfur atom (Figure 3.8). The evaluated reducing agents were able to induce the activity of *Af*AA9C being PyrA the most efficient while L-cys was the less effective in the tested conditions for both hemi- and cellulosic substrates.

Compared to monophenols and sulfur-based the chemical compounds containing the portion 1,2,3-benzenotriol were already reported to promote better efficiency in LPMO activation (Frommhagen et al., 2016). To understand these results is necessary to consider the donation of an electron by a hydroxyl group which is not energetically favorable, leading to a displacement of the π-electron sextet. However, in phenolic compounds with 1,2,3-benzenetriol structure the stabilization of the displacement of π-electrons by their additional hydroxyl groups may occur due to the resonance effect. Thus, these chemical compounds present low reducing potential as compared to monophenols and compounds containing sulfur, which can benefit the reduction of copper ion in the LPMO active site (Ingold, 1934; Kracher et al., 2016). In addition, the best performance of PyrA can also be associated with the redox potential of the molecule, since PyrA has one-electron redox potential 24 mV lower than AscA (which is commonly applied in LPMO studies) increasing the reducing efficiency as electron donor, and besides of that is more stable than AscA (Kracher et al., 2016; Steenken and Neta, 1982). The evaluation of recombinants LPMOs from other microorganisms showed that incubation time in reactions can influence the stability of reducing agent demonstrating that PyrA at pH 6.0, compared to AscA is almost 10-fold more stable in tested condition. However, stability of the compound can also be pH and/or temperature dependent since this stability was verified for AscA which decreases at temperatures higher than 30 °C and pH above 5.0 (Frommhagen et al., 2018b; Kracher et al., 2016). Figure 3.8 shows that *Af*AA9C in presence of the different reducing agents achieved for both polysaccharides a continuous product release over the time suggesting that reaction condition was not able to affect neither reducing agent or enzyme stability. It is important to note that in each evaluated time the oxidation of both polysaccharides by LPMO was higher when PyrA was the reducing agent.

The idea of LPMO selectivity, specificity or preference for a chemical reducing agent must be carefully analyzed, because it can be associated to factors like the reduction potential of both enzyme and reductant (Kracher et al., 2016), reaction parameters (pH, temperature and reducing agent concentration) (Bissaro et al., 2017), conditions fostered by LPMO-chemical reducing agent interaction (being ROS and H_2O_2 generation a preponderant factor), reducing agent stability and LPMO susceptibility for H_2O_2 (Bissaro et al., 2017; Frommhagen et al., 2018b; Kracher et al., 2016).

3.4.6 Activation of recombinant *Af*AA9C by light

Initially, a Photo-LPMO-Catalysis system (PLC) for cellulose oxidation composed by chlorophyllin, light and the recombinant enzyme *Af*AA9C was configured to investigate the effect of electron transfer induced by light in LPMO activity. The reactions were performed using PASC as a substrate and AscA was added as a reducing agent followed by incubation times of 10, 30 and 60 min (Figure 3.9A and B). The control experiments were carried out including reactions in the dark (Figure 3.10).

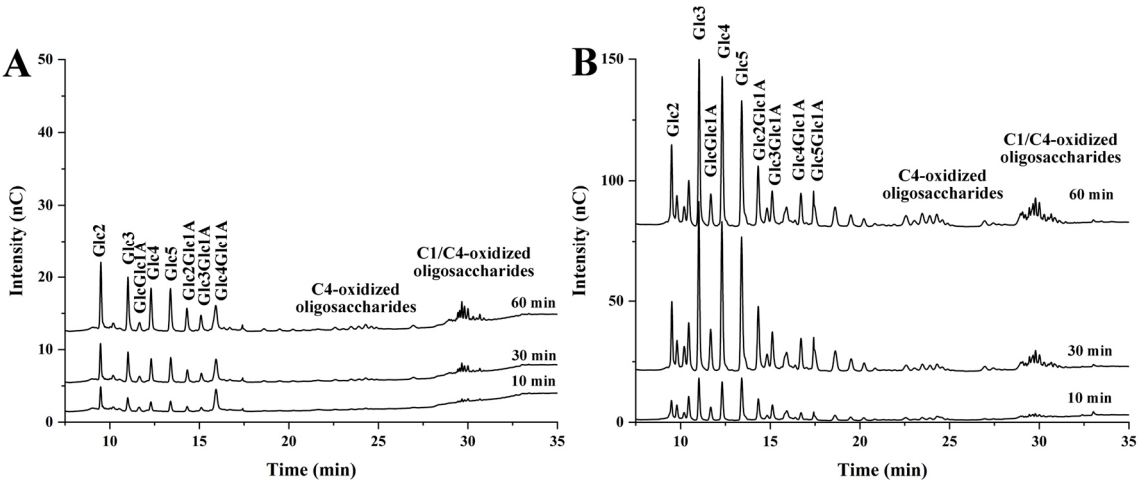

Figure 3.9. Evaluation of PASC oxidation at different times (10, 30, 60 min) using Photo-LPMO-Catalysis (PLC) system. (**A**) Time reaction of PLC system in the absence of a chemical reducing agent and (**B**) in the presence of 1mM ascorbic acid. Products were detected using HPAEC-PAD. The reaction controls appear in figure 3.10A.

The PLC was able to promote oxidative cleavage of cellulose mediated by *Af*AA9C both in the presence and absence of AscA in the reaction. However, the coupling of the reducing agent to the PLC favored the enzyme activity allowing the detection of a large amounts of products (Figure 3.9A and B). Two different pathways have been proposed to the mechanism of electron transfer induced by light in AA9 LPMOs. In the first mechanism the pigment under the light-induced state (excited state) delivers the electron needed to reduce the copper atom present in active site of the enzyme. Thus, the pigment remains in its oxidized form and the presence of reducing agents into the reaction like AscA will preserve the pigment in excitation-donation cycle since this molecule is able to reduce the pigment (Cannella et al., 2016). In the second mechanism, the photo-excited pigment reduces O_2 in

to the superoxide radical ($O_2^{\bullet-}$), which is subsequently converted into H_2O_2 promoting the activation of LPMO to oxidize cellulose. In this scenario, the priming LPMO reduction can be carried out by $O_2^{\bullet-}$ or the direct electron transfer from the photo-excited pigment with the contribution of reducing agent in the formation of H_2O_2 from $O_2^{\bullet-}$ (Bissaro et al., 2020).

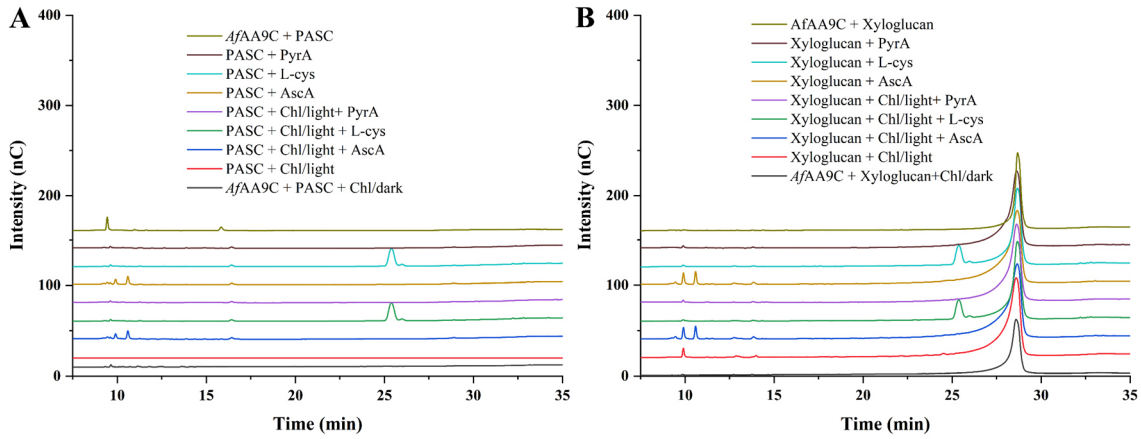

Figure 3.10. Control reactions. HPAEC-PAD analysis from control LPMO reactions using PASC (**A**) and xyloglucan (**B**) as substrates.

Both proposed mechanisms allow to explain the improved activity of *Af*AA9C when it is part of PLC systems coupled to a reducing agent for polysaccharides oxidation, for example, was already demonstrated how the coupling of Chl/light and reducing agent promoted an increase in the activity of an AA9 LPMO family from *Thermothielavioides terrestris* (*Tt*LPMO9E) and an AA10 LPMO from *Thermobifida fusca* (*Tf*LPMO10A) (Cannella et al., 2016). The activity of the enzyme *Tt*LPMO9E using only thylakoids/light or Chl/light without the addition of reducing agents was 10-fold lower compared to full light-induced system including the reducing agent (Cannella et al., 2016). The low reducing power of pigment/light systems on LPMOs have been described for *Sc*AA10C from *Streptomyces coelicolor* and *Mt*LPMO9A from *T. thermophilus* (Bissaro et al., 2020; Sepulchro et al., 2021).

It is important to emphasize that PLC system constantly increased the product formation over the evaluated periods of 10, 30 and 60 min of incubation, while AscA added to PLC did not present apparent changes between 30 and 60 min of incubation. To understand better the coupling of reducing agents to the PLC for polysaccharides oxidation, *Af*AA9C was used as catalyst with three different reducing agents (AscA, PyrA, L-cys), and two types of substrates (PASC and xyloglucan). Regardless of the type of electron donor used in the assay the combination between each reducing agent and PLC promoted the cellulose

oxidation, since the detection of solubilized products in the reaction using PASC as substrate was larger than that using the reducing agent and Chl/light separately (Figure 3.11A, B and C).

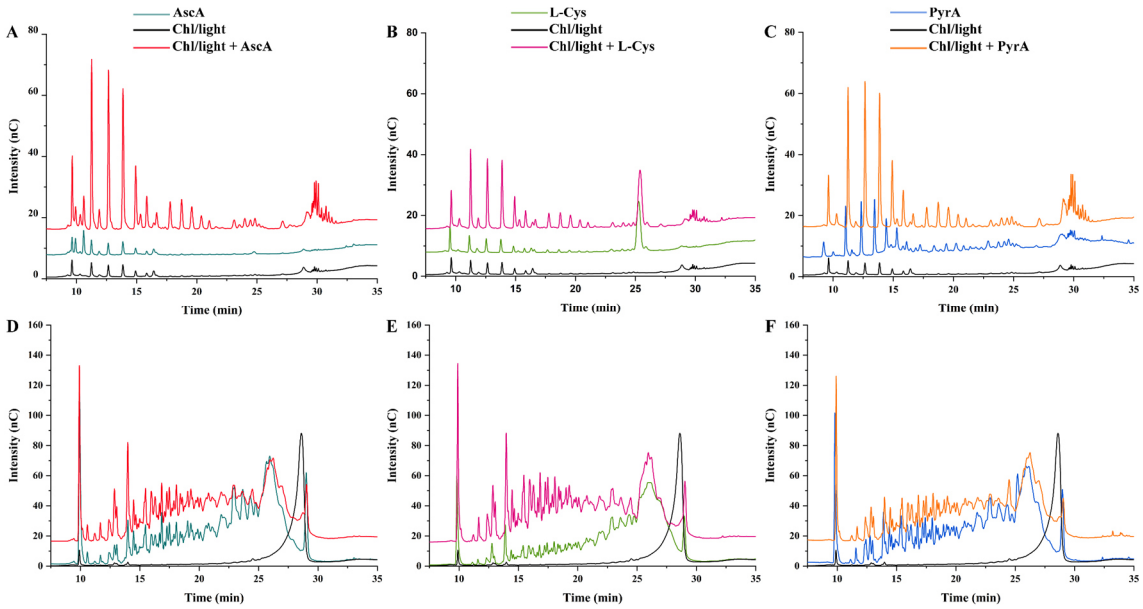

Figure 3.11. Evaluation of the coupling of different chemical reductants at 1mM (AscA: **A** and **D**; L-Cys: **B** and **E**; PyrA: **C** and **F**) with the electron transfer system composed by chlorophyllin and light (Chl/light) on *Af*AA9C activity. The reactions were carried out for 30 min with *Af*AA9C in PASC (**A- C)** and xyloglucan (**D**-**F**). Products were detected using HPAEC-PAD and the reaction controls are shown in figure 3.10.

A collaborative effect between the chemical reducing agent and the light-induced electron transfer system to stimulate the enzymatic action is evident, however the results show different levels of collaborative effect which is depending of the type of reducing agent. As can be seen in figure 3.11A, the coupling of AscA in PLC increased the amounts of products detected in the reaction as compared with the conditions containing only AscA or Chl/light (red, spindrift and black lines, respectively). Comparing the assays coupled with L-Cys or PyrA (showed by pink and orange lines in figure 3.11B and C) the amounts of released products was improved in assay when PLC was coupled to AscA. Furthermore, comparison of the non-coupled reducing agents to the PLC shows that the highest amount of products was achieved in the presence of PyrA (see figures 3.8B-red line and 3.11C-blue line). This demonstrates a change in the catalytic behavior of *Af*AA9C in the presence of reducing agents coupled to the PLC, since AscA promote a better performance in cellulose photo-oxidation mediated by *Af*AA9C under the tested conditions.

For the assays using xyloglucan as substrate, it was not possible to detect the soluble products using only the PLC which is a different behavior of the enzyme when compared to

that using PASC as a substrate (black line in figure 3.11D, E and F). The concept that light-induced electron transfer systems can affect the substrate selectivity of LPMOs have been described for *Tt*LPMO9E that acted strictly on cellulose in reactions using only AscA, however, the subjection of *Tt*LPMO9E to the pigment/light/AscA condition stimulated the action of enzyme to oxidize xyloglucan (Cannella et al., 2016). of the possible explanation of this fact is that the degradation of xyloglucan by *Tt*LPMO9E in absence of light was very low to be detected and that LPMO activity increased substantially due the coupling of AscA with the photosystem. Therefore, the mode how the light-induced electron transfer system influences the relation among enzyme and different substrates still require additional investigations. Again, the coupling of chemical reducing agents to the PLC favored the polysaccharide oxidation mediated by *Af*AA9C, and also showed differences in the collaborative levels influenced by reducing agents and photosystem (Chl/light). Quite surprisingly, here, the collaborative effect was greater for L-cys (compare green and pink lines in figure 3.11E) while this effect was much smaller for AscA and PyrA (Figure 3.11D and F, respectively). The complexity of PLC makes it difficult to explain the observed phenomena and pinpoint the factors that govern collaborative effect of chemical reducing agents and the light-inducing electron transfer in boosting the LPMO activities, since the effect may depend on the redox potentials, chemical reducing agents, the biochemical characteristics of the enzyme and photo-excited pigment. However, compared to previous reports related to light-stimulated LPMO activity our results demonstrated: (*i*) the Chl/light system promotes the LPMO activity, but to a lesser degree as compared to traditionally employed chemical reducing agents such as AscA and PyrA; (*ii*) there is a combined collaborative effect between chemical reducing agents and the photosystems to boost the activity of LPMOs which can be low or less accentuated depending of the used compound and (*iii*) the reducing agent showing better activation of LPMO separately not necessarily will be the best reducing compound when coupled to PLC. In summary, the preference of an LPMO for a specific reducing agent can be affected by coupling with a pigment/light system. Currently, studies of photobiocatalysis processes involving LPMOs are scarce, even those contemplating the pigment/light/enzyme system and absent of chemical reducing agents. The increase in the number of studies and available data related to this approach will allow to build the necessary knowledge to evaluate the feasibility in using light as an energy source to activate LPMOs in plant biomass saccharification processes.

3.5 Conclusions

The ability of LPMOs to perform photobiocatalysis reactions is potentially promising for the conversion of lignocellulosic material into sugars for biofuels and green chemicals production. The recombinant *Af*AA9C is the first reported AA9-LPMO from the thermotolerant fungi *A. fumigatus* with the demonstrated capacity to oxidatively cleave xyloglucan as well as to be activated by photosystems (pigment/light) coupled (or not) to chemical reducing agents. This is the first study to evaluate the effect of different reducing agents coupled with photosystems and to analyze the LPMO activity against model hemi- and cellulosic substrates. The obtained results confirm the existence of a collaborative effect between photosystem and chemical reducing agents to boost the enzyme activity as well as to show a preference of LPMO for specific reducing agent and suggest that this preference can be modified when the electron donor is coupled in PLC. In addition, our study describes a three-dimensional model of the enzyme used for *in-silico* analyses and identifies an extra C-terminal region in the recombinant LPMO which is only found in *Aspergillus* species opening an opportunity for further studies regarding of its biological function. The characteristics of *Af*AA9C presented here demonstrates its potential for plant biomass photo-bioconversion processes.

REFERENCES

Aachmann, F.L., Sørlie, M., Skjåk-bræk, G., Eijsink, V.G.H., Vaaje-kolstad, G., 2012. NMR structure of a lytic polysaccharide monooxygenase provides insight into copper binding , protein dynamics , and substrate interactions. Proc. Natl. Acad. Sci. 109, 18779–18784. https://doi.org/10.1073/pnas.1208822109

Agger, J.W., Isaksen, T., Varnai, A., Vidal-Melgosa, S., Willats, W.G.T., Ludwig, R., Horn, S.J., Eijsink, V.G.H., Westereng, B., 2014. Discovery of LPMO activity on hemicelluloses shows the importance of oxidative processes in plant cell wall degradation. Proc. Natl. Acad. Sci. 111, 6287–6292. https://doi.org/10.1073/pnas.1323629111

Bar-On, Y.M., Phillips, R., Milo, R., 2018. The biomass distribution on Earth. Proc. Natl. Acad. Sci. 115, 6506–6511. https://doi.org/10.1073/pnas.1711842115

Beeson, W.T., Phillips, C.M., Cate, J.H.D., Marletta, M.A., 2012. Oxidative Cleavage of Cellulose by Fungal Copper-Dependent Polysaccharide Monooxygenases. J. Am. Chem. Soc. 134, 890–892.

Beeson, W.T., Vu, V. V., Span, E.A., Phillips, C.M., Marletta, M.A., 2015. Cellulose Degradation by Polysaccharide Monooxygenases. Annu. Rev. Biochem. 84, 923–946. https://doi.org/10.1146/annurev-biochem-060614-034439

Benkert, P., Biasini, M., Schwede, T., 2011. Toward the estimation of the absolute quality of individual protein structure models. Bioinformatics 27, 343–350. https://doi.org/10.1093/bioinformatics/btq662

Bennati-Granier, C., Garajova, S., Champion, C., Grisel, S., Haon, M., Zhou, S., Fanuel, M., Ropartz, D., Rogniaux, H., Gimbert, I., Record, E., Berrin, J.G., 2015. Substrate specificity and regioselectivity of fungal AA9 lytic polysaccharide monooxygenases secreted by Podospora anserina. Biotechnol. Biofuels 8, 1–14. https://doi.org/10.1186/s13068-015-0274-3

Berka, R.M., Grigoriev, I. V, Otillar, R., Salamov, A., Grimwood, J., Reid, I., Ishmael, N., John, T., Darmond, C., Moisan, M.C., Henrissat, B., Coutinho, P.M., Lombard, V., Natvig, D.O., Lindquist, E., Schmutz, J., Lucas, S., Harris, P., Powlowski, J., Bellemare, A., Taylor, D., Butler, G., de Vries, R.P., Allijn, I.E., van den Brink, J., Ushinsky, S., Storms, R., Powell, A.J., Paulsen, I.T., Elbourne, L.D., Baker, S.E., Magnuson, J., Laboissiere, S., Clutterbuck, A.J., Martinez, D., Wogulis, M., de Leon, A.L., Rey, M.W., Tsang, A., 2011. Comparative genomic analysis of the thermophilic biomass-degrading fungi Myceliophthora thermophila and Thielavia terrestris. Nat Biotechnol 29, 922–927. https://doi.org/10.1038/nbt.1976

Bernardinelli, O.D., Lima, M.A., Rezende, C.A., Polikarpov, I., DeAzevedo, E.R., 2015. Quantitative 13C MultiCP solid-state NMR as a tool for evaluation of cellulose crystallinity index measured directly inside sugarcane biomass. Biotechnol. Biofuels 8, 1–11. https://doi.org/10.1186/s13068-015-0292-1

Berto, G., Velasco, J., Tasso, C., Ribeiro, C., Maria, L., Noronha, M., Tyago, M., Polikarpov, I., 2019. Functional characterization and comparative analysis of two heterologous endoglucanases from diverging subfamilies of glycosyl hydrolase family 45. Enzyme

Microb. Technol. 120, 23–35. https://doi.org/10.1016/j.enzmictec.2018.09.005

Bey, M., Zhou, S., Poidevin, L., Henrissat, B., Coutinho, P.M., Berrin, J.-G., Sigoillot, J.-C., 2012. Cello-Oligosaccharide Oxidation Reveals Differences between Two Lytic Polysaccharide Monooxygenases (Family GH61) from Podospora anserina. Appl. Environ. Microbiol. 79, 488–496. https://doi.org/10.1128/aem.02942-12

Bissaro, B., Forsberg, Z., Ni, Y., Hollmann, F., Vaaje-Kolstad, G., Eijsink, V.G.H., 2016. Fueling biomass-degrading oxidative enzymes by light-driven water oxidation. Green Chem. 18, 5357–5366. https://doi.org/10.1039/c6gc01666a

Bissaro, B., Kommedal, E., Røhr, Å.K., Eijsink, V.G.H., 2020. Controlled depolymerization of cellulose by light-driven lytic polysaccharide oxygenases. Nat. Commun. 11, 890. https://doi.org/10.1038/s41467-020-14744-9

Bissaro, B., Røhr, Å.K., Müller, G., Chylenski, P., Skaugen, M., Horn, S.J., Vaaje-kolstad, G., Eijsink, V.G.H., 2017. Oxidative cleavage of polysaccharides by monocopper enzymes depends on H 2 O 2. Nat. Chem. Biol. 13, 1123–1128. https://doi.org/10.1038/nchembio.2470

Blossom, B.M., Russo, D.A., Singh, R.K., van Oort, B., Keller, M.B., Simonsen, T.I., Perzon, A., Gamon, L.F., Davies, M.J., Cannella, D., Croce, R., Jensen, P.E., Bjerrum, M.J., Felby, C., 2020. Photobiocatalysis by a Lytic Polysaccharide Monooxygenase Using Intermittent Illumination. ACS Sustain. Chem. Eng. 8, 9301–9310. https://doi.org/10.1021/acssuschemeng.0c00702

Bond, C.S., Schüttelkopf, A.W., 2009. ALINE: A WYSIWYG protein-sequence alignment editor for publication-quality alignments. Acta Crystallogr. Sect. D Biol. Crystallogr. 65, 510–512. https://doi.org/10.1107/S0907444909007835

Borisova, A.S., Isaksen, T., Dimarogona, M., Kognole, A.A., Mathiesen, G., Varnai, A., Rohr, A.K., Payne, C.M., Sorlie, M., Sandgren, M., Eijsink, V.G., 2015. Structural and Functional Characterization of a Lytic Polysaccharide Monooxygenase with Broad Substrate Specificity. J Biol Chem 290, 22955–22969. https://doi.org/10.1074/jbc.M115.660183

Brenelli, L., Squina, F.M., Felby, C., Cannella, D., 2018. Laccase-derived lignin compounds boost cellulose oxidative enzymes AA9. Biotechnol. Biofuels 11, 1–12. https://doi.org/10.1186/s13068-017-0985-8

Breslmayr, E., Daly, S., Požgajčić, A., Chang, H., Rezić, T., Oostenbrink, C., Ludwig, R., 2019. Improved spectrophotometric assay for lytic polysaccharide monooxygenase. Biotechnol. Biofuels 12, 1–12.

Breslmayr, E., Hanžek, M., Hanrahan, A., Leitner, C., Kittl, R., Šantek, B., Oostenbrink, C., Ludwig, R., 2018. A fast and sensitive activity assay for lytic polysaccharide monooxygenase. Biotechnol. Biofuels 11, 1–13. https://doi.org/10.1186/s13068-018-1063-6

Cannella, D., Jørgensen, H., 2014. Do new cellulolytic enzyme preparations affect the industrial strategies for high solids lignocellulosic ethanol production? Biotechnol. Bioeng. 111, 59–68. https://doi.org/10.1002/bit.25098

Cannella, D., Möllers, K.B., Frigaard, N.U., Jensen, P.E., Bjerrum, M.J., Johansen, K.S.,

Felby, C., 2016. Light-driven oxidation of polysaccharides by photosynthetic pigments and a metalloenzyme. Nat. Commun. 7, 1–8. https://doi.org/10.1038/ncomms11134

Carmona-Cabello, M., Garcia, I.L., Leiva-Candia, D., Dorado, M.P., 2018. Valorization of food waste based on its composition through the concept of biorefinery. Curr. Opin. Green Sustain. Chem. 14, 67–79. https://doi.org/10.1016/j.cogsc.2018.06.011

Chandel, A.K., Garlapati, V.K., Singh, A.K., Antunes, F.A.F., da Silva, S.S., 2018. The path forward for lignocellulose biorefineries: Bottlenecks, solutions, and perspective on commercialization. Bioresour. Technol. 264, 370–381. https://doi.org/10.1016/j.biortech.2018.06.004

Chaplin, A.K., Wilson, M.T., Hough, M.A., Svistunenko, D.A., Hemsworth, G.R., Walton, P.H., Vijgenboom, E., Worrall, J.A.R., 2016. Heterogeneity in the Histidine-brace Copper Coordination Sphere in Auxiliary Activity Family 10 (AA10) Lytic Polysaccharide Monooxygenases *. J. Biol. Chem. 291, 12838–12850. https://doi.org/10.1074/jbc.M116.722447

Chen, Chen, J., Geng, Z., Wang, M., Liu, N., Li, D., 2018. Regioselectivity of oxidation by a polysaccharide monooxygenase from Chaetomium thermophilum. Biotechnol. Biofuels 11, 1–16. https://doi.org/10.1186/s13068-018-1156-2

Chen, J., Guo, X., Zhu, M., Chen, C., Li, D., 2019. Polysaccharide monooxygenase-catalyzed oxidation of cellulose to glucuronic acid-containing cello-oligosaccharides. Biotechnol. Biofuels 12, 42. https://doi.org/10.1186/s13068-019-1384-0

Chen, Y., Jiang, Y., Wan, J., Wu, Q., Wei, Z., 2018. Effects of wet-pressing induced fiber hornification on hydrogen bonds of cellulose and on properties of eucalyptus paper sheets. Holzforschung 1–9.

Choi, S., Song, C.W., Shin, J.H., Lee, S.Y., 2015. Biorefineries for the production of top building block chemicals and their derivatives. Metab. Eng. 28, 223–239. https://doi.org/10.1016/j.ymben.2014.12.007

Chylenski, P., Bissaro, B., Sørlie, M., Røhr, Å.K., Várnai, A., Horn, S.J., Eijsink, V.G.H., 2019. Lytic Polysaccharide Monooxygenases in Enzymatic Processing of Lignocellulosic Biomass. ACS Catal. 9, 4970–4991. https://doi.org/10.1021/acscatal.9b00246

Ciano, L., Davies, G.J., Tolman, W.B., Walton, P.H., 2018. Bracing copper for the catalytic oxidation of C–H bonds. Nat. Catal. 1, 571–577. https://doi.org/10.1038/s41929-018-0110-9

Coletta, V.C., Rezende, C.A., Da Conceição, F.R., Polikarpov, I., Guimarães, F.E.G., 2013. Mapping the lignin distribution in pretreated sugarcane bagasse by confocal and fluorescence lifetime imaging microscopy. Biotechnol. Biofuels 6, 1–10. https://doi.org/10.1186/1754-6834-6-43

Couger, B., Weirick, T., Damasio, A.R.L., Segato, F., Polizeli, M.L.T.M., de Almeida, R.S.C., Goldman, G.H., Prade, R.A., 2018. The Genome of a Thermo Tolerant, Pathogenic Albino Aspergillus fumigatus. Front. Microbiol. Microbiol 9, 1827–1838. https://doi.org/10.3389/fmicb.2018.01827

Courtade, G., Forsberg, Z., Heggset, E., Eijsink, V.G.H., Aachmann, F.L., 2018. The

carbohydrate-binding module and linker of a modular lytic polysaccharide monooxygenase promote localized cellulose oxidation. J. Biol. Chem. 293, 13006–13015. https://doi.org/10.1074/jbc.RA118.004269

Couturier, M., Ladevèze, S., Sulzenbacher, G., Ciano, L., Fanuel, M., Moreau, C., Villares, A., Cathala, B., Chaspoul, F., Frandsen, K.E., Labourel, A., Herpoël-Gimbert, I., Grisel, S., Haon, M., Lenfant, N., Rogniaux, H., Ropartz, D., Davies, G.J., Rosso, M.N., Walton, P.H., Henrissat, B., Berrin, J.G., 2018. Lytic xylan oxidases from wood-decay fungi unlock biomass degradation. Nat. Chem. Biol. 14, 306–310. https://doi.org/10.1038/nchembio.2558

Danneels, B., Tanghe, M., Desmet, T., 2019. Structural Features on the Substrate-Binding Surface of Fungal Lytic Polysaccharide Monooxygenases Determine Their Oxidative Regioselectivity. Biotechnol. J. 14. https://doi.org/10.1002/biot.201800211

de Gouvêa, P.F., Bernardi, A.V., Gerolamo, L.E., de Souza Santos, E., Riaño-Pachón, D.M., Uyemura, S.A., Dinamarco, T.M., 2018. Transcriptome and secretome analysis of Aspergillus fumigatus in the presence of sugarcane bagasse. BMC Genomics 19, 1–18. https://doi.org/10.1186/s12864-018-4627-8

Di Tommaso, P., Moretti, S., Xenarios, I., Orobitg, M., Montanyola, A., Chang, J.M., Taly, J.F., Notredame, C., 2011. T-Coffee: A web server for the multiple sequence alignment of protein and RNA sequences using structural information and homology extension. Nucleic Acids Res. 39. https://doi.org/10.1093/nar/gkr245

Dimarogona, M., Topakas, E., Olsson, L., Christakopoulos, P., 2012. Lignin boosts the cellulase performance of a GH-61 enzyme from Sporotrichum thermophile. Bioresour. Technol. 110, 480–487. https://doi.org/10.1016/j.biortech.2012.01.116

Dolinsky, T.J., Czodrowski, P., Li, H., Nielsen, J.E., Jensen, J.H., Klebe, G., Baker, N.A., 2007. PDB2PQR: Expanding and upgrading automated preparation of biomolecular structures for molecular simulations. Nucleic Acids Res. 35, 522–525. https://doi.org/10.1093/nar/gkm276

Edgar, R.C., 2004. MUSCLE: A multiple sequence alignment method with reduced time and space complexity. BMC Bioinformatics 5, 1–19. https://doi.org/10.1186/1471-2105-5-113

Eijsink, V.G.H., Petrovic, D., Forsberg, Z., Mekasha, S., Røhr, Å.K., Várnai, A., Bissaro, B., Kolstad, G.V., 2019. On the functional characterization of lytic polysaccharide monooxygenases (LPMOs). Biotechnol. Biofuels 12, 1–16.

Eriksson, K., Pettersson, B., 1974. Oxydation: an inportant enzyme reaction in fungal degradation of cellulose. FEBS Lett 49, 282–285.

Espírito Santo, M.C. do, Cardoso, E.B., Guimaraes, F.E.G., deAzevedo, E.R., Cunha, G.P. da, Novotny, E.H., Pellegrini, V. de O.A., Chandel, A.K., Silveira, M.H.L., Polikarpov, I., 2019. Multifaceted characterization of sugarcane bagasse under different steam explosion severity conditions leading to distinct enzymatic hydrolysis yields. Ind. Crops Prod. 139, 111542. https://doi.org/10.1016/j.indcrop.2019.111542

Espirito Santo, M., Rezende, C.A., Bernardinelli, O.D., Pereira, N., Curvelo, A.A.S., deAzevedo, E.R., Guimarães, F.E.G., Polikarpov, I., 2018. Structural and

compositional changes in sugarcane bagasse subjected to hydrothermal and organosolv pretreatments and their impacts on enzymatic hydrolysis. Ind. Crops Prod. 113, 64–74. https://doi.org/10.1016/j.indcrop.2018.01.014

Filiatrault-Chastel, C., Navarro, D., Haon, M., Grisel, S., Herpoël-Gimbert, I., Chevret, D., Fanuel, M., Henrissat, B., Heiss-Blanquet, S., Margeot, A., Berrin, J.-G., 2019. AA16, a new lytic polysaccharide monooxygenase family identified in fungal secretomes. Biotechnol. Biofuels 12, 55. https://doi.org/10.1186/s13068-019-1394-y

Forsberg, Z., Bissaro, B., Gullesen, J., Dalhus, B., Vaaje-kolstad, G., Eijsink, V.G.H., 2017. Structural determinants of bacterial lytic polysaccharide monooxygenase functionality. J. Biol. Chem. 293, 1397–1412. https://doi.org/10.1074/jbc.M117.817130

Frandsen, K.E.H., Poulsen, J.N., Tandrup, T., Leggio, L. Lo, 2017. Unliganded and substrate bound structures of the cellooligosaccharide active lytic polysaccharide monooxygenase Ls AA9A at low pH. Carbohydr. Res. 448, 187–190. https://doi.org/10.1016/j.carres.2017.03.010

Frandsen, K.E.H., Tovborg, M., Jørgensen, C.I., Spodsberg, N., Hemsworth, G.R., Garman, E.F., Grime, G.W., Poulsen, J.N., Batth, T.S., Miyauchi, S., Lipzen, A., Daum, C., Grigoriev, I. V, Katja, S., Leggio, L., 2019. Insights into an unusual Auxiliary Activity 9 family member lacking the histidine brace motif of lytic polysaccharide monooxygenases. J. Biol. Chem. 294, 17117–17130. https://doi.org/10.1074/jbc.RA119.009223

Frommhagen, M., Koetsier, M.J., Westphal, A.H., Visser, J., Hinz, S.W.A., Vincken, J.P., Van Berkel, W.J.H., Kabel, M.A., Gruppen, H., 2016. Lytic polysaccharide monooxygenases from Myceliophthora thermophila C1 differ in substrate preference and reducing agent specificity. Biotechnol. Biofuels 9, 1–17. https://doi.org/10.1186/s13068-016-0594-y

Frommhagen, M., Mutte, S.K., Westphal, A.H., Koetsier, M.J., Hinz, S.W.A., Visser, J., Vincken, J.P., Weijers, D., Berkel, W.J.H. Van, Gruppen, H., Kabel, M.A., 2017. Boosting LPMO - driven lignocellulose degradation by polyphenol oxidase - activated lignin building blocks. Biotechnol. Biofuels 10, 1–16. https://doi.org/10.1186/s13068-017-0810-4

Frommhagen, M., Westphal, A.H., Berkel, W.J.H. Van, Kabel, M.A., 2018a. Distinct substrate specificities and electron-donating systems of fungal lytic polysaccharide monooxygenases. Front. Microbiol. 9, 1–22. https://doi.org/10.3389/fmicb.2018.01080

Frommhagen, M., Westphal, A.H., Hilgers, R., Koetsier, M.J., Hinz, S.W.A., Visser, J., Gruppen, H., van Berkel, W.J.H., Kabel, M.A., 2018b. Quantification of the catalytic performance of C1-cellulose-specific lytic polysaccharide monooxygenases. Appl. Microbiol. Biotechnol. 102, 1281–1295. https://doi.org/10.1007/s00253-017-8541-9

Garajova, S., Mathieu, Y., Beccia, M.R., Bennati-Granier, C., Biaso, F., Fanuel, M., Ropartz, D., Guigliarelli, B., Record, E., Rogniaux, H., Henrissat, B., Berrin, J.G., 2016. Single-domain flavoenzymes trigger lytic polysaccharide monooxygenases for oxidative degradation of cellulose. Sci. Rep. 6, 1–9. https://doi.org/10.1038/srep28276

Gasteiger, E., Hoogland, C., Gattiker, A., Duvaud, S., Wilkins, M.R., Appel, R.D., Bairoch, A., 2005. Protein Analysis Tools on the ExPASy Server, in: Walker, J.M. (Ed.), The

Proteomics Protocol Handbook. Humana Press, pp. 571–607.

Gibson, Young, L., Chuang, R.Y., Venter, J.C., Hutchison, C.A., Smith, H.O., 2009. Enzymatic assembly of DNA molecules up to several hundred kilobases. Nat. Methods 6, 343–345. https://doi.org/10.1038/nmeth.1318

Gouvêa, P.F., Gerolamo, L.E., Bernardi, A.V., Pereira, L.M.S., Uyemura, S.A., Dinamarco, T.M., 2019. Lytic Polysaccharide Monooxygenase from Aspergillus fumigatus can Improve Enzymatic Cocktail Activity During Sugarcane Bagasse Hydrolysis. Protein Pept. Lett. 26, 377–385. https://doi.org/10.2174/0929866526666190228163629

Hangasky, J.A., Iavarone, A.T., Marletta, M.A., 2018. Reactivity of O2 versus H2O2 with polysaccharide monooxygenases. Proc. Natl. Acad. Sci. U. S. A. 115, 4915–4920. https://doi.org/10.1073/pnas.1801153115

Harris, P. V, Xu, F., Kreel, N.E., Kang, C., Fukuyama, S., 2014. New enzyme insights drive advances in commercial ethanol production. Curr. Opin. Chem. Biol. 19, 162–170. https://doi.org/10.1016/j.cbpa.2014.02.015

Harris, Welner, D., Mcfarland, K.C., Re, E., Poulsen, J.N., Brown, K., Salbo, R., Ding, H., Vlasenko, E., Merino, S., Xu, F., Cherry, J., Larsen, S., Leggio, L. Lo, 2010. Stimulation of Lignocellulosic Biomass Hydrolysis by Proteins of Glycoside Hydrolase Family 61 : Structure and Function of a Large , Enigmatic Family †. Biochemistry 49, 3305–3316. https://doi.org/10.1021/bi100009p

Hegnar, O., Petrovi´c, D.M., Bissaro, B., Alfredsen, G., Várnai, A., Eijsink, V.G.H., 2019. pH-Dependent Relationship between Catalytic Activity and Hydrogen Peroxide Production Shown via Characterization of a Lytic Polysaccharide Monooxygenase from Gloeophyllum trabeum. Appl. Environ. Microbiol. 85, 1–15.

Hemsworth, G.R., Henrissat, B., Davies, G.J., Walton, P.H., 2014. Discovery and characterization of a new family of lytic polysaccharide monooxygenases. Nat. Chem. Biol. 10, 122–126. https://doi.org/10.1038/nchembio.1417

Hemsworth, G.R., Johnston, E.M., Davies, G.J., Walton, P.H., 2015. Lytic Polysaccharide Monooxygenases in Biomass Conversion. Trends Biotechnol. 33, 747–761. https://doi.org/10.1016/j.tibtech.2015.09.006

Hemsworth, G.R., Taylor, E.J., Kim, R.Q., Gregory, R.C., Lewis, S.J., Turkenburg, J.P., Parkin, A., Davies, G.J., Walton, P.H., 2013. The copper active site of CBM33 polysaccharide oxygenases. J. Am. Chem. Soc. 135, 6069–6077. https://doi.org/10.1021/ja402106e

Higasi, P.M.R., Velasco, J.A., Pellegrini, V.O.A., de Araújo, E.A., França, B.A., Keller, M.B., Labate, C.A., Blossom, B.M., Segato, F., Polikarpov, I., 2021. Light-stimulated T. thermophilus two-domain LPMO9H: low-resolution SAXS model and synergy with cellulases. Carbohydr. Polym. 260, 117814. https://doi.org/10.1016/j.carbpol.2021.117814

Himmel, M.E., Ding, S.-Y., Johnson, D.K., Adney, W.S., Nimlos, M.R., Brady, J.W., Foust, T.D., 2007. Biomass Recalcitrance: Engineering Plants and Enzymes for Biofuels Production. Science (80-.). 315, 804–807. https://doi.org/10.1126/science.1137016

Horn, S.J., Vaaje-Kolstad, G., Westereng, B., Eijsink, V.G.H., 2012. Novel enzymes for the

degradation of cellulose. Biotechnol. Biofuels 5, 12. https://doi.org/10.1186/1754-6834-5-45

Hu, J., Arantes, V., Pribowo, A., Gourlay, K., Saddler, J.N., 2014. Substrate factors that influence the synergistic interaction of AA9 and cellulases during the enzymatic hydrolysis of biomass. Energy Environ. Sci. 7, 2308–2315. https://doi.org/10.1039/c4ee00891j

Hu, J., Chandra, R., Arantes, V., Gourlay, K., Dyk, J.S. Van, Saddler, J.N., 2015. The addition of accessory enzymes enhances the hydrolytic performance of cellulase enzymes at high solid loadings. Bioresour. Technol. 186, 149–153. https://doi.org/10.1016/j.biortech.2015.03.055

Ingold, C.K., 1934. Principles of an electronic theory of organic reactions. Chem. Rev. 15, 225–274. https://doi.org/10.1021/cr60051a003

Isaksen, T., Westereng, B., Finn, L., Agger, J.W., Kracher, D., Kittl, R., Ludwig, R., Eijsink, V.G.H., Svein, J., Isaksen, T., Westereng, B., Aachmann, F.L., Agger, J.W., Kracher, D., Kittl, R., 2014. A C4-oxidizing Lytic Polysaccharide Monooxygenase Cleaving Both Cellulose and Cello-oligosaccharides *. J. Biol. Chem. 289, 2632–2642. https://doi.org/10.1074/jbc.M113.530196

Jagadeeswaran, G., Gainey, L., Prade, R., Mort, A.J., 2016. A family of AA9 lytic polysaccharide monooxygenases in Aspergillus nidulans is differentially regulated by multiple substrates and at least one is active on cellulose and xyloglucan. Appl. Microbiol. Biotechnol. 100, 4535–4547. https://doi.org/10.1007/s00253-016-7505-9

Johansen, K.S., 2016. Discovery and industrial applications of lytic polysaccharide mono-oxygenases. Biochem. Soc. Trans. 44, 143–149. https://doi.org/10.1042/BST20150204

Jones, P., Binns, D., Chang, H.Y., Fraser, M., Li, W., McAnulla, C., McWilliam, H., Maslen, J., Mitchell, A., Nuka, G., Pesseat, S., Quinn, A.F., Sangrador-Vegas, A., Scheremetjew, M., Yong, S.Y., Lopez, R., Hunter, S., 2014. InterProScan 5: Genome-scale protein function classification. Bioinformatics 30, 1236–1240. https://doi.org/10.1093/bioinformatics/btu031

Kadowaki, M.A.S., Várnai, A., Jameson, J.-K., T. Leite, A.E., Costa-Filho, A.J., Kumagai, P.S., Prade, R.A., Polikarpov, I., Eijsink, V.G.H., 2018. Functional characterization of a lytic polysaccharide monooxygenase from the thermophilic fungus Myceliophthora thermophila. PLoS One 13, 16. https://doi.org/10.1371/journal.pone.0202148

Keller, M.B., Felby, C., Labate, C.A., Pellegrini, V.O.A., Higasi, P., Singh, R.K., Polikarpov, I., Blossom, B.M., 2020. Simple enzymatic assay for the quantification of C1-specific cellulose oxidation by lytic polysaccharide monooxygenases. Biotechnol. Lett. 42, 93–102. https://doi.org/10.1007/s10529-019-02760-9

Kern, M., Mcgeehan, J.E., Streeter, S.D., Martin, R.N.A., Besser, K., Elias, L., Eborall, W., Malyon, G.P., Payne, C.M., Himmel, M.E., Schnorr, K., Beckham, G.T., McQueen-Mason, S.J., 2013. Structural characterization of a unique marine animal family 7 cellobiohydrolase suggests a mechanism of cellulase salt tolerance. Proc. Natl. Acad. Sci. 110, 10189–10194. https://doi.org/10.1073/pnas.1301502110

Kim, D.E., Chivian, D., Baker, D., 2004. Protein structure prediction and analysis using the

Robetta server. Nucleic Acids Res. 32, 526–531. https://doi.org/10.1093/nar/gkh468

Kittl, R., Kracher, D., Burgstaller, D., Haltrich, D., Ludwig, R., 2012. Production of four Neurospora crassa lytic polysaccharide monooxygenases in Pichia pastoris monitored by a fluorimetric assay. Biotechnol. Biofuels 5, 13. https://doi.org/10.1186/1754-6834-5-79

Kracher, D., Scheiblbrandner, S., Felice, A.K.G., Breslmayr, E., Preims, M., Ludwicka, K., Haltrich, D., Eijsink, V.G.H., Ludwig, R., 2016. Extracellular electron transfer systems fuel cellulose oxidative degradation. Science 352, 1098–1101. https://doi.org/10.1126/science.aaf3165

Kubicek, C.P., Kubicek, E.M., 2016. Enzymatic deconstruction of plant biomass by fungal enzymes. Curr. Opin. Chem. Biol. 35, 51–57. https://doi.org/10.1016/j.cbpa.2016.08.028

Kües, U., 2015. Fungal enzymes for environmental management. Curr. Opin. Biotechnol. 33, 268–278. https://doi.org/10.1016/j.copbio.2015.03.006

Kumar, S., Stecher, G., Li, M., Knyaz, C., Tamura, K., 2018. MEGA X: Molecular Evolutionary Genetics Analysis across Computing Platforms. Mol. Biol. Evol. 35, 1547–1549. https://doi.org/10.1093/molbev/msy096

Labourel, A., Frandsen, K.E.H., Zhang, F., Brouilly, N., Grisel, S., Haon, M., Ciano, L., Ropartz, D., Fanuel, M., Martin, F., Navarro, D., Rosso, M.N., Tandrup, T., Bissaro, B., Johansen, K.S., Zerva, A., Walton, P.H., Henrissat, B., Leggio, L. Lo, Berrin, J.G., 2020. A fungal family of lytic polysaccharide monooxygenase-like copper proteins. Nat. Chem. Biol. 16, 345–350. https://doi.org/10.1038/s41589-019-0438-8

Latgé, J.P., 1999. Aspergillus fumigatus and aspergillosis. Clin. Microbiol. Rev. 12, 310–350. https://doi.org/10.1128/CMR.00140-18

Lenfant, N., Hainaut, M., Terrapon, N., Drula, E., Lombard, V., Henrissat, B., 2017. A bioinformatics analysis of 3400 lytic polysaccharide oxidases from family AA9. Carbohydr. Res. 448, 166–174. https://doi.org/10.1016/j.carres.2017.04.012

Levasseur, Drula, E., Lombard, V., Coutinho, P.M., Henrissat, B., 2013. Expansion of the enzymatic repertoire of the CAZy database to integrate auxiliary redox enzymes. Biotechnol. Biofuels 6, 41. https://doi.org/10.1186/1754-6834-6-41

Li, P.Y., Zhang, Y., Xie, B. Bin, Zhang, Y.Q., Hao, J., Wang, Y., Wang, P., Li, C.Y., Qin, Q.L., Zhang, X.Y., Su, H.N., Shi, M., Zhang, Y.Z., Chen, X.L., 2017. Structural and mechanistic insights into the improvement of the halotolerance of a marine microbial esterase by increasing intra- and interdomain hydrophobic interactions. Appl. Environ. Microbiol. 83, 1–12. https://doi.org/10.1128/AEM.01286-17

Li, X., Beeson IV, W.T., Phillips, C.M., Marletta, M.A., Cate, J.H.D., 2012. Structural basis for substrate targeting and catalysis by fungal polysaccharide monooxygenases. Structure 20, 1051–1061. https://doi.org/10.1016/j.str.2012.04.002

Lo Leggio, L., Simmons, T.J., Poulsen, J.C.N., Frandsen, K.E.H., Hemsworth, G.R., Stringer, M.A., Von Freiesleben, P., Tovborg, M., Johansen, K.S., De Maria, L., Harris, P. V., Soong, C.L., Dupree, P., Tryfona, T., Lenfant, N., Henrissat, B., Davies, G.J., Walton, P.H., 2015. Structure and boosting activity of a starch-degrading lytic

polysaccharide monooxygenase. Nat. Commun. 6, 9. https://doi.org/10.1038/ncomms6961

Lo Leggio, L., Weihe, C.D., Poulsen, J.C.N., Sweeney, M., Rasmussen, F., Lin, J., De Maria, L., Wogulis, M., 2018. Structure of a lytic polysaccharide monooxygenase from Aspergillus fumigatus and an engineered thermostable variant. Carbohydr. Res. 469, 55–59. https://doi.org/10.1016/j.carres.2018.08.009

Loose, J.S.M., Forsberg, Z., Fraaije, M.W., Eijsink, V.G.H., Vaaje-kolstad, G., 2014. A rapid quantitative activity assay shows that the Vibrio cholerae colonization factor GbpA is an active lytic polysaccharide monooxygenase. FEBS Lett. 588, 3435–3440. https://doi.org/10.1016/j.febslet.2014.07.036

López, M.J., Jurado, M.M., López-González, J.A., Estrella-González, M.J., Martínez-Gallardo, M.R., Toribio, A., Suárez-Estrella, F., 2021. Characterization of Thermophilic Lignocellulolytic Microorganisms in Composting. Front. Microbiol. 12, 1–13. https://doi.org/10.3389/fmicb.2021.697480

Maciá-Agulló, J.A., Corma, A., Garcia, H., 2015. Photobiocatalysis: The Power of Combining Photocatalysis and Enzymes. Chem. - A Eur. J. 21, 10940–10959. https://doi.org/10.1002/chem.201406437

Magri, S., Nazerian, G., Segato, T., Vieira, A., Zarattini, M., Segato, F., Polikarpov, I., Cannella, D., 2021. Polymer ultrastructure governs AA9 lytic polysaccharide monooxygenases functionalization and deconstruction efficacy on cellulose nano-crystals. Bioresour. Technol. 126375. https://doi.org/10.1016/j.biortech.2021.126375

Martínez, A.T., 2016. How to break down crystalline cellulose. Science 352, 1050–1. https://doi.org/10.1126/science.aaf8920

Meier, K.K., Jones, S.M., Kaper, T., Hansson, H., Koetsier, M.J., Karkehabadi, S., Solomon, E.I., Sandgren, M., Kelemen, B., 2018. Oxygen Activation by Cu LPMOs in Recalcitrant Carbohydrate Polysaccharide Conversion to Monomer Sugars. Chem. Rev. 118, 2593–2635. https://doi.org/10.1021/acs.chemrev.7b00421

Miao, Y., Liu, D., Li, G., Li, P., Xu, Y., Shen, Q., Zhang, R., 2015. Genome-wide transcriptomic analysis of a superior biomass-degrading strain of A. fumigatus revealed active lignocellulose-degrading genes. BMC Genomics 16, 1–20. https://doi.org/10.1186/s12864-015-1658-2

Miller, Gail Lorenz, 1959. Use of Dinitrosalicylic Acid Reagent for Determination of Reducing Sugar. Anal. Chem. 31, 426–428. https://doi.org/10.1021/ac60147a030

Miyauchi, S., Rancon, A., Drula, E., Hage, H., Chaduli, D., Favel, A., Grisel, S., Henrissat, B., Herpoël-Gimbert, I., Ruiz-Dueñas, F.J., Chevret, D., Hainaut, M., Lin, J., Wang, M., Pangilinan, J., Lipzen, A., Lesage-Meessen, L., Navarro, D., Riley, R., Grigoriev, I. V., Zhou, S., Raouche, S., Rosso, M.N., 2018. Integrative visual omics of the white-rot fungus Polyporus brumalis exposes the biotechnological potential of its oxidative enzymes for delignifying raw plant biomass. Biotechnol. Biofuels 11, 1–14. https://doi.org/10.1186/s13068-018-1198-5

Möllers, K.B., Mikkelsen, H., Simonsen, T.I., Cannella, D., Johansen, K.S., Bjerrum, M.J., Felby, C., 2017. On the formation and role of reactive oxygen species in light-driven

LPMO oxidation of phosphoric acid swollen cellulose. Carbohydr. Res. 448, 182–186. https://doi.org/10.1016/j.carres.2017.03.013

Momeni, M.H., Fredslund, F., Bissaro, B., Raji, O., Vuong, T. V, Meier, S., So, T., Lombard, V., Guigliarelli, B., Biaso, F., Haon, M., Grisel, S., Henrissat, B., Welner, D.H., Master, E.R., Berrin, J., Hachem, M.A., 2021. Discovery of fungal oligosaccharide-oxidising flavo-enzymes with previously unknown substrates, redox-activity profiles and interplay with LPMOs. Nat. Commun. 12. https://doi.org/10.1038/s41467-021-22372-0

Monclaro, A.V., Filho, E.X.F., 2017. Fungal lytic polysaccharide monooxygenases from family AA9: Recent developments and application in lignocelullose breakdown. Int. J. Biol. Macromol. 102, 771–778. https://doi.org/10.1016/j.ijbiomac.2017.04.077

Monclaro, A. V., Petrović, D.M., Alves, G.S.C., Costa, M.M.C., Midorikawa, G.E.O., Miller, R.N.G., Filho, E.X.F., Eijsink, V.G.H., Várnai, A., 2020. Characterization of two family AA9 LPMOs from Aspergillus tamarii with distinct activities on xyloglucan reveals structural differences linked to cleavage specificity. PLoS One 15, 1–19. https://doi.org/10.1371/journal.pone.0235642

Monshi, A., Foroughi, M.R., Monshi, M.R., 2012. Modified Scherrer Equation to Estimate More Accurately Nano-Crystallite Size Using XRD. World J. Nano Sci. Eng. 02, 154–160. https://doi.org/10.4236/wjnse.2012.23020

Moreau, C., Tapin-Lingua, S., Grisel, S., Gimbert, I., Le Gall, S., Meyer, V., Petit-Conil, M., Berrin, J.G., Cathala, B., Villares, A., 2019. Lytic polysaccharide monooxygenases (LPMOs) facilitate cellulose nanofibrils production. Biotechnol. Biofuels 12, 13–17. https://doi.org/10.1186/s13068-019-1501-0

Moreno, J., López-González, J.A., Arcos-Nievas, M.A., Suárez-Estrella, F., Jurado, M.M., Estrella-González, M.J., López, M.J., 2021. Revisiting the succession of microbial populations throughout composting: A matter of thermotolerance. Sci. Total Environ. 773, 145587. https://doi.org/10.1016/j.scitotenv.2021.145587

Müller, G., Chylenski, P., Bissaro, B., Eijsink, V.G.H., Horn, S.J., 2018. The impact of hydrogen peroxide supply on LPMO activity and overall saccharification efficiency of a commercial cellulase cocktail. Biotechnol. Biofuels 11, 1–17. https://doi.org/10.1186/s13068-018-1199-4

Nakamura, A.M., Antonio, M., Kadowaki, S., Godoy, A., Nascimento, A.S., Polikarpov, I., 2018. Low-resolution envelope , biophysical analysis and biochemical characterization of a short-chain specific and halotolerant carboxylesterase from Bacillus licheniformis. Int. J. Biol. Macromol. 120, 1893–1905. https://doi.org/10.1016/j.ijbiomac.2018.10.003

Nishikimi, M., 1975. Oxidation of ascorbic acid with superoxide Anion generated by the xanthine- xanthine oxidase system. Biochem. Biophys. Res. Commun. 63, 65–94.

O`Dell, W.B., Pratul, A., Flora, M., 2017. Oxygen activation at the active site of a fungal lytic polysaccharide monooxygenase. Angew. Chemie 56, 767–770. https://doi.org/10.1002/anie.201610502.Oxygen

Obeng, E.M., Adam, S.N.N., Budiman, C., Ongkudon, C.M., Maas, R., Jose, J., 2017.

Lignocellulases: a review of emerging and developing enzymes, systems, and practices. Bioresour. Bioprocess. 4, 16. https://doi.org/10.1186/s40643-017-0146-8

Park, S., Baker, J.O., Himmel, M.E., Parilla, P.A., Johnson, D.K., 2010. Cellulose crystallinity index: measurement techniques and their impact on interpreting cellulase performance. Biotechnol. Biofuels 3, 1–14. https://doi.org/10.1080/02773818608085213

Peralta-Yahya, P.P., Zhang, F., Del Cardayre, S.B., Keasling, J.D., 2012. Microbial engineering for the production of advanced biofuels. Nature 488, 320–328. https://doi.org/10.1038/nature11478

Petrovic, D.M., Bissaro, B., Chylenski, P., Skaugen, M., Sørlie, M., Jensen, M.S., Aachmann, F.L., Courtade, G., Várnai, A., Eijsink, V.G.H., 2018. Methylation of the N-terminal histidine protects a lytic polysaccharide monooxygenase from auto-oxidative inactivation. Protein Sci. 27, 1636–1650. https://doi.org/10.1002/pro.3451

Pettersen, E.F., Goddard, T.D., Huang, C.C., Couch, G.S., Greenblatt, D.M., Meng, E.C., Ferrin, T.E., 2004. UCSF Chimera - A visualization system for exploratory research and analysis. J. Comput. Chem. 25, 1605–1612. https://doi.org/10.1002/jcc.20084

Phillips, C.M., Beeson, W.T., Cate, J.H., Marletta, M.A., 2011. Cellobiose Dehydrogenase and a Copper-Dependent Polysaccharide Monooxygenase Potentiate Cellulose Degradation by Neurospora crassa. Chem. Biol. 6, 1399–1406.

Pielhop, T., Larrazábal, G.O., Studer, M.H., Brethauer, S., Seidel, C.M., Rudolf Von Rohr, P., 2015. Lignin repolymerisation in spruce autohydrolysis pretreatment increases cellulase deactivation. Green Chem. 17, 3521–3532. https://doi.org/10.1039/c4gc02381a

Pierce, B.C., Wittrup, J., Wichmann, J., Meyer, A.S., 2017. Oxidative cleavage and hydrolytic boosting of cellulose in soybean spent flakes by Trichoderma reesei Cel61A lytic polysaccharide monooxygenase. Enzyme Microb. Technol. 98, 58–66. https://doi.org/10.1016/j.enzmictec.2016.12.007

Quinlan, Sweeney, M.D., Lo Leggio, L., Otten, H., Poulsen, J.-C.N., Johansen, K.S., Krogh, K.B.R.M., Jorgensen, C.I., Tovborg, M., Anthonsen, A., Tryfona, T., Walter, C.P., Dupree, P., Xu, F., Davies, G.J., Walton, P.H., 2011. Insights into the oxidative degradation of cellulose by a copper metalloenzyme that exploits biomass components. Proc. Natl. Acad. Sci. 108, 15079–15084. https://doi.org/10.1073/pnas.1105776108

Ragauskas, A.J., Williams, C.K., Davison, B.H., Britovsek, G., Cairney, J., Eckert, C.A., Frederick, W.J., Hallett, J.P., Leak, D.J., Liotta, C.L., Mielenz, J.R., Murphy, R., Templer, R., Tschaplinski, T., 2006. The path forward for biofuels and biomaterials. Science (80-.). 311, 484–489. https://doi.org/10.1126/science.1114736

Rodríguez-Zúñiga, U.F., Cannella, D., Giordano, R. de C., Giordano, R.D.L.C., Jørgensen, H., Felby, C., 2015a. Lignocellulose pretreatment technologies affect the level of enzymatic cellulose oxidation by LPMO. Green Chem. 17, 2896–2903. https://doi.org/10.1039/C4GC02179G

Rodríguez-Zúñiga, U.F., Cannella, D., Giordano, R.D.C., Giordano, R.D.L.C., Jørgensen, H., Felby, C., 2015b. Lignocellulose pretreatment technologies affect the level of

enzymatic cellulose oxidation by LPMO. Green Chem. 17, 2896–2903. https://doi.org/10.1039/c4gc02179g

Rodríguez-zúñiga, U.F., Cannella, D., Giordano, R.D.C., Lima, R. De, Giordano, C., Jørgensen, H., Felby, C., 2015. Lignocellulose pretreatment technologies affec the level of enzymatic cellulose oxidation by. Green Chem. 17, 2896–2903. https://doi.org/10.1039/c4gc02179g

Rubio, M.V., Zubieta, M.P., Franco Cairo, J.P.L., Calzado, F., Paes Leme, A.F., Squina, F.M., Prade, R.A., De Lima Damásio, A.R., 2016. Mapping N-linked glycosylation of carbohydrate-active enzymes in the secretome of Aspergillus nidulans grown on lignocellulose. Biotechnol. Biofuels 9, 1–19. https://doi.org/10.1186/s13068-016-0580-4

Sabbadin, F., Hemsworth, G.R., Ciano, L., Henrissat, B., Dupree, P., Tryfona, T., Marques, R.D.S., Sweeney, S.T., Besser, K., Elias, L., Pesante, G., Li, Y., Dowle, A.A., Bates, R., Gomez, L.D., Simister, R., Davies, G.J., Walton, P.H., Bruce, N.C., McQueen-Mason, S.J., 2018. An ancient family of lytic polysaccharide monooxygenases with roles in arthropod development and biomass digestion. Nat. Commun. 9. https://doi.org/10.1038/s41467-018-03142-x

Sabbadin, F., Urresti, S., Henrissat, B., Avrova, A.O., Welsh, L.R.J., Lindley, P.J., Csukai, M., Squires, J.N., Walton, P.H., Davies, G.J., Bruce, N.C., Whisson, S.C., McQueen-Mason, S.J., 2021. Secreted pectin monooxygenases drive plant infection by pathogenic oomycetes. Science (80-.). 373, 774–779. https://doi.org/10.1126/science.abj1342

Sarkar, S., Witham, S., Zhang, J., Zhenirovskyy, M., Rocchia, W., Alexov, E., 2013. DelPhi web server: A comprehensive online suite for electrostatic calculations of biological macromolecules and their complexes. Commun. Comput. Phys. 13, 269–284. https://doi.org/10.4208/cicp.300611.201011s

Scheller, H.V., Ulvskov, P., 2010. Hemicelluloses. Annu. Rev. Plant Biol. 61, 263–289. https://doi.org/10.1146/annurev-arplant-042809-112315

Segato, F., Damásio, A.R.L., de Lucas, R.C., Squina, F.M., Prade, R.A., 2014a. Genomics Review of Holocellulose Deconstruction by Aspergilli. Microbiol. Mol. Biol. Rev. 78, 588–613. https://doi.org/10.1128/MMBR.00019-14

Segato, F., Damásio, A.R.L., de Lucas, R.C., Squina, F.M., Prade, R.A., 2014b. Genomics Review of Holocellulose Deconstruction by Aspergilli. Microbiol. Mol. Biol. Rev. 78, 588–613. https://doi.org/10.1128/MMBR.00019-14

Segato, F., Damásio, A.R.L., Gonc, T. a, Lucas, R.C. De, 2012a. High-yield secretion of multiple client proteins in Aspergillus. Enzyme Microb. Technol. 51, 100–106.

Segato, F., Damásio, A.R.L., Gonc, T.A., Lucas, R.C. De, Squina, F.M., Decker, S.R., Prade, R.A., 2012b. High-yield secretion of multiple client proteins in Aspergillus. Enzyme Microb. Technol. 51, 100–106. https://doi.org/10.1016/j.enzmictec.2012.04.008

Semenova, Gusakov, A. V, Telitsin, V.D., Rozhkova, A.M., Kondratyeva, E.G., Sinitsyn, A.P., 2020. Purification and characterization of two forms of the homologously expressed lytic polysaccharide monooxygenase (PvLPMO9A) from Penicillium verruculosum. BBA - Proteins Proteomics 1868.

https://doi.org/10.1016/j.bbapap.2019.140297

Sepulchro, A.G. V., Pellegrini, V.V.O.A., Dias, L.D., Kadowaki, M.M.A.S., Cannella, D., Polikarpov, I., 2021. Combining pieces: a thorough analysis of light activation boosting power and co-substrate preferences for the catalytic efficiency of lytic polysaccharide monooxygenase MtLPMO9A. Biofuel Res. J. 8, 1454–1464. https://doi.org/10.18331/BRJ2021.8.3.5

Shapiro, A.L., Viñuela, E., V. Maizel Jr., J., 1967. Molecular weight estimation of polypeptide chains by electrophoresis in SDS-polyacrylamide gels. Biochem. Biophys. Res. Commun. 28, 815–820. https://doi.org/10.1016/0006-291X(67)90391-9

Sheldon, R.A., 2014. Green and sustainable manufacture of chemicals from biomass: State of the art. Green Chem. 16, 950–963. https://doi.org/10.1039/c3gc41935e

Shevchenko, A., Wilm, M., Vorn, O., Mann, M., 1996. Mass spectrometric sequencing of proteins from silver-stained polyacrylamide gels. Anal. Chem. 68, 850–858.

Siglioccolo, A., Paiardini, A., Piscitelli, M., Pascarella, S., 2011. Structural adaptation of extreme halophilic proteins through decrease of conserved hydrophobic contact surface. BMC Struct. Biol. 11, 50. https://doi.org/10.1186/1472-6807-11-50

Simmons, T.J., Frandsen, K.E.H., Ciano, L., Tryfona, T., Lenfant, N., Poulsen, J.C., Wilson, L.F.L., Tandrup, T., Tovborg, M., Schnorr, K., Johansen, K.S., Henrissat, B., Walton, P.H., Lo Leggio, L., Dupree, P., 2017. Structural and electronic determinants of lytic polysaccharide monooxygenase reactivity on polysaccharide substrates. Nat. Commun. 8, 12. https://doi.org/10.1038/s41467-017-01247-3

Span, E.A., Suess, D.L.M., Deller, M.C., Britt, R.D., Marletta, M.A., 2017. The Role of the Secondary Coordination Sphere in a Fungal Polysaccharide Monooxygenase. ACS Chem. Biol. 12, 1095–1103. https://doi.org/10.1021/acschembio.7b00016

Steenken, S., Neta, P., 1982. One-Electron Redox Potentials of Phenols . Hydroxy- and Aminophenols and Related Compounds of Biological Interest1. J. Phys. Chem. Chem. 86, 3661–3667. https://doi.org/10.1021/j100215a033

Steentoft, C., Vakhrushev, S.Y., Joshi, H.J., Kong, Y., Vester-Christensen, M.B., Schjoldager, K.T.-B.G., Lavrsen, K., Dabelsteen, S., Pedersen, N.B., Marcos-Silva, L., Gupta, R., Paul Bennett, E., Mandel, U., Brunak, S., Wandall, H.H., Levery, S.B., Clausen, H., 2013. Precision mapping of the human O-GalNAc glycoproteome through SimpleCell technology. EMBO J. 32, 1478–1488. https://doi.org/10.1038/emboj.2013.79

Stepnov, A.A., Forsberg, Z., Sørlie, M., Nguyen, G.S., Wentzel, A., Røhr, Å.K., Eijsink, V.G.H., 2021. Unraveling the roles of the reductant and free copper ions in LPMO kinetics. Biotechnol. Biofuels 14, 1–14. https://doi.org/10.1186/s13068-021-01879-0

Studer, G., Rempfer, C., Waterhouse, A.M., Gumienny, R., Haas, J., Schwede, T., 2020. QMEANDisCo—distance constraints applied on model quality estimation. Bioinformatics 36, 1765–1771. https://doi.org/10.1093/bioinformatics/btz828

Sugui, J.A., Kwon-Chung, K.J., Juvvadi, P.R., Latgé, J.P., Steinbach, W.J., 2015. Aspergillus fumigatus and related species. Cold Spring Harb. Perspect. Med. 5, 1–17. https://doi.org/10.1101/cshperspect.a019786

Sun, P., Laurent, C.V.F.P., Scheiblbrandner, S., Frommhagen, M., Kouzounis, D., Sanders, M.G., Berkel, W.J.H. Van, Ludwig, R., Kabel, M.A., 2020. Configuration of active site segments in lytic polysaccharide monooxygenases steers oxidative xyloglucan degradation. Biotechnol. Biofuels 13, 1–20. https://doi.org/10.1186/s13068-020-01731-x

Sun, P., Valenzuela, S. V, Chunkrua, P., Pastor, F.I.J., Laurent, C.V.F.P., Ludwig, R., Berkel, W.J.H. Van, Kabel, M.A., 2021. Oxidized Product Profiles of AA9 Lytic Polysaccharide Monooxygenases Depend on the Type of Cellulose. ACS Sustain. Chem. Eng. https://doi.org/10.1021/acssuschemeng.1c04100

Sygmund, C., Kracher, D., Scheiblbrandner, S., Zahma, K., Felice, A.K.G., Harreither, W., Kittl, R., Ludwig, R., 2012. Characterization of the Two Neurospora crassa Cellobiose Dehydrogenases and Their Connection to Oxidative Cellulose Degradation. Appl. Environ. Microbiol. 78, 6161–6171. https://doi.org/10.1128/AEM.01503-12

Tamburrini, K.C., Terrapon, N., Lombard, V., Bissaro, B., Longhi, S., Berrin, J., 2021. Bioinformatic Analysis of Lytic Polysaccharide Monooxygenases Reveals the Pan-Families Occurrence of Intrinsically Disordered C-Terminal Extensions. Biomolecules 11, 19.

Tandrup, T., Frandsen, K.E.H., Johansen, K.S., Berrin, J.G., Leggio, L. Lo, 2018. Recent insights into lytic polysaccharide monooxygenases (LPMOs). Biochem. Soc. Trans. 46, 1431–1447. https://doi.org/10.1042/BST20170549

Tanghe, M., Danneels, B., Camattari, A., Glieder, A., Vandenberghe, I., Devreese, B., Stals, I., Desmet, T., 2015. Recombinant Expression of Trichoderma reesei Cel61A in Pichia pastoris: Optimizing Yield and N-terminal Processing. Mol Biotechnol 57, 1010–1017. https://doi.org/10.1007/s12033-015-9887-9

Textor, L.C., Colussi, F., Silveira, R.L., Serpa, V., De Mello, B.L., Muniz, J.R.C., Squina, F.M., Pereira, N., Skaf, M.S., Polikarpov, I., 2013. Joint X-ray crystallographic and molecular dynamics study of cellobiohydrolase i from Trichoderma harzianum: Deciphering the structural features of cellobiohydrolase catalytic activity. FEBS J. 280, 56–69. https://doi.org/10.1111/febs.12049

Tilburn, J., Scazzoccbio, C., Taylor, G.G., Zabicky-Zissman, J.H., Lockington, R.A., Davies, R.W., 1983. Transformation by integration in Aspergillus nidulans (Ascomycetes; acetamidase gene; ribosomal repeat; mitochondrial replication origin). Gene 26, 236.

Touw, W.G., Baakman, C., Black, J., Te Beek, T.A.H., Krieger, E., Joosten, R.P., Vriend, G., 2015. A series of PDB-related databanks for everyday needs. Nucleic Acids Res. 43, D364–D368. https://doi.org/10.1093/nar/gku1028

Vaaje-kolstad, G., Forsberg, Z., Loose, J.S.M., Bissaro, B., Eijsink, V.G.H., 2017. Structural diversity of lytic polysaccharide monooxygenases. Curr. Opin. Struct. Biol. 44, 67–76. https://doi.org/10.1016/j.sbi.2016.12.012

Vaaje-kolstad, G., Westereng, B., Horn, S.J., Liu, Z., Zhai, H., 2010. An Oxidative Enzyme Boosting the. Science 1795, 219–223.

Vaaje-Kolstad, G., Westereng, B., Horn, S.J., Liu, Z., Zhai, H., Sorlie, M., Eijsink, V.G.H.,

2010. An Oxidative Enzyme Boosting the enzymatic conversion of Recalcitrant Polysaccharides. Science (80-.). 330, 219–222. https://doi.org/10.1126/science.1192231

Vandhana, T.M., Reyre, J. Lou, Sushmaa, D., Berrin, J.G., Bissaro, B., Madhuprakash, J., 2022. On the expansion of biological functions of lytic polysaccharide monooxygenases. New Phytol. 233, 2380–2396. https://doi.org/10.1111/nph.17921

Velasco, J., de Oliveira Arnoldi Pellegrini, V., Sepulchro, A.G.V., Kadowaki, M.A.S., Santo, M.C.E., Polikarpov, I., Segato, F., 2021. Comparative analysis of two recombinant LPMOs from Aspergillus fumigatus and their effects on sugarcane bagasse saccharification. Enzyme Microb. Technol. 144, 109746. https://doi.org/10.1016/j.enzmictec.2021.109746

Velasco, J., Oliva, B., Gonçalves, A.L., Lima, A.S., Ferreira, G., França, B.A., Mulinari, E.J., Gonçalves, T.A., Squina, F.M., Kadowaki, M.A.S., Maiorano, A., Polikarpov, I., Oliveira, L.C. de, Segato, F., 2020. Functional characterization of a novel thermophilic exo-arabinanase from Thermothielavioides terrestris. Appl. Microbiol. Biotechnol. 104, 8309–8326. https://doi.org/10.1007/s00253-020-10806-6

Velasco, J., Oliva, B., José, E., Patricia, L., Lima, S., Larissa, A., Augusto, T., Damasio, A., Marcio, F., Maria, A., Milagres, F., Abdella, A., Wilkins, M.R., Segato, F., 2019. Heterologous expression and functional characterization of a GH10 endoxylanase from Aspergillus fumigatus var . niveus with potential biotechnological application. Biotechnol. Reports 24. https://doi.org/10.1016/j.btre.2019.e00382

Veneault-Fourrey, C., Commun, C., Kohler, A., Morin, E., Balestrini, R., Plett, J., Danchin, E., Coutinho, P., Wiebenga, A., de Vries, R.P., Henrissat, B., Martin, F., 2014. Genomic and transcriptomic analysis of Laccaria bicolor CAZome reveals insights into polysaccharides remodelling during symbiosis establishment. Fungal Genet. Biol. 72, 168–181. https://doi.org/10.1016/j.fgb.2014.08.007

Venkata, S., Nikhil, G.N., Chiranjeevi, P., Nagendranatha Reddy, C., Rohit, M. V., Kumar, A.N., Sarkar, O., 2016. Waste biorefinery models towards sustainable circular bioeconomy: Critical review and future perspectives. Bioresour. Technol. 215, 2–12. https://doi.org/10.1016/j.biortech.2016.03.130

Vivek-Ananth, R.P., Mohanraj, K., Vandanashree, M., Jhingran, A., Craig, J.P., Samal, A., 2018. Comparative systems analysis of the secretome of the opportunistic pathogen Aspergillus fumigatus and other Aspergillus species. Sci. Rep. 8, 1–16. https://doi.org/10.1038/s41598-018-25016-4

Vries, R.P. De, Riley, R., Wiebenga, A., Aguilar-osorio, G., Amillis, S., Uchima, C.A., Anderluh, G., Asadollahi, M., Askin, M., Barry, K., Battaglia, E., Bayram, Ö., Benocci, T., Braus-stromeyer, S.A., Caldana, C., Cánovas, D., Ricardo, A., Damásio, D.L., Diallinas, G., Emri, T., Fekete, E., Flipphi, M., 2017. Comparative genomics reveals high biological diversity and specific adaptations in the industrially and medically important fungal genus Aspergillus. Genome Biol. 18, 1–45. https://doi.org/10.1186/s13059-017-1151-0

Vu, V. V, Beeson, W.T., Phillips, C.M., Cate, J.H.D., Marletta, M.A., 2014. Determinants of Regioselective Hydroxylation in the Fungal Polysaccharide Monooxygenases. J. Am. Chem. Soc. 136, 562–565.

Vu, V. V, Marletta, M.A., 2016. Starch-degrading polysaccharide monooxygenases. Cell. Mol. Life Sci. 298–300. https://doi.org/10.1007/s00018-016-2251-9

Walseth, C.S., 1952. Occurrence of Cellulases in enzyme preparations from microorganisms. TAPPI 35, 228–233.

Walton, P.H., Davies, G.J., 2016. On the catalytic mechanisms of lytic polysaccharide monooxygenases. Curr. Opin. Chem. Biol. 31, 195–207. https://doi.org/10.1016/j.cbpa.2016.04.001

Wanderley, M.C. de A., Martín, C., Rocha, G.J. de M., Gouveia, E.R., 2013. Increase in ethanol production from sugarcane bagasse based on combined pretreatments and fed-batch enzymatic hydrolysis. Bioresour. Technol. 128, 448–453. https://doi.org/10.1016/j.biortech.2012.10.131

Wang, B., Walton, P.H., Rovira, C., 2019. Molecular Mechanisms of Oxygen Activation and Hydrogen Peroxide Formation in Lytic Polysaccharide Monooxygenases. ACS Catal. 9, 4958–4969. https://doi.org/10.1021/acscatal.9b00778

Wang, B., Wang, Z., Davies, G.J., Walton, P.H., Rovira, C., 2020. Activation of O 2 and H 2 O 2 by Lytic Polysaccharide Monooxygenases. ACS Catal. 10, 12760–12769. https://doi.org/10.1021/acscatal.0c02914

Waterhouse, A., Bertoni, M., Bienert, S., Studer, G., Tauriello, G., Gumienny, R., Heer, F.T., de Beer, T.A.P., Rempfer, C., Bordoli, L., Lepore, R., Schwede, T., 2018. SWISS-MODEL: homology modelling of protein structures and complexes. Nucleic Acids Res. 46, W296–W303. https://doi.org/10.1093/nar/gky427

Westereng, B., Arntzen, M.T., Aachmann, F.L., Várnai, A., Eijsink, V.G.H., Agger, J.W., 2016. Simultaneous analysis of C1 and C4 oxidized oligosaccharides, the products of lytic polysaccharide monooxygenases acting on cellulose. J. Chromatogr. A 1445, 46–54. https://doi.org/10.1016/j.chroma.2016.03.064

Westereng, B., Cannella, D., Wittrup Agger, J., Jørgensen, H., Larsen Andersen, M., Eijsink, V.G.H., Felby, C., 2015. Enzymatic cellulose oxidation is linked to lignin by long-range electron transfer. Sci. Rep. 5, 18561. https://doi.org/10.1038/srep18561

Wood, T.M., 1988. Preparation of crystalline, amorphous, and dyed cellulase substrates. Methods Enzymol. 160, 19–25.

Wu, M., Beckham, G.T., Larsson, A.M., Ishida, T., Kim, S., Payne, C.M., Himmel, M.E., Crowley, M.F., Horn, S.J., Westereng, B., Igarashi, K., Samejima, M., Ståhlberg, J., Eijsink, V.G.H., Sandgren, M., 2013. Crystal structure and computational characterization of the lytic polysaccharide monooxygenase GH61D from the basidiomycota fungus Phanerochaete chrysosporium. J. Biol. Chem. 288, 12828–12839. https://doi.org/10.1074/jbc.M113.459396

Yang, J., Yan, R., Roy, A., Xu, D., Poisson, J., Zhang, Y., 2015. The I-TASSER Suite: protein structure and function prediction. Nat. Methods 12, 7–8. https://doi.org/10.1038/nmeth.3213

Yu, Z., Gwak, K.S., Treasure, T., Jameel, H., Chang, H.M., Park, S., 2014. Effect of lignin chemistry on the enzymatic hydrolysis of woody biomass. ChemSusChem 7, 1942–1950. https://doi.org/10.1002/cssc.201400042

Zarattini, M., Corso, M., Kadowaki, M.A., Monclaro, A., Magri, S., Milanese, I., Jolivet, S., Godoy, M.O. De, Hermans, C., Fagard, M., Cannella, D., 2021. LPMO-oxidized cellulose oligosaccharides evoke immunity in Arabidopsis conferring resistance towards necrotrophic fungus B. cinerea. Commun. Biol. 4, 1–13. https://doi.org/10.1038/s42003-021-02226-7

Zhang, R., 2020. Functional characterization of cellulose-degrading AA9 lytic polysaccharide monooxygenases and their potential exploitation. Appl. Microbiol. Biotechnol. 104, 3229–3243. https://doi.org/10.1007/s00253-020-10467-5

Zhang, R., Liu, Y., Zhang, Y., Feng, D., Hou, S., Guo, W., Niu, K., Jiang, Y., Han, L., Sindhu, L., Fang, X., 2019. Identification of a thermostable fungal lytic polysaccharide monooxygenase and evaluation of its effect on lignocellulosic degradation. Appl. Microbiol. Biotechnol. 103, 5739–5750. https://doi.org/10.1007/s00253-019-09928-3

Zhou, X., Qi, X., Huang, H., Zhu, H., 2019. Sequence and structural analysis of AA9 and AA10 LPMOs: An insight into the basis of substrate specificity and regioselectivity. Int. J. Mol. Sci. 20. https://doi.org/10.3390/ijms20184594